

PALLADIUM METAL MEMBRANES FOR HYDROGEN PURIFICATION WITH TITANIUM AS AN INTERMEDIATE LAYER

G. Krishnamurthy

11/30/16

TU Delft

PALLADIUM METAL MEMBRANES FOR HYDROGEN PURIFICATION WITH TITANIUM AS AN INTERMEDIATE LAYER

MASTER THESIS

by

G. Krishnamurthy

(4416120)

In partial fulfilment of the requirements for the degree of

Master of Science

in Materials Science and Engineering

at the Delft University of Technology,

to be defended publicly on Wednesday November 30, 2016 at 09:15.

Supervisor: Dr. Amarante Böttger

Thesis committee: Dr. Yaiza Gonzalez Garcia

Neha Verma Dhingra



PREFACE

Curiosity in taking part of tackling the climatic change has drawn me towards research on renewable energy materials. At the beginning of second year of my master's program at TU Delft, I approached Dr. Amarante Böttger to discuss about my interests in thin films which eventually landed me on this project. Working on this project gave me an immense pleasure and helped me gain knowledge in a wider perspective. This project would not have been possible without the efforts and support of many individuals.

First and foremost, I would like to express my heartfelt thanks to Dr. Amarante Böttger for being so encouraging and trusting me throughout the project. Her constructive suggestions and guidance helped me a lot during this research project. Her passion towards scientific research left a deep impression on me.

I would like extend my heartfelt thanks to my PhD supervisor Neha Verma Dhingra for her guidance, time, motivation and encouragement during this research project and for being there helping me all the time.

I would also thank Dr. Yaiza Gonzalez Garcia for helping me with AFM analysis and also for accepting the offer to be one of my thesis committee member.

A special thanks to Ing. Ruud Hendriks and Ing. Niek van der Pers for assisting me with the XRD lab work and spending time by answering my queries and clearing up doubts related to the project at various stages of my research. I thank Ing. Kees Kwakernaak for training and helping me with SEM. Also I extend my thanks to Ing. Rob Luttjeboer for helping me with sputtering machine all the time. I thank Dr. Marcel bus for helping and training me with AFM.

I express my sincere gratitude to my grandparents, mother, father, sister and also to my extended family members for all the sacrifices they have done to help me to do what I want. I am greatly indebted to Radesh, Ashwathi, Shravan, Hephzibah, Devina, Rujuta, Aravindh, Maria, Kashmira, Prashob who have created a home away from home for me and supporting me all the time. I am also grateful to my colleagues in the department Aakarshit, Yiming, Jeff, Mao yo, Qiyu, Syam for encouraging me during my ups and downs while doing this project.

Finally, I dedicate this work to all the researchers and explorers for their unceasing efforts towards the greener, modern and a sustainable future.

Giridharan Krishnamurthy

Delft, November 2016.

ABSTRACT

Palladium (Pd) metal membranes are used for the production and effective storage of high purity hydrogen. To overcome the crack and de-lamination of Pd membranes at room temperature during several hydrogen loading and de-loading cycles, a Titanium (Ti) of very small thickness of less than 10 nm is introduced as an intermediate layer between the palladium film and an oxidized Si wafer substrate. The objective of the project is to study the thin film growth of Ti and Pd films deposited for different titanium thickness at different argon sputtering pressures over oxidized Si wafer substrate. The surface roughness analysis of titanium and palladium films with its corresponding AFM images is done by Gwyddion software which shows the initial deposition and growth of films for corresponding film thicknesses. Introducing titanium reduces the surface roughness of palladium and enhances the hydrogen flux through palladium films. Texture and stress measurements of the films from XRD also accounts for the growth of the films on the substrate. The hydrogen loading and de-loading process carried out for Pd and Ti films resulted in an elimination of the crack and de-lamination of the palladium film from the substrate with titanium acting as a good adhesion layer.

Keywords: thin films, hydrogen storage, Ti adhesive layer, AFM, Pd/Ti Ultra-thin film, X-ray Diffraction.

TABLE OF CONTENTS

| | |
|---|-----|
| List of Figures..... | ix |
| List of Tables..... | xii |
| 1. Introduction..... | 1 |
| 1.1. Thesis overview..... | 4 |
| 2. Characterization techniques..... | 5 |
| 2.1. Magnetron sputtering method..... | 5 |
| 2.2. Scanning electron microscope..... | 6 |
| 2.3. Atomic force microscope..... | 8 |
| 2.3.1. AFM image analysis by Gwyddion software..... | 10 |
| 2.4. X-Ray Diffraction..... | 12 |
| 3. Experimental part..... | 18 |
| 3.1. Optimization of sputtering parameters..... | 18 |
| 3.1.1. Argon pressure optimization..... | 19 |
| 3.1.2. Thickness optimization..... | 19 |
| 3.2. Film preparation..... | 22 |
| 3.3. Quantification of Texture..... | 23 |
| 4. Results and Discussion..... | 24 |
| 4.1. Before Hydrogenation..... | 24 |
| 4.1.1. RMS Surface roughness by AFM..... | 24 |
| 4.1.1.1. Substrate roughness..... | 24 |
| 4.1.1.2. Ti intermediate layer on Si and SiO ₂ /Si substrates..... | 25 |
| 4.1.1.3. Pd film with Ti intermediate layer (PdTi/SiO ₂ /Si)..... | 31 |
| 4.1.1.4. Pd film without Ti intermediate layer (Pd/SiO ₂ /Si)..... | 33 |

| | |
|--|----|
| 4.1.2. Texture results..... | 34 |
| 4.1.3. Stress measurements..... | 36 |
| 4.1.4. Discussion..... | 40 |
| 4.2. After Hydrogenation and De-hydrogenation..... | 43 |
| 4.2.1. Hydrogen Loading and De-loading (H-L&DL) processes..... | 43 |
| 4.2.2. Texture results..... | 50 |
| 4.2.3. Stress measurements..... | 53 |
| 4.2.4. Discussion..... | 54 |
| 5. Conclusion..... | 56 |
| 6. Recommendations for Future work..... | 57 |
| A. Appendix I- AFM..... | 59 |
| B. Appendix II- SEM..... | 63 |
| C. Appendix III- Texture results..... | 66 |
| D. Appendix IV- Hydrogen Loading and de-loading process results..... | 70 |
| Bibliography..... | 71 |

LIST OF FIGURES

| | |
|---|----|
| 1. Hydrogen permeability through different metals..... | 1 |
| 2. Plot of equilibrium solubility isotherms of PdH_n for bulk Pd at different temperatures where $n = \text{H/Pd}$ ratio. Inset plots shows the low pressure region of the solubility isotherms..... | 3 |
| 3. Lattice parameter of α and β phase of PdH at different temperatures..... | 3 |
| 4. Working principle of Magnetron Sputtering system..... | 6 |
| 5. AJA Magnetron Sputter System..... | 7 |
| 6. Scanning Electron Microscopy..... | 7 |
| 7. Principle of AFM..... | 8 |
| 8. Atomic Force Microscopy..... | 9 |
| 9. Roughness profile..... | 10 |
| 10. Three individual spaces in surface profile. The mean spacing is the average of the three individual spaces on the evaluation length..... | 11 |
| 11. Working Principle of X-ray Diffraction..... | 12 |
| 12. Bruker-AXS-D8-Discover (PSI) XRD diffractometer equipped with Eulerian cradle of Parallel beam geometry..... | 13 |
| 13. Bruker-AXS-D5005 [Theta-Theta (TT)] XRD diffractometer with Bragg-Brentano focusing geometry..... | 14 |
| 14. Structure Zone Model by Thornton..... | 19 |
| 15. X'Pert Reflectivity thickness analysis of Ti sample sputtered for 180 s at 3 Pa argon pressure..... | 20 |
| 16. Average RMS Roughness of Ti deposited on Si substrate for different thickness and argon sputtering pressures..... | 26 |
| 17. Average RMS Roughness of Ti deposited on oxidized Si substrate for different thickness and argon sputtering pressures..... | 27 |
| 18. AFM images of 1 nm thick intermediate layer Ti deposited at 3 Pa on (a) Si substrate and (b) SiO_2/Si substrate..... | 28 |

| | |
|--|----|
| 19. AFM images of Ti intermediate layer deposited on SiO ₂ /Si substrate at argon pressures of (a) 0.4 Pa (3 nm Ti thickness) and (b) 3 Pa (1 nm Ti thickness)..... | 30 |
| 20. AFM images of Ti intermediate layer deposited on SiO ₂ /Si substrate at 3 Pa for (a) 1.0 nm Ti thickness and (b) 6.4 nm Ti thickness..... | 31 |
| 21. Average RMS Roughness of Pd deposited on Ti of various thickness and argon pressures..... | 33 |
| 22. Weak {111} fibre texture pole figure of Pd/SiO ₂ /Si film..... | 35 |
| 23. Weak {111} fibre texture pole figure for 6 nm Ti intermediate layer deposited at 3 Pa argon pressure of Pd/Ti/SiO ₂ /Si film..... | 35 |
| 24. Strong {111} fibre texture pole figure for 6 nm Ti intermediate layer deposited at 0.4 Pa argon pressure of Pd/Ti/SiO ₂ /Si film..... | 36 |
| 25. Strong textured Pd/Ti film with 6 nm Ti deposited at 0.4 Pa argon pressure for {111} reflection. [111] oriented grains are selected for stress measurements..... | 39 |
| 26. Weak textured Pd/Ti film with 6 nm Ti deposited at 3 Pa argon pressure for {111} reflection. [111] oriented grains are selected for stress measurements..... | 40 |
| 27. SEM surface topographic images of 100 nm thick Pd layer (3 Pa) (a) without Ti intermediate layer and (b) with 6 nm thick Ti intermediate layer (3 Pa) deposited on SiO ₂ /Si substrate..... | 41 |
| 28. TEM Bright Field (BF) image of Pd/Ti/SiO ₂ /Si film with 1 nm Ti intermediate layer sputtered at 3 Pa argon pressure..... | 42 |
| 29. Elemental EDX maps of the layers of Pd/Ti/SiO ₂ /Si film..... | 42 |
| 30. Hydrogen Loading and De-loading intensity scans for a weak textured Pd/Ti film with 6 nm Ti intermediate layer deposited at 3 Pa..... | 45 |
| 31. Hydrogen Loading and De-loading intensity scans for a strong textured Pd/Ti film with 3 nm Ti layer deposited at 0.4 Pa..... | 45 |
| 32. Hydrogen Loading and De-loading intensity scans Pd film without Ti intermediate layer..... | 46 |
| 33. Formation and decrease of β - Phase (PdH) during respective hydrogen loading and de-loading processes in strong textured Pd/Ti films..... | 47 |
| 34. Formation and decrease of β - Phase (PdH) during respective hydrogen loading and de-loading processes in weak textured Pd/Ti film and Pd film without Ti intermediate layer..... | 48 |
| 35. Suppression and formation of α -Phase (Pd) during respective hydrogen loading and de-loading processes in strong textured Pd/Ti films..... | 48 |

| | |
|---|----|
| 36. Suppression and formation of α -Phase (Pd) during respective hydrogen loading and de-loading processes in weak textured Pd/Ti film and Pd film without Ti intermediate layer..... | 49 |
| 37. Normalization of β -PdH peak area to before hydrogenated α -Pd peak area with respect to hydrogen loading time..... | 50 |
| 38. Weak {111} texture pole figure of Pd/SiO ₂ /Si film after H-L&DL processes..... | 51 |
| 39. Weak {111} texture pole figure for 6.4 nm thick Ti intermediate layer deposited at 3 Pa argon pressure of Pd/Ti/SiO ₂ /Si film after H-L&DL processes..... | 52 |
| 40. Strong {111} texture pole figure for 6 nm thick Ti intermediate layer deposited at 0.4 Pa argon pressure of Pd/Ti/SiO ₂ /Si film after H-L&DL processes..... | 52 |
| 41. SEM surface topographic images at 100000x magnification for a strong textured Pd/Ti film with 3 nm Ti deposited at 0.4 Pa before and after H-L&DL..... | 55 |
| 42. SEM surface topographic images at 100000x magnification for a weak textured Pd/Ti film with 6 nm Ti deposited at 3 Pa before and after H-L&DL..... | 55 |
| C.1. Strong {111} texture pole figure for 3 nm thick Ti intermediate layer deposited at 0.4 Pa argon pressure of Pd/Ti/SiO ₂ /Si film..... | 66 |
| C.2. Strong {111} texture pole figure for 1 nm thick Ti intermediate layer deposited at 3 Pa argon pressure of Pd/Ti/SiO ₂ /Si film..... | 67 |
| C.3. Strong {111} texture pole figure for 3 nm thick Ti intermediate layer deposited at 0.4 Pa argon pressure of Pd/Ti/SiO ₂ /Si film after hydrogen loading and de-loading processes..... | 68 |
| C.4. Strong {111} texture pole figure for 1 nm thick Ti intermediate layer deposited at 3 Pa argon pressure of Pd/Ti/SiO ₂ /Si film after hydrogen loading and de-loading processes..... | 69 |
| D.1. Hydrogen Loading and De-loading intensity scans for a strong textured Pd/Ti film with 6 nm Ti layer deposited at 0.4 Pa..... | 70 |
| D.2. Hydrogen Loading and De-loading intensity scans for a strong textured Pd/Ti film with 1 nm Ti layer deposited at 3 Pa..... | 70 |

LIST OF TABLES

| | |
|---|----|
| 1. Approximate Ti thickness obtained by XRR for different sputter times and argon pressures deposited on both Si and oxidized Si wafer substrates..... | 21 |
| 2. RMS Roughness values of Ti deposited films on both Si and oxidized Si wafer substrates at two argon sputtering pressures..... | 25 |
| 3. Average RMS Roughness values of Ti only deposited films on both Si and oxidized Si wafer substrates at two argon sputtering pressures..... | 26 |
| 4. Roughness parameters for Ti intermediate layer deposited on SiO ₂ /Si substrate..... | 28 |
| 5. Approximate thin film growth schematic diagrams for Ti intermediate layer deposited on oxidized Si substrate..... | 29 |
| 6. RMS surface Roughness of Pd/Ti/SiO ₂ /Si samples..... | 32 |
| 7. RMS surface roughness of Pd film without Ti intermediate layer..... | 33 |
| 8. Texture results of Pd/SiO ₂ /Si and Pd/Ti/SiO ₂ /Si films..... | 34 |
| 9. Stress values for [111] oriented grains from {311} reflection of Pd/SiO ₂ /Si and Pd/Ti films..... | 37 |
| 10. Hydrogen loading and de-loading times of Pd film with and without Ti intermediate layer..... | 44 |
| 11. {111} Texture results of Pd film without and with Ti intermediate layer before and after hydrogen loading and de-loading processes..... | 51 |
| 12. Stress values for [111] oriented grains from {311} reflection of Pd/SiO ₂ /Si and Pd/Ti/SiO ₂ /Si films before and after hydrogen loading and de-loading processes..... | 53 |
| A.1. AFM images of reference Pd sample on Si and oxidized Si substrates..... | 59 |
| A.2. AFM images of Titanium samples deposited at 0.4 Pa (3 mTorr) argon pressure..... | 60 |
| A.3. AFM images of Titanium samples deposited at 3 Pa (23 mTorr) argon pressure..... | 61 |
| A.4. AFM images of Pd/Ti samples with Ti sputtered at different pressures and thickness..... | 62 |
| B.1. SEM surface topographic images of Pd film without Ti layer before and after H-L&DL processes..... | 63 |
| B.2. SEM surface topographic images of Pd/Ti films with Ti deposited at 0.4 Pa argon pressure before and after H-L&DL processes..... | 64 |

| | |
|---|----|
| B.3. SEM surface topographic images of Pd/Ti film with Ti deposited at 3 Pa argon pressure before and after H-L&DL processes..... | 65 |
|---|----|

INTRODUCTION

The production of pure hydrogen provides a good renewable source of energy eliminating the industrialized world's dependence on fossil fuels and also reducing the greenhouse effect [1]. The fuel cells in automobiles which are hydrogen gas operated, usually require pure hydrogen to avoid the contamination of the catalyst of the fuel cell. The hydrogen gas is normally present with the mixture of other gases. The hydrogen gas is separated by using palladium (Pd) based membranes [2].

The hydrogen permeability is higher for niobium (Nb), vanadium (V) and tantalum (Ta) than palladium (Pd) in a temperature range of 273 K (0 °C) and 973 K (700 °C) as shown in Figure 1. But the above metals give a stronger surface resistance to hydrogen transport than the Pd. So for the above mentioned reason, dense Pd membranes are preferentially used [3, 4].

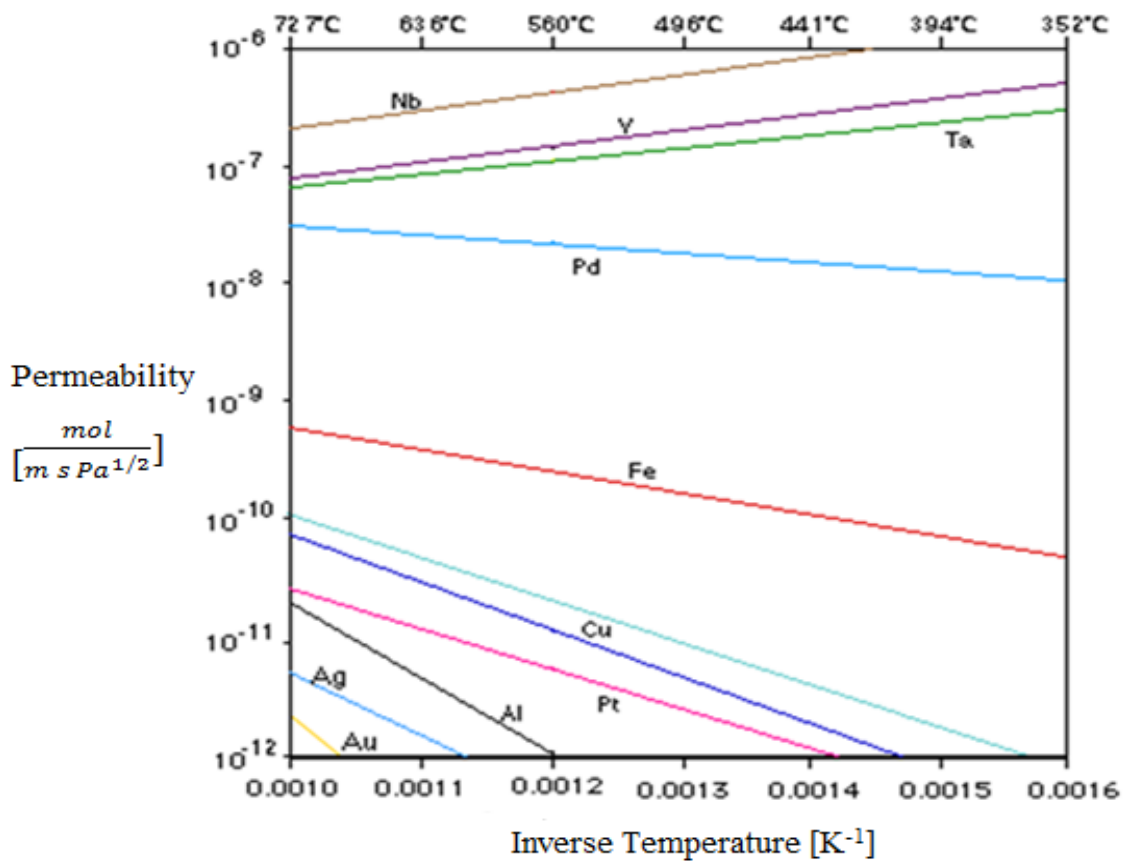


Figure 1. Hydrogen permeability through different metals [3].

The Pd is used for the hydrogen gas separation because the Pd layer could serve as a dissociation layer which has high solubility and diffusivity of H^+ through the bulk of the metal [1, 2]. The hydrogen molecular transport in the palladium membranes occurs through a solution/diffusion mechanism [3], which follows the following activated steps:

- Dissociation of molecular hydrogen at the gas/metal interface
- Adsorption of the atomic hydrogen on the membrane surface
- Dissolution of atomic hydrogen into the palladium lattice
- Diffusion of atomic hydrogen through the membrane
- Recombination of atomic hydrogen to form hydrogen molecules at the gas/metal interface
- Desorption of hydrogen molecules

The face centered cubic (f.c.c.) structure of palladium lattice has four octahedral sites and eight tetrahedral sites. It is at these two sites in the Pd lattice that the surface potential energy of the hydrogen atom is minimum [4]. Thus, the atomic diffusion of hydrogen through the bulk of Pd occurs by the H atom jumping between the nearest neighbour octahedral sites while passing through the tetrahedral sites.

The most important problem associated with the use of pure palladium membranes is the “hydrogen embrittlement” phenomenon. When the temperature is below 573 K (300 °C) and the pressure is below 2 MPa, the β -hydride phase may nucleate from the α -phase as shown in the Figure 2 of the Pd-H phase diagram [3, 4]. At room temperature, absorption of small amounts of hydrogen in palladium cause the α -phase to form up to a maximum composition of $PdH_{0.03}$. Figure 3 shows that the lattice parameter of the α -phase (0.3889 nm) is close to that of pure palladium (0.3890 nm) [4]. However, with the further absorption of hydrogen, β -phase hydride ($PdH_{0.6}$) is formed and the transformation causes the expansion of the lattice to 0.4018 nm. Thus after a few cycles of $\alpha \rightleftharpoons \beta$ transition, the Pd membrane can become brittle due to the strains caused by the Pd lattice expansion. Delamination of the Pd membrane also occurs due to the defects or the cracks that arises in the membrane leading to a very low mechanical stability [3, 4].

In order to overcome the delamination and hydrogen embrittlement, an intermediate layer of titanium (Ti) was introduced between the deposited Pd metal and the substrate. The selection of titanium (Ti) as an intermediate layer is because the Ti layer acts as a good adhesive layer between the Pd membrane and the substrate. The Pd acts as a catalyst for gathering hydrogen in Ti and its diffusion through the layers. Also Ti is selected due to its high hydrogen storage capacity of 67 % in its lattice [5].

In this thesis, a very small thickness of 1 and 6 nm were considered for Ti intermediate layer and 100 nm thickness for Pd layer as the thinner membranes offers higher permeability [3]. An oxidized Si wafer was used as a substrate which has an oxide layer of 188 nm over silicon. The influence of Ti as an intermediate layer was studied and analysed by comparing the results of Pd membrane without Ti

(Pd/SiO₂/Si) and the Pd membrane with Ti as an intermediate layer (Pd/Ti/SiO₂/Si) deposited on an oxidized Si substrates.

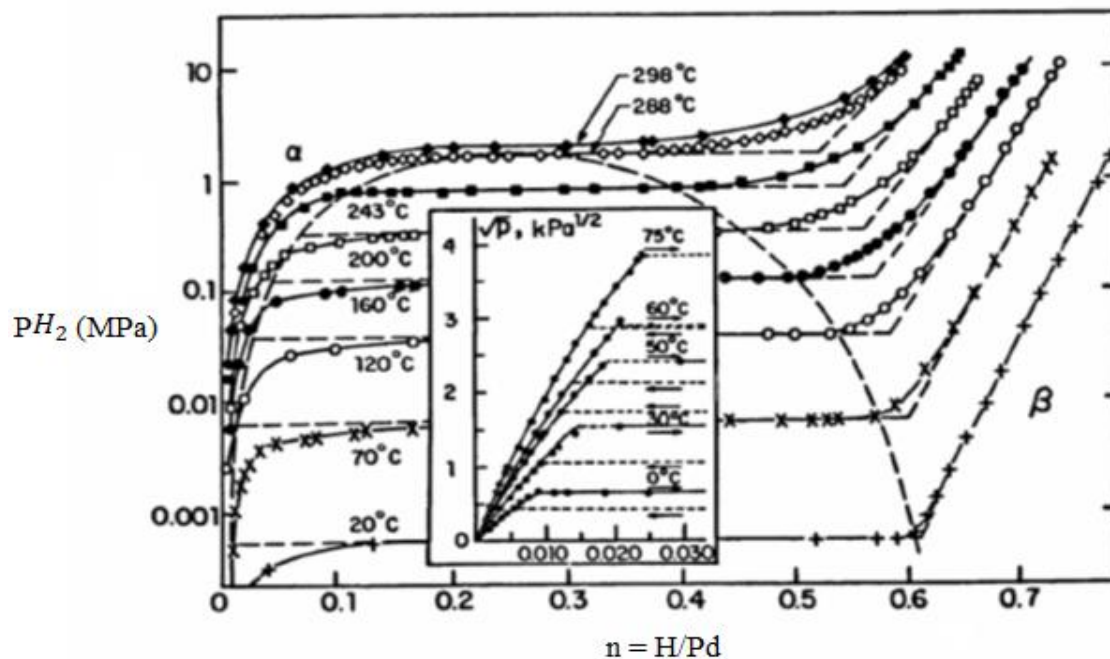


Figure 2. Plot of equilibrium solubility isotherms of PdH_n for bulk Pd at different temperatures where $n = \text{H/Pd}$ ratio. Inset plots shows the low pressure region of the solubility isotherms [4].

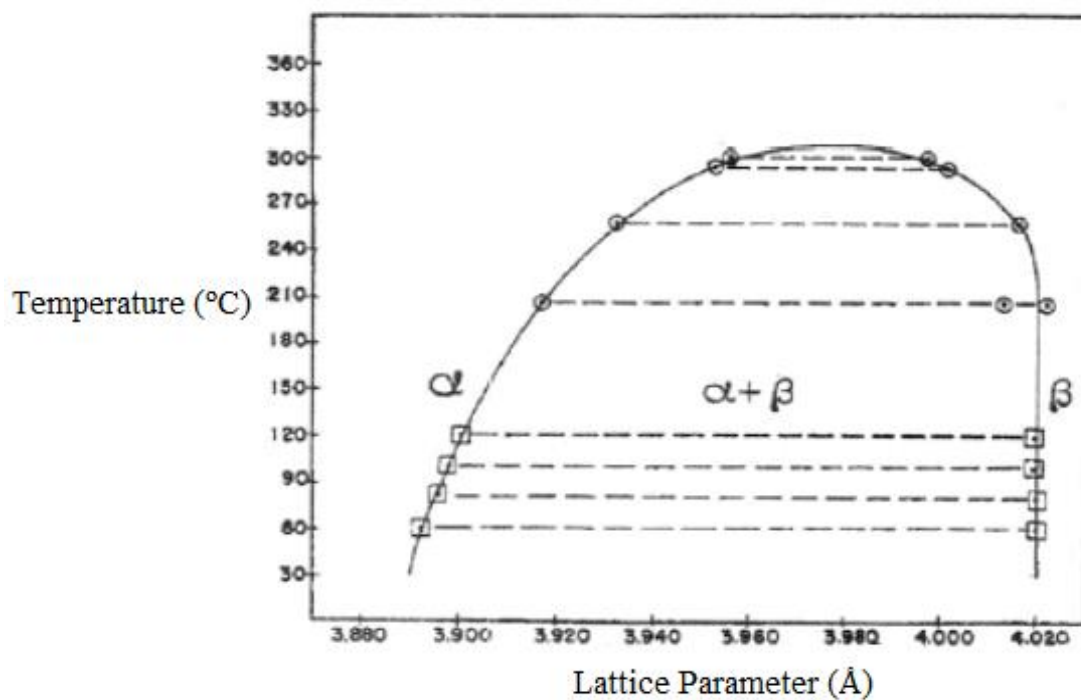


Figure 3. Lattice parameter of α and β phase of PdH at different temperatures [4].

1.1. Thesis Overview

In chapter 2, a brief description of the different characterization techniques used for analysing the thin film samples are provided.

In chapter 3, information is provided regarding the experimental parameters optimization and preparation of the sample.

In chapter 4, before and after hydrogenation results are presented and analysed with different characterization techniques for different Pd and Ti deposited films.

In chapter 5, significant conclusions that emerged from this research are stated.

In chapter 6, recommendations are made for the future work that should be carried out for enhancing and extending the present research.

In the end, appendices are enclosed to supplement the information presented in the report. The appendices present the ancillary results.

CHARACTERIZATION TECHNIQUES

The Pd membranes with Ti as an intermediate layer was deposited over the substrate by Magnetron sputtering deposition technique. And the post-deposition techniques like X-Ray Reflectometry (XRR), Scanning Electron Microscopy (SEM), Atomic Force Microscopy (AFM) and X-Ray Diffraction (XRD) were carried out for examining the deposited film structures and properties like film thickness, film surface structure, film roughness, film texture and stresses respectively. The characterization techniques used for the preparation and studying the Ti and Pd thin films are described below.

2.1. Magnetron sputtering method

Magnetron sputtering system was chosen as sputter deposition process in depositing thin film in this thesis. The adhesion of the sputtered films is stronger when sputtered by Magnetron sputtering method than other physical vapour deposition (PVD) techniques like evaporation deposited films [4]. The Sputtering is defined as the process whereby particles are ejected from the target material due to the bombardment of the target by energetic material [6]. Magnetron sputtering is the plasma vapour deposition in which a plasma is created and positively charged ions from the plasma are accelerated by an electric field super imposed on a negatively charged electrode or target. The ions strike target and eject atoms from the target that are to be deposited on the substrate [6]. Figure 4 shows the brief explanation of the working principle of the magnetron sputtering system.

In sputter deposition, the nature of the substrate, deposition rate and temperature, deposition pressure and vacuum quality are some of the parameters that influence the film properties like stress, texture and morphology predicting reliability of thin film systems [8]. Magnetron sputtering method was used for depositing the Ti and Pd materials sequentially on the oxidised silicon wafer substrate at different argon pressures. The sputtering was done for the optimal required thickness of the sputtering material by adjusting the sputtering parameters like argon pressure, power, current and sputtering rate [9]. The sputtering instrument used for the deposition process is ATC 1500-F SPUTTER SYSTEM (AJA International., Inc.).

The substrate was first loaded into the load lock chamber of the AJA magnetron system and allowed to achieve vacuum with pressure of about 1.33 mPa [10]. After the vacuum is created, the sample is then transferred to the main chamber from the load lock chamber. The main chamber is the place where the sputtering process is carried out. The stage where the sample is loaded in the chamber is allowed to

rotate for the uniform deposition of the material on the entire area of the substrate during its operation. The rotation of the sample stage is optimized to be about 20 rpm.

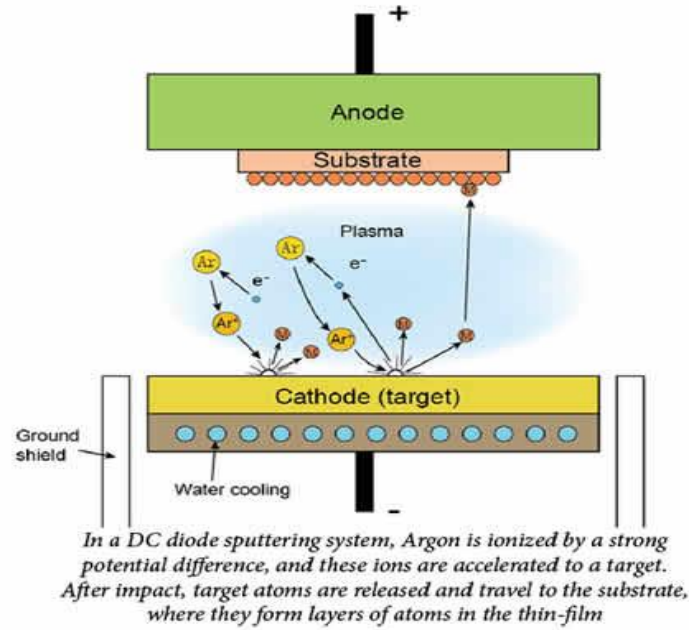


Figure 4. Working principle of Magnetron Sputtering system [7].

The working distance between the target (the material to be deposited on the substrate) and the substrate (over which the material should be deposited) is optimized to be about 60 cm for the maximum deposition of the target material on the substrate. The base pressure of the chamber was kept at about 13.3 μ Pa for better deposition process [10]. An optimized argon pressure was used in the sputtering to get better deposition of the target material on the substrate. Adjusting the sputtering parameters like power, current, sputtering time and argon pressure will produce the different sputtering rates as well as different thickness of the target material that are to be deposited on the substrate [9].

A typical magnetron sputtering instrument used for the sputtering process is shown in Figure 5 [11]. The arrangement of the main chamber and load lock chamber as well as the position of the operators for controlling the sputtering parameters are clearly seen from Figure 5.

2.2. Scanning Electron Microscope (SEM)

A Scanning Electron Microscope (SEM) is a type of electron microscope that produces images of a sample by scanning it with a focused beam of electrons. The electrons interact with the sample producing various signals that can be detected, which contain information about the sample's surface topography and composition. The electron beam is generally scanned in a raster scan pattern, and the

2. Characterization Techniques

beam's position is combined with the detected signal to produce an image [12]. The surface topography of thin Ti and Pd films were examined with JOEL JSM-6500F Field Emission Scanning Electron Microscope as shown in Figure 6 using an acceleration voltage of 15 kV.

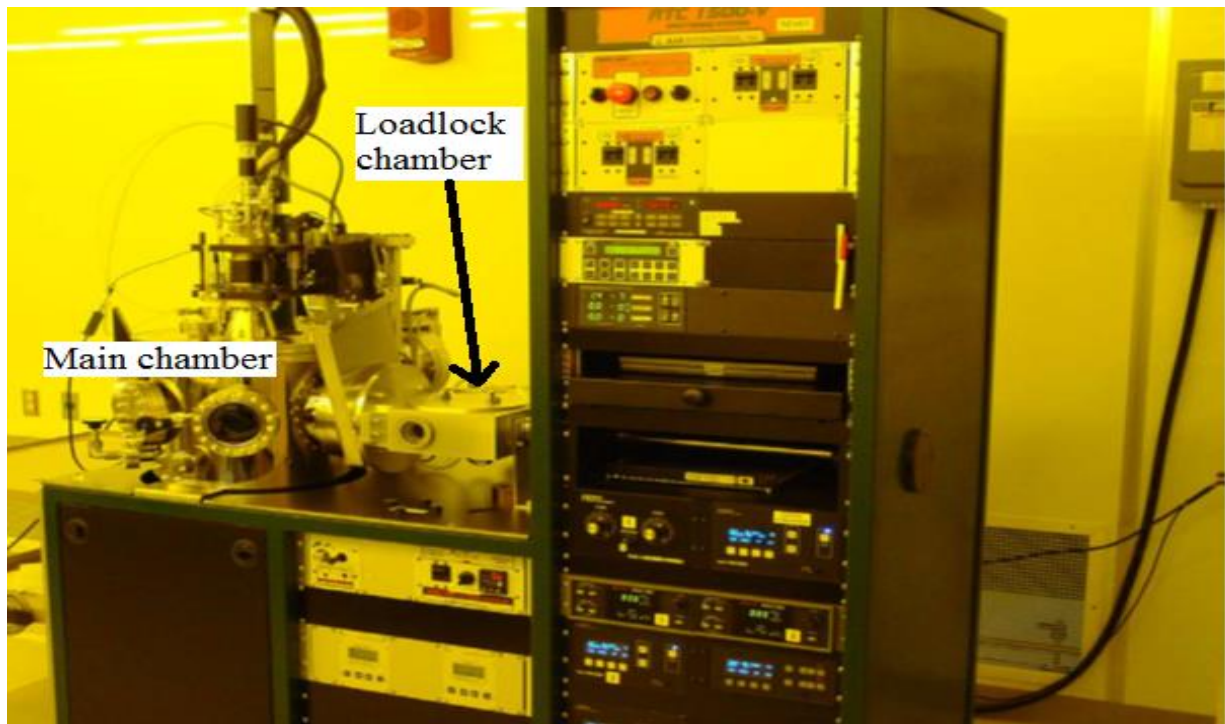


Figure 5. AJA Magnetron Sputter System [11].



Figure 6. Scanning Electron Microscopy (SEM).

2.3. Atomic Force Microscopy (AFM)

Atomic force microscopy (AFM) is an imaging technique used to determine the topography of surfaces. It allows quantitative characterization of the surface morphology, including determination of surface roughness [13]. The AFM provides a 3D profile on a nanoscale, by measuring forces between a sharp probe and surface at very short distance (0.2-10 nm probe-sample separation) [14]. The probe is supported on a flexible cantilever and the AFM tip gently touches the surface and records the small force between the probe and the surface. The basic components of an AFM are the probe, the cantilever, the scanner, the laser, a data processor and a photodetector as shown in the Figure 7.

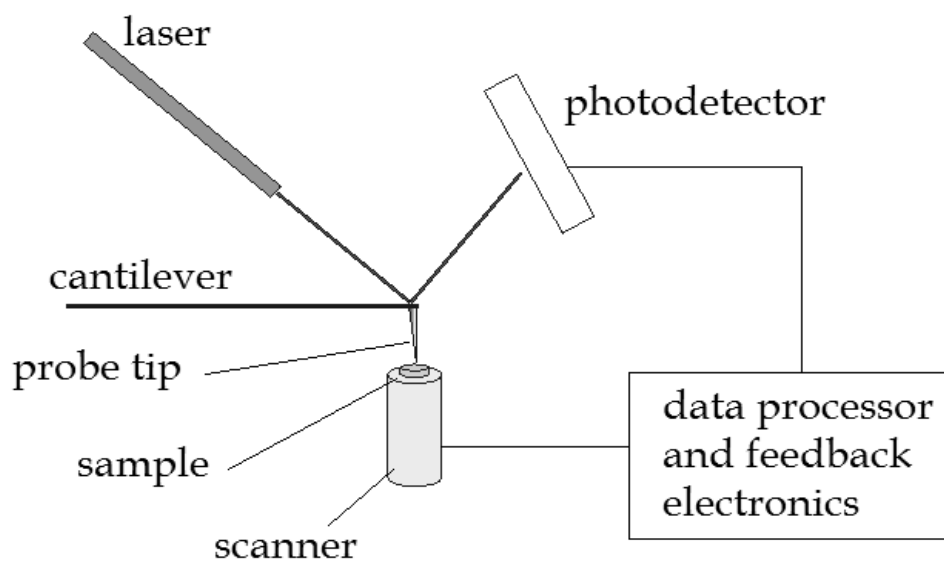


Figure 7. Principle of AFM [14].

There are three primary imaging modes in AFM: the contact mode where the probe-surface separation is less than 0.5 nm, the intermittent contact (tapping mode) with probe-surface separation occurs in the range 0.5 and 2 nm and the non-contact mode where the probe-surface-separation ranges from 0.1 to 10 nm [14].

Contact mode: This mode is most useful for hard surfaces; a tip in contact with a surface, however, is subjected to contamination from removable material on the surface. Excessive force in contact mode can also damage the surface or blunt the probe tip.

Non-contact mode: This mode is useful for imaging soft surfaces, but its low resolution and its sensitivity to external vibrations often cause problems in the engagement and retraction of the tip.

Tapping mode: This mode takes the advantages of the above two modes, as it eliminates the frictional forces by intermittently contacting the surface and oscillating with sufficient amplitude to prevent the tip from being trapped by adhesive meniscus forces from the contaminant layer. Tapping mode is usually preferred to image samples that are soft like polymers and thin films. Due to this reason, the tapping mode was chosen for the surface analysis with AFM in this thesis.

A Digital Instrument NTMDT Ntegra AFM device operating in the tapping mode, with Si tip cantilever of radius 10 nm nominal curvature and resonance frequency of 296-358 KHz shown in Figure 8 is used to determine the surface morphology of the thin films. A raster scan method probes over a small area of $1 \times 1 \mu\text{m}^2$, $3 \times 3 \mu\text{m}^2$ and $10 \times 10 \mu\text{m}^2$ of the sample measuring the surface roughness property.



Figure 8. Atomic Force Microscopy [15].

Surface Roughness:

The surface roughness is a component of surface texture. The roughness is often described as closely spaced irregularities (Figure 9). It is quantified by the vertical spacing of a real surface from its ideal form [14]. If the spacing and height are large, the surface is rough; if they are small, the surface is smooth.

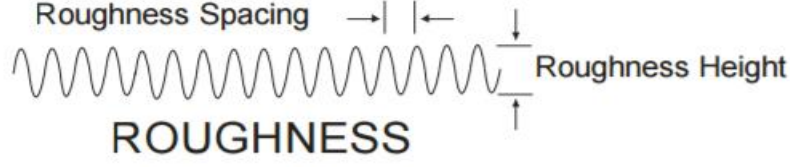


Figure 9. Roughness profile [14].

The roughness can be characterized by several parameters and functions such as height and spacing parameters [14, 18]. The height parameters include the roughness average (R_a) and Root mean square roughness (R_q).

Average Roughness (R_a): R_a is the most widely used among the height parameters because it is simple to obtain when compared to others. R_a is the arithmetic mean of the absolute values of the height of the surface profile over the evaluation length (L):

$$R_a = \frac{1}{L} \int_0^L |y(x)| dx$$

Where $y(x)$ is the function that describes the surface profile analysed in terms of height y and position (x) of the sample over the evaluation length ' L '. But the average roughness can be the same for surfaces with roughness profile totally different because it depends only on the average profile of the heights. For this reason, R_a is not used for analysis in this thesis.

Root-Mean-Square Roughness (R_q): R_q is a function that takes the square of the measures. The Root-Mean-Square (RMS) roughness of a surface is similar to the average roughness, with the only difference being the mean squared absolute values of surface roughness profile:

$$R_q = \sqrt{\frac{1}{L} \int_0^L y^2(x) dx}$$

The R_q depends on the swept area of the sample, the scan size, as it represents the standard deviation of the height distribution. The R_q is more sensitive to peaks and valleys than the average roughness due to the squaring of the amplitude in its calculation. Due to the above reason, the root mean square (RMS) roughness is taken for surface analysis in this thesis.

2.3.1. AFM image analysis by Gwyddion software

The AFM images obtained are analysed by using Gwyddion software for extracting more information about the deposition of the thin films [16]. The line scans are obtained from the AFM image by using

Gwyddion software [16, 17]. The line scan is the surface roughness profile, from which the height of roughness, a deposited island size, the spacing between the islands and the shape of the film top surface were obtained. The following are the parameters which explains the surface roughness profile.

Skewness (R_{sk}): It measures the symmetry of the variation of a profile about its mean line [18].

$$R_{sk} = \frac{1}{LR_q^3} \int_0^L y^3(x) dx$$

Surfaces with positive skewness have fairly high spikes that protrude above the average. Surfaces with negative skewness, such as porous surfaces have fairly deep valleys in a smoother plateau. More random surfaces have a skew near zero. The skewness is non-dimensional parameter.

Kurtosis (R_{ku}): It relates to the uniformity of the surface line profile or to the spikiness of the profile [18].

$$R_{ku} = \frac{1}{LR_q^4} \int_0^L y^4(x) dx$$

The kurtosis value less than 3 implies an uneven surface and greater than 3 implies a spiky surface. The kurtosis is non-dimensional parameter.

Mean Spacing (S_m): It is the average spacing between peaks in the length of evaluation [14]. The spacing between peaks is the horizontal distance between the points where two peaks cross above the midline. The mean spacing as shown in Figure 10 is defined as the average of spacing individual (S_i):

$$S_m = \frac{1}{L} \sum_{i=1}^L S_i$$

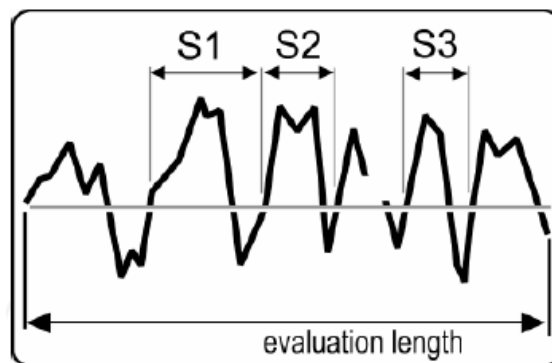


Figure 10. Three individual spaces in surface profile. The mean spacing is the average of the three individual spaces on the evaluation length [14].

The spacing between the islands and the island size can be calculated from the mean spacing parameter. The mean spacing is generally described in nm or μm .

2.4. X-Ray Diffraction (XRD)

The X-ray Diffraction technique can be used for the measurement of different thin film structure properties like stress, texture and also carrying out the processes like annealing and hydrogenation of the samples [19]. The XRD instrument is shown in Figure 12.

The basic working principle of XRD is explained in Figure 11 where the incident beam of X-rays are allowed to hit the sample and the reflected beam is detected by the detector. This detection of the reflected X-rays gives the X-ray diffraction pattern [20]. The method for the study of the internal structure of the sample is based on the Bragg equation given by,

$$2d \sin\theta = n\lambda$$

Where, d is inter-planar distance or the distance between the successive lattice planes.

θ is the angle between the incident X-rays and the sample surface.

n is an integer.

λ is the wavelength.

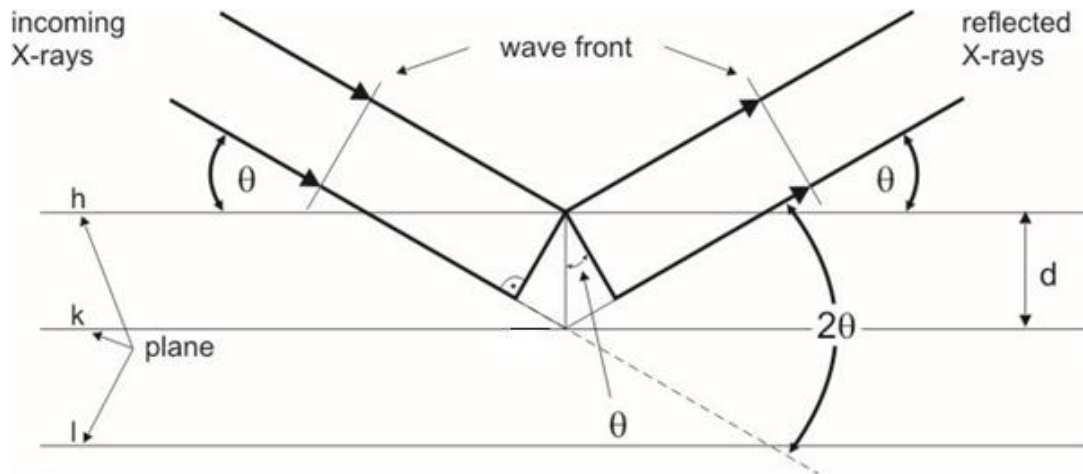


Figure 11. Working Principle of X-ray Diffraction [21].

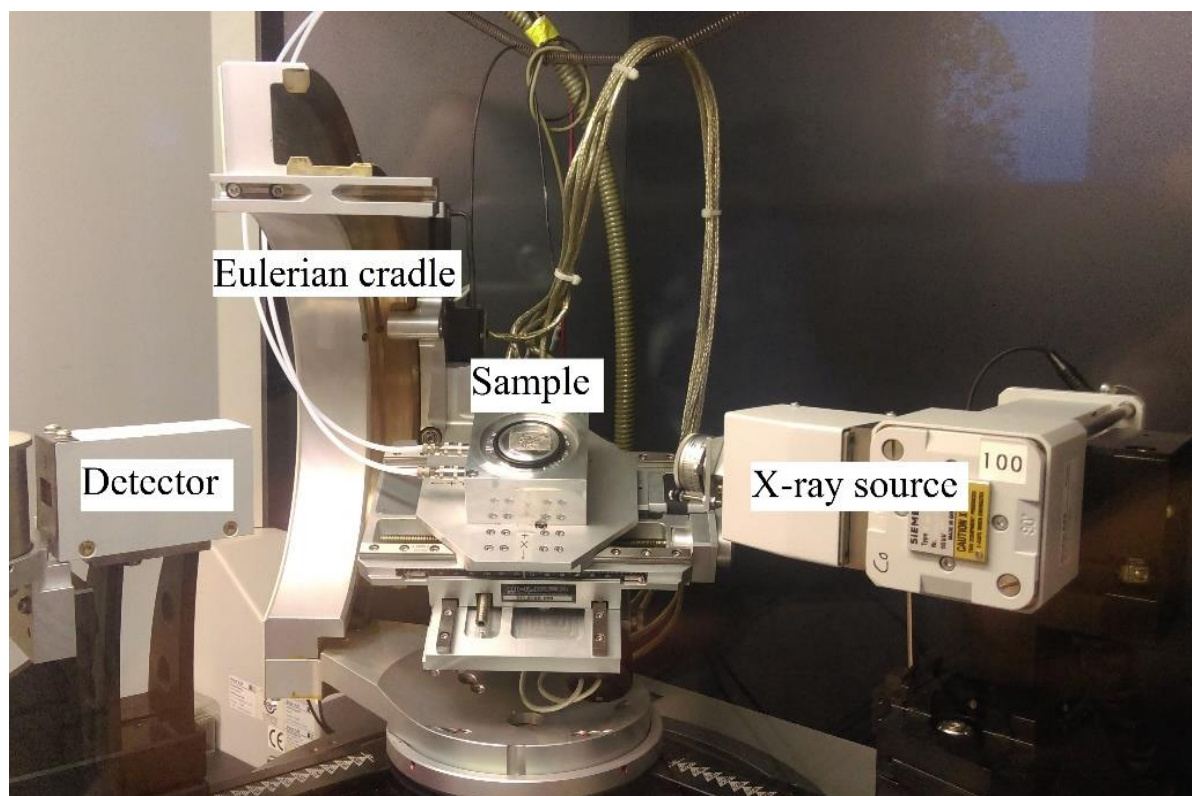


Figure 12(a). PSI-XRD diffractometer equipped with Eulerian cradle.

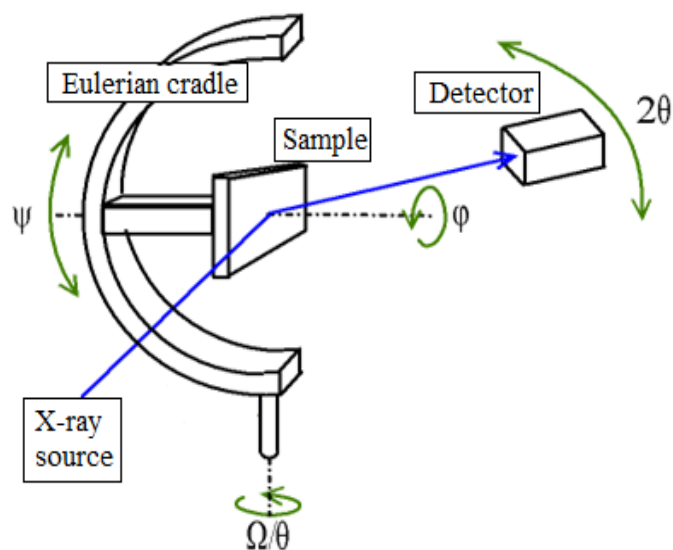


Figure 12(b). PSI-XRD equipped with Eulerian cradle of Parallel beam geometry.

Figure 12. Bruker-AXS-D8-Discover (PSI) XRD diffractometer equipped with Eulerian cradle of Parallel beam geometry.

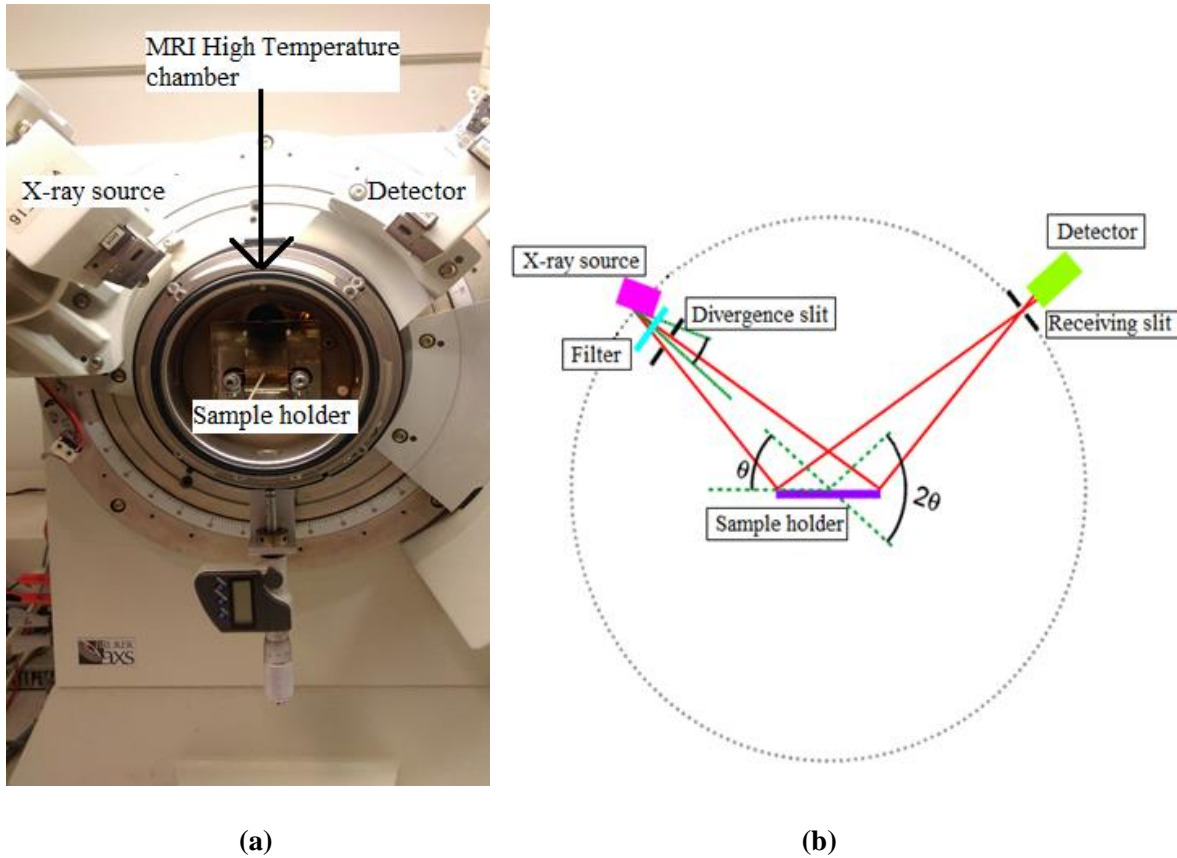


Figure 13. Bruker-AXS-D5005 [Theta-Theta (TT)] XRD diffractometer with Bragg-Brentano focusing geometry (a) TT-XRD machine (b) Bragg-Brentano focussing geometry [15].

Two XRD instruments were used for Pd and Ti thin film analysis in this thesis:

(i) Bruker-AXS-D5005 [Theta-Theta (TT)] diffractometer in Bragg-Brentano focusing geometry, equipped with a graphite monochromator in the diffracted beam of $\text{CuK}\alpha$ radiation of wavelength 0.554 nm as shown in Figure 13. The X-ray source was operated at the voltage of 45 kV and current of 30 mA. The divergence slit of 0.6 mm, anti-scatter slit of 0.6 mm and detector slit of 0.6 mm are used. The samples are fixed on a Pt heater strip in a MRI high temperature chamber. The variable slits (divergence slits) are used which will maintain the irradiated area constant for all theta angle measurements. The thin films prepared are then measured for the deposited film thickness by reflectivity measurements and the process of hydrogenation and dehydrogenation are also carried out in the XRD machine.

Thickness measurement:

The X-Ray Reflectivity (XRR) measurements for finding the thickness of the film deposited on the substrate can also be done with XRD [23]. The X-ray reflectance curves of intensity versus 2θ were obtained for the 2θ angle range starting from 0.2° to 5° for the samples during XRR measurements. Interference occurs between the X-rays reflected from the surface of the film and the substrate [23].

This interference results in the oscillations as seen in the reflectivity profile as shown in Figure 14 in Section 3.1.2. The oscillation depends on the film thickness and the thicker film, the shorter period of the oscillation.

Hydrogenation and De-Hydrogenation process:

The processes of hydrogen loading and de-loading in the Pd and Ti films deposited on oxidized Si (SiO₂/Si) substrate are carried out at room temperature and with the pressure of 10⁵ Pa (1 bar). The H₂-N₂ gas mixture (5 % H₂ and 95 % N₂) is used during the hydrogen loading (hydrogenation) process with the flow rate of 0.5 L/min and N₂ (100%) gas is used during hydrogen de-loading (De-hydrogenation) process with the flow rate of 0.5 L/min. The samples are loaded and the intensity versus 2 θ scans of {111} reflection were carried out for the 2 θ angle range starting from 37° to 42° during hydrogen loading and de-loading process. A stable α -Pd phase occurs at 2 θ angle of 40.12°. During hydrogenation of Pd film, α -Pd to β -PdH phase transition occurs resulting in the peak shift as described later in Section 4.2.1 [3, 4]. And during de-hydrogenation, the β phase of PdH is transformed back to a stable α -Pd phase. The hydrogen absorption and desorption time taken for the Pd and Ti films are also explained later in Section 4.2.1.

(ii) **Bruker-AXS-D8-Discover (PSI)** machine with parallel beam geometry, equipped with graphite monochromatic of CoK α radiation of wavelength 0.178 nm. The diffractometer is equipped with an Eulerian cradle that allows to rotate for 360° (ϕ) angles and also be tilted up to the maximum (ψ) angle of 90° as shown in Figure 12(a) and (b). The X-ray source was operated at the voltage of 45 kV and current of 25 mA. The specimen holder used is HP42. The texture and stress measurements of the thin films are carried out with this XRD machine.

Texture:

Measurement of texture - the non-random, or preferred, orientation of crystallites – involves measurement of the variations in intensity of a single Bragg reflection as the sample is both tilted (ψ) and rotated (ϕ) [20]. The thin film textures are fibre textures as the orientation of a certain lattice plane is parallel to the substrate plane. The result can be plotted as a ‘pole figure’, which is the map of the density of a specific crystal direction with respect to the sample reference frame. The contours in the pole figures indicate the intensity levels as a function of sample orientation as can be seen in Figure 10 of Section 4.1.2.

The Pd and Ti films deposited on the substrate were texture measured for {111} orientation. As Pd being f.c.c, the growth plane is {111} due to its high packing density and low surface energy [24]. The samples loaded are then tilted from 0° to 75° angle and also rotated 360° angle for {111} fibre texture measurements. The texture results obtained for the as-deposited Pd and Ti films can be seen in Section 4.1.2 and for Pd and Ti films after hydrogenation and dehydrogenation process in Section 4.2.2.

Stress:

Stress or strain commonly exist in thin films as a result of constraints imposed by the substrates. The intrinsic stress is due to the accumulating effect of the crystallographic flaws that are built into the coating during deposition. The absorption of hydrogen during hydrogenation process causes the films to expand resulting in stress.

The Psi-2 θ scans are carried out for {111} and {311} reflections for Pd and Ti films deposited on oxidized Si wafer substrate. The {311} reflection have the peak position at 2 θ angle of 99.4° for Pd and this reflection was chosen for analysis because the shifts in diffraction lines are more prominent due to stress at higher diffraction angles and also d-spacing is very small giving more sensitive values [8]. The sample tilt angle range was from 0° to 75°. The scans were done for the sample with 2 θ angle range of 44° to 50° for {111} reflection with rotation angle ϕ (Phi) of 90° and with 2 θ angle range of 95° to 104° for {311} reflection with ϕ angle of 35° to avoid the interference of single crystal Si.

The Psi-2 θ scans actually provides a measure of strain in the films, from which the stress can be deduced using $\sin^2\psi$ - method employing suitable X-ray elastic constants [26, 27]. All the data evaluation was done with the programs, Bruker EVA and PANalytical X'Pert Stress Plus [27]. The lattice spacing d_ψ was then calculated and plotted as a function of $\sin^2\psi$ to deduce in-plane stress in the Pd films. In-plane stress for the case of planar, rotationally symmetric biaxial state of stress ($\sigma_{11} = \sigma_{22} = \sigma$), was calculated from the following equation [8, 27]:

$$\varepsilon_\psi^{hkl} = \frac{d_\psi^{hkl} - d_0^{hkl}}{d_0^{hkl}}; \varepsilon_\psi^{hkl} = (2S_1^{hkl} + \frac{1}{2}S_2^{hkl} \sin^2\psi)\sigma$$

The residual stress analysis involving particular hkl reflections measures the lattice strain of particular reflection. This can be taken into account by using the so-called grain-interaction models that describe the distribution of stresses and strains over the crystallographically differently oriented crystallites in the specimen [27]. The available conventional grain interaction models in the X'Pert Stress Plus software are Reuss model, Voigt model and Hill Weighted average model. The different grain interaction models has different elastic constants which are used to convert the lattice strain obtained from the diffraction into the stress. Reuss model assumes each grain to have the same stress and Voigt model assumes each grain to have the same strain. The Hill weighted average model, which is the arithmetic average of x-ray and macroscopic elastic constants as calculated with the Reuss and the Voigt grain-interaction model [27], was selected for stress analysis in thin Pd and Ti films before and after hydrogen loading and de-loading process.

The available X'Pert Stress Plus software was suitable only for isotropic materials but the Pd and Ti films prepared are anisotropic. So the grain interaction models are incompatible with the non-linear

$\sin^2\psi$ - plots obtained for $\{111\}$ and $\{311\}$ reflections. Due to this, only $[111]$ oriented grains are chosen for stress calculation to obtain more accurate values (See discussion in section 4.1.4 and 4.2.4).

To overcome the limitation of the only use of isotropic calculations in X'Pert stress plus software, a newly introduced software called ISODEC was used for anisotropic materials [28]. ISODEC is a program for the calculation of diffraction elastic constants (DEC). DEC are used to convert lattice strain measured by diffraction into macroscopic stress [27]. It can also calculate stress from measured d-spacing and vice versa. In case of materials with preferred orientation DEC reads the crystallite orientation distribution function (ODF) for calculation of stress values. The selection of grain shape parameters can also be done with ISODEC software as the stress factors are sensitive to the grain shape. Due to no ODF obtained for different orientations and with many unknown parameters in ISODEC software, this software was no longer used in this thesis for stress calculations. The stress values were calculated by X'Pert stress plus software with the assumption that the material is isotropic as described in Sections 4.1.3 and 4.2.3.

EXPERIMENTAL PART

3.1. Optimization of sputtering parameters

The thin films of Titanium and Palladium are sputtered on the oxidized silicon wafer substrate. The sputtering was performed at room temperature in Volmer-Weber growth mode to achieve loose columnar morphology [27]. The sputtering parameters were chosen based on Thornton's Structure Zone Model (SZM) to develop a particular thin film growth structure [29, 31].

Structure Zone Model

Structure Zone Models (SZM) are used in characterizing microstructure evolution in pure elemental films [29]. The structural zone model by Thornton is shown in Figure 14. According to this model, the film surface structure is dominated by the substrate temperature (T). There are three main structure zones with boundary temperatures $T_1=0.3T_m$ and $T_2=0.5T_m$, where T_m (K) is the melting point of the film material [29, 30].

At relatively low temperatures ($T < T_1$, zone 1), the surface diffusion of ad-atoms is too weak to ensure the filling of the shadowed surface regions (self-shadowing effect). During the surface growth of thin films, the particles can approach the surface at oblique angles and be captured by higher surface points (hills) due to shadowing effect. This usually occurs at higher argon sputtering pressures. This leads to the formation of the characteristic well-defined columnar structure [29, 31].

The films deposited at higher temperatures ($T_1 < T < T_2$, zone 2) exhibit much larger columns with domed tops. The surface diffusion of ad-atoms becomes sufficient which leads to surface recrystallization under these conditions. The films deposited at $T > T_2$ (zone 3) consists of big grains with flat and faceted faces [31]. Also for different pressures, either compact structure at lower pressure or porous structures at higher pressures develops.

During the sputtering of Ti and Pd metal, the main parameters that are to be optimized are argon pressure, substrate temperature and the sputter time. A temperature of 303 K (30 °C) was maintained in the chamber during the sputtering process. The T/T_m (substrate temperature/melting temperature of the particular material) for Ti metal with its melting point temperature of 1668°C is 0.017. And for Pd metal with its melting temperature of 1555°C, the T/T_m is 0.019. According to Thornton's SZM for a low T/T_m of Pd and Ti material, Zone T of dense film growth structure results when sputtered at argon

pressures less than 0.67 Pa (5 mTorr) and Zone 1 of porous structure results when sputtered at argon pressures greater than 0.67 Pa as seen in Figure 14.

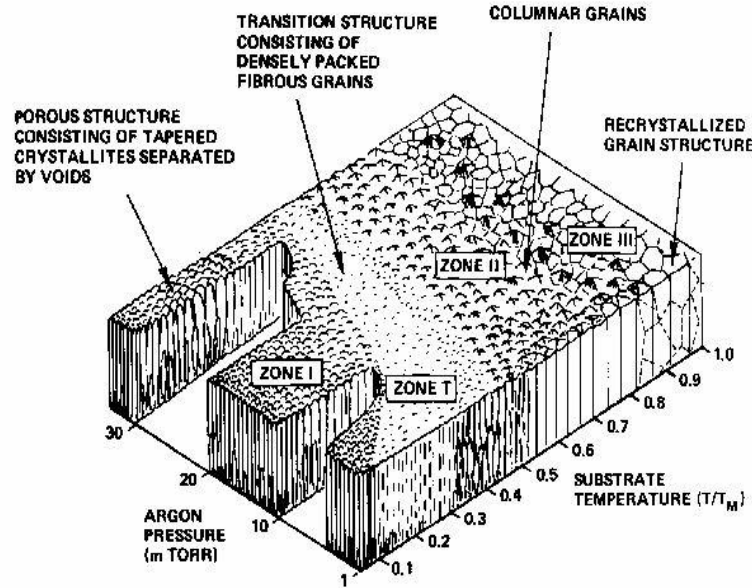


Figure 14. Structure Zone Model by Thornton [31].

3.1.1. Argon pressure optimization

According to Thornton's SZM, the Pd was sputtered only at 23 mTorr (3 Pa) to develop porous structures which will help in high diffusivity of H^+ through the Pd material [3]. And for Ti, an argon pressures of 3 mTorr (0.4 Pa) and 23 mTorr (3 Pa) was selected for sputtering to develop a different film growth structure of Ti and to study the influence of Ti on Pd membrane before and after hydrogenation and de-hydrogenation process.

3.1.2. Thickness optimization

The thickness of the Pd membrane without and with Ti as an intermediate layer deposited on the substrate should be optimized. In both cases of Pd layer without and with Ti intermediate layer, Pd was sputtered for 100 nm thickness at 3 Pa argon pressure. In this thesis for the Pd membrane with Ti as an intermediate layer, a very small Ti thickness of 1, 3 and 6 nm were considered to study its influence on Pd membrane. Thinner membranes are selected for both Pd and Ti because of its higher permeability [3].

To optimize Ti and Pd deposition thickness in sputtering, a different sputter times were used to obtain the required Ti thickness of 1, 3 and 6 nm and Pd of 100 nm thickness for the above specified argon

sputtering pressures. Both Si and oxidised Si (SiO_2/Si) wafer substrates are used for initial analysis of thickness optimization.

The thickness of Pd metal deposited was obtained from gravimetric method by weighing the oxidized Si substrate wafer before and after sputtering. An approximate Pd thickness value of 100 nm was obtained from the gravimetric method. With trial and error method, the sputter time to deposit Pd at 3 Pa for 100 nm thickness was found to be about 15 min (900 s). The sputtering rate of Pd obtained for 3 Pa argon pressure was 0.11 nm/s (sputter rate = thickness deposited/sputter time = 100 nm/900 s).

On the other hand for Ti, because of its very small deposition thickness, the thickness measurement were done by X-Ray Reflectometry (XRR). With X'Pert Reflectivity software, the reflectivity scans obtained from XRR are fitted along the fringes to obtain an approximate thickness as shown in Figure 15 [23].

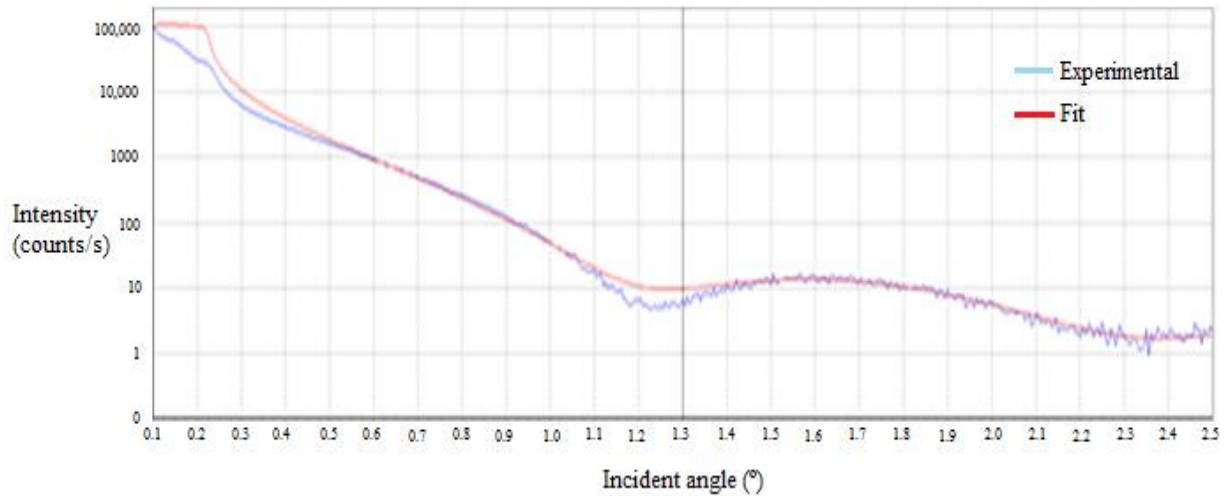


Figure 15. X'Pert Reflectivity thickness analysis of Ti sample sputtered for 180 s at 3 Pa argon pressure. The Ti thickness obtained from this fringe fitting method was 4 nm.

An approximate thickness obtained for Ti with corresponding sputter times are listed in Table 1. The thickness obtained from XRR are approximate values because the fringes fitted for the XRR thickness scans are not accurate as seen from the experimental and the fitted line shown in the Figure 15. With the trial and error method and also with the above XRR fitting method, the anticipated Ti of 1, 3 and 6 nm thickness for different sputter times were measured for Ti layer deposited on both Si and oxidized Si wafer substrates as shown in Table 1.

An optimized sputter timings to obtain the required Ti thickness of 1, 3 and 6 nm sputtered in case of 3 Pa (23 mTorr) argon pressure are 1, 3 and 6 minutes respectively. And for 0.4 Pa (3 mTorr) argon

3. Experimental Part

sputtering pressure, the optimized sputter times to obtain the required Ti thickness of 1, 3 and 6 nm are 12, 38, 70 seconds. The substrate inside the chamber rotates at 20 rpm. In case of 0.4 Pa for 1 nm Ti thickness, the substrate rotates only 4 times during its deposition time of 12 seconds. This less rotation of the substrate might lead to many areas of the substrate left un-deposited. So the sputter time was increased for deposition of 1 nm Ti at 0.4 Pa from 12 to 20 seconds. This increase in sputter time will increase the number of substrate rotation to 7 which enhance the deposition of the material by having enough time for the material to deposit over all areas of the substrate. The sputter time increase also resulted in an increase of an anticipated Ti thickness from 1 to 3 nm as seen in Table 1.

| Deposited film | Substrate | Argon Sputtering Pressure (Pa) | Sputter Time (s) | Anticipated Film Thickness (nm) | Approximate Film Thickness obtained from XRR (nm) |
|----------------|----------------------|--------------------------------|------------------|---------------------------------|---|
| Titanium | Si | 0.4 (3 mTorr) | 20 | 1 | 3.0 |
| | | | 38 | 3 | 4.4 |
| | | | 70 | 6 | 5.8 |
| | | 3 (23 mTorr) | 60 (1 min) | 1 | 0.2 |
| | | | 180 (3 min) | 3 | 4.0 |
| | | | 360 (6 min) | 6 | 6.5 |
| | SiO ₂ /Si | 0.4 (3 mTorr) | 20 | 1 | 3.0 |
| | | | 38 | 3 | 4.3 |
| | | | 70 | 6 | 6.0 |
| | | 3 (23 mTorr) | 60 (1 min) | 1 | 1.0 |
| | | | 180 (3 min) | 3 | 3.8 |
| | | | 360 (6 min) | 6 | 6.4 |

Table 1. Approximate Ti thickness obtained by XRR for different sputter times and argon pressures deposited on both Si and oxidized Si wafer substrates.

The sputtering rate of Ti obtained for 3 Pa argon pressure was 0.0167 nm/s (rate = thickness deposited/sputter time = 1 nm/60 s). And the sputtering rate of Ti at 0.4 Pa argon pressure was 0.08 nm/s (rate = 3 nm/38 s).

3.2. Film preparation

With the obtained optimized sputtering parameters, initially the intermediate layer of Ti was deposited on both Si and oxidized Si wafer substrate for the corresponding Ti thickness and argon sputtering pressures as shown in Table 1. The Ti only deposited films are analysed with AFM for the deposition and the growth behaviour of Ti films on different substrates and at different argon sputtering pressures. But only oxidized Si wafer substrates were used for further analysis by depositing Pd film over intermediate Ti layer which was deposited on SiO₂/Si substrate. The reason for the selection of an oxidized Si (SiO₂/Si) substrate was due to the presence of an oxide layer which acts as a diffusion barrier eliminating the silicide formation between the Si wafer and the metal interface in case of Si substrate. Another reason could be due to the higher surface roughness resulted for Ti film deposited on Si substrate [32] as explained later in Section 4.1.4.

The Pd layer was sputtered for 100 nm thickness at 3 Pa argon pressure on oxidized Si substrate without Ti intermediate layer (Pd/SiO₂/Si) for an expected porous structure according to Thornton's SZM [29]. The Pd film without Ti layer (Pd/SiO₂/Si) was analysed and compared with the 100 nm thick Pd film (3 Pa) deposited over different thickness of Ti intermediate layer on oxidized Si substrate (Pd/Ti/SiO₂/Si). In Pd/Ti/SiO₂/Si films, the Ti intermediate layer was sputtered for two extreme thickness of 3.0 and 6.0 nm in case of 0.4 Pa and 1.0 and 6.4 nm in case of 3 Pa as shown in Table 1. The two extreme thickness of Ti was chosen to show the influence of Ti thickness and its corresponding film growth on Pd layer in Pd/Ti/SiO₂/Si films.

Thus four Pd/Ti/SiO₂/Si (Pd/Ti) films were prepared with Ti sputtered for different thickness and at different argon pressures which will result in an expected compact and porous structures of Ti according to Thornton's SZM [29] as listed below:

1. Ti – 0.4 Pa (3 mTorr) – 3 nm – compact structure
2. Ti – 0.4 Pa (3 mTorr) – 6nm – compact structure
3. Ti – 3 Pa (23 mTorr) – 1 nm – porous structure
4. Ti – 3 Pa (23 mTorr) – 6 nm – porous structure

The Pd was sputtered at 3 Pa (23 mTorr) argon pressure for 100 nm thickness for an expected porous structure according to Thornton's SZM for all Pd/Ti samples over Ti intermediate layer. After sputtering, the Pd/Ti samples were analysed with different characterization techniques to study about the Ti and Pd film growth on oxidized Si substrates at different argon pressures.

3.3. Quantification of Texture

The Pd and Ti films deposited on oxidized Si (SiO_2/Si) wafer substrate were texture measured for $\{111\}$ orientation. The corresponding pole figure obtained shown in Section 4.1.2 and 4.2.2 are quantified in terms of random crystallite orientation. The crystallite (grain) orientations obtained are expressed with respect to a specimen with a random crystallite orientation as follows: the values for a random crystallite orientation is obtained by averaging the total measured intensity over all measured volume elements ($\Delta\phi, \Delta\psi$) of the pole figure (Figures 22, 23, 24, 38, 39 and 40). The actually measured values are then compared to this random value. A 4 times random texture means that the measured maximum value is 4 times the value expected in the case of a specimen with a random crystallite orientation. The maximum pole density obtained for the respective Pd/Ti films before and after hydrogenation are shown in Tables 6 and 11.

RESULTS AND DISCUSSION

The as-deposited Pd film with and without Ti intermediate layer deposited are analysed and explained in Section 4.1. The hydrogenation and de-hydrogenation processes are carried out in the as-deposited films and the results obtained are analysed and explained in Section 4.2.

4.1. BEFORE HYDROGENATION

The Pd layer without and with Ti intermediate layer were analysed by different characterization techniques and the results obtained are described in this section. Initially the RMS roughness values were measured for both Pd film with and without Ti intermediate layer with help of AFM as explained in Section 4.1.1. Then the texture and stress measurements for Pd/SiO₂/Si and Pd/Ti films were carried out with XRD and the results obtained are shown in Sections 4.1.2 and 4.1.3 respectively. The obtained results of surface roughness, texture and stress of Pd/SiO₂/Si and Pd/Ti films were discussed and the influence of Ti on Pd/Ti films were deduced in Section 4.1.4.

4.1.1. RMS Surface Roughness by AFM

In this section the surface roughness of the films deposited on the respective Si and SiO₂/Si substrates were measured. The RMS roughness of the substrates used were measured and the results are shown in Section 4.1.1.1. The intermediate layer Ti was sputtered at different argon pressures and for different thickness as shown in Table 1 over both Si and SiO₂/Si substrates and the corresponding RMS surface roughness results obtained were listed in Section 4.1.1.2. The 100 nm thick Pd layer was then sputtered over Ti intermediate layer deposited on SiO₂/Si substrate and the roughness of the four Pd/Ti films prepared as described in Section 3.2 were measured and the results are shown in Section 4.1.1.3. The roughness of 100 nm thick Pd film sputtered over SiO₂/Si substrate without Ti intermediate layer were measured and shown in Section 4.1.1.4. The obtained AFM images for Pd film with and without Ti intermediate layer were then analysed by Gwyddion software and the corresponding film deposition and the effect of Ti intermediate layer on Pd layer in Pd/Ti films were explained in Sections 4.1.2 and 4.1.3. The results obtained are discussed later in Section 4.1.4.

4.1.1.1. Substrate roughness

The silicon (Si) wafer was initially selected as a substrate for depositing Ti and Pd films. But the roughness for the Si substrate could not be measured due to its very low roughness which was below the detection limit of the available AFM instrument. For the oxidized Si wafer (SiO₂/Si), the RMS

4. Results and Discussion

roughness measured was about 0.253 nm. This roughness was due to the presence of an oxide layer of 188 nm over Si layer.

4.1.1.2. Ti intermediate layer on Si and SiO₂/Si substrates

The Ti film was sputtered on both Si and SiO₂/Si substrates at two argon pressures of 0.4 Pa and 3 Pa for different Ti thickness as mentioned earlier in Table 1 of Section 3.1.2. The RMS roughness were measured for three different scan size areas of 1 μm x 1 μm , 3 μm x 3 μm and 10 μm x 10 μm for a Ti deposited film and the values obtained are shown in Table 2.

| Deposited film | Argon Sputtering Pressure (Pa) | Substrate | Film Thickness (nm) | RMS Roughness (nm) | | |
|----------------|--------------------------------|----------------------|---------------------|--------------------------------------|--------------------------------------|--|
| | | | | Scan Size | | |
| | | | | 1 x 1 (μm) ² | 3 x 3 (μm) ² | 10 x 10 (μm) ² |
| Titanium | 0.4 (3 mTorr) | Si | 3.0 | 0.22 | 0.34 | 0.49 |
| | | | 4.4 | 0.33 | 0.40 | 0.64 |
| | | | 5.8 | 0.3 | N.A. | N.A. |
| | | SiO ₂ /Si | 3.0 | 0.24 | 0.26 | 0.21 |
| | | | 4.3 | 0.23 | 0.26 | 0.30 |
| | | | 6.0 | N.A. | 0.27 | N.A. |
| | 3 (23 mTorr) | Si | 0.2 | 0.30 | 0.52 | 0.72 |
| | | | 4.0 | 0.41 | N.A. | N.A. |
| | | | 6.5 | 0.23 | 0.39 | 0.43 |
| | | SiO ₂ /Si | 1.0 | 0.15 | 0.17 | 0.22 |
| | | | 3.8 | N.A. | 0.26 | N.A. |
| | | | 6.4 | 0.21 | 0.21 | 0.32 |

N.A. - No AFM scans were done for that respective scan size areas.

Table 2. RMS Roughness values of Ti deposited films on both Si and oxidized Si wafer substrates at two argon sputtering pressures.

The average RMS roughness values for a particular Ti deposited film were calculated with an error bars shown in Table 3 from the RMS roughness values obtained for different scan size areas as shown in Table 2 for that particular Ti deposited film. An average RMS roughness values obtained for Ti films deposited on Si and SiO₂/Si substrates are shown in Figures 16 and 17 respectively for different Ti thickness and argon pressures.

| Deposited film | Argon Sputtering Pressure (Pa) | Substrate | Film Thickness (nm) | Average RMS surface roughness value (nm) |
|----------------|--------------------------------|----------------------|---------------------|--|
| Titanium | 0.4 (3 mTorr) | Si | 3.0 | 0.348 ± 0.13 |
| | | | 4.4 | 0.457 ± 0.13 |
| | | | 5.8 | 0.300 ± 0.00 |
| | | SiO ₂ /Si | 3.0 | 0.234 ± 0.02 |
| | | | 4.3 | 0.259 ± 0.03 |
| | | | 6.0 | 0.269 ± 0.00 |
| | 3 (23 mTorr) | Si | 0.2 | 0.515 ± 0.21 |
| | | | 4.0 | 0.414 ± 0.00 |
| | | | 6.5 | 0.347 ± 0.08 |
| | | SiO ₂ /Si | 1.0 | 0.178 ± 0.03 |
| | | | 3.8 | 0.261 ± 0.00 |
| | | | 6.4 | 0.246 ± 0.04 |

Table 3. Average RMS Roughness values of Ti only deposited films on both Si and oxidized Si wafer substrates at two argon sputtering pressures.

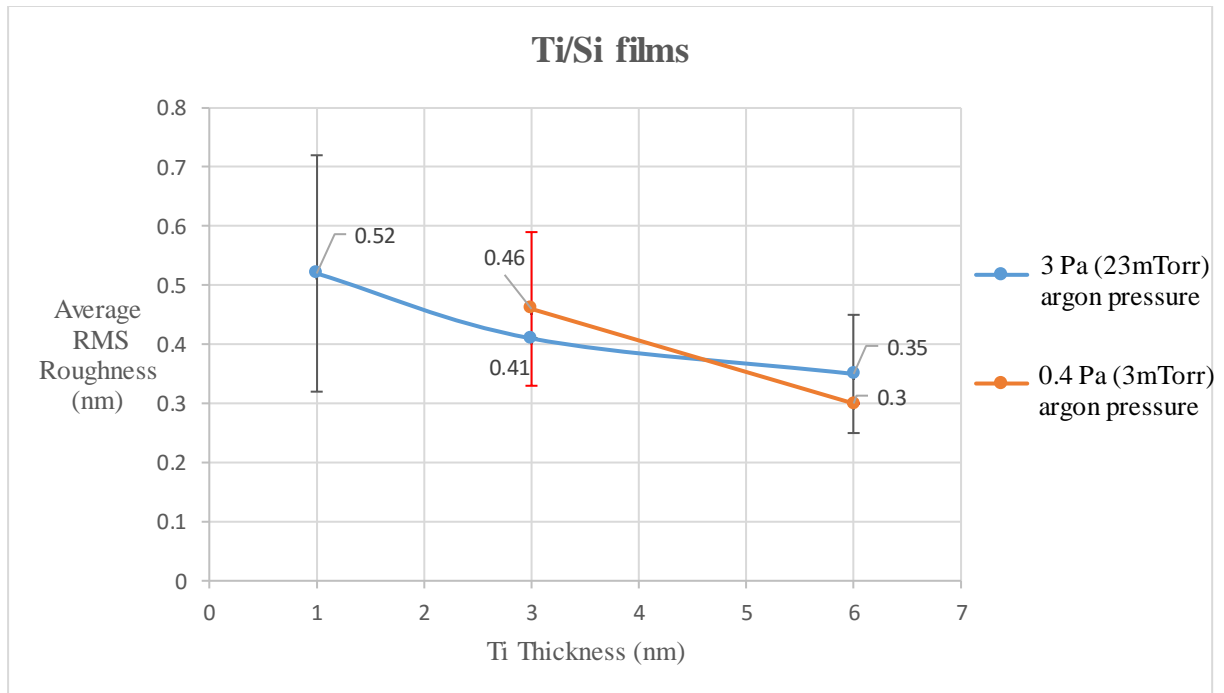


Figure 16. Average RMS Roughness of Ti deposited on Si substrate for different thickness and argon sputtering pressures.

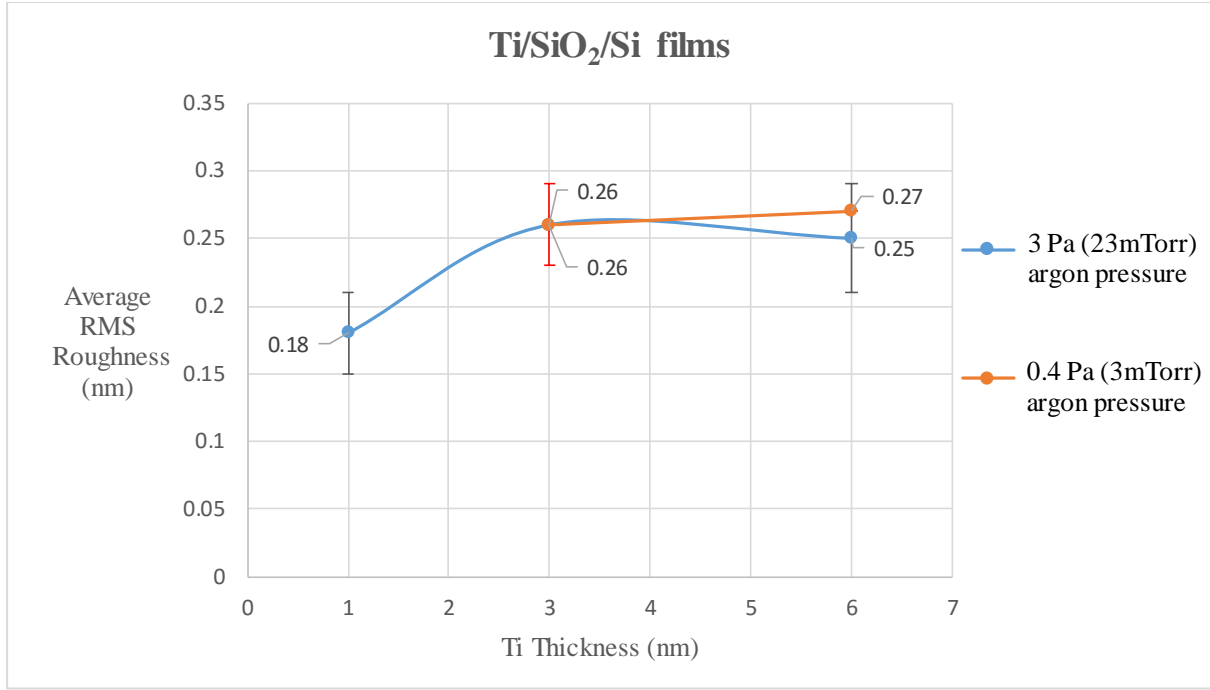


Figure 17. Average RMS Roughness of Ti deposited on oxidized Si substrate for different thickness and argon sputtering pressures.

The average RMS surface roughness obtained is same for the bare SiO₂/Si substrate and the Ti/SiO₂/Si films with an approximate value of 0.253 nm. Thus depositing Ti intermediate layer results in no change of surface roughness on SiO₂/Si substrate. The lower roughness of Ti films on SiO₂/Si substrate was due to the presence of 188 nm oxide layer on Si substrate. The incoming Ti atoms diffuse easily on an oxide layer and results in a uniform spreading of the deposited film on substrate surface as seen from the AFM image shown in Figure 18(b) [35]. As the Ti has a higher affinity for oxygen, a very good bonding results between Ti and SiO₂/Si substrate. This bonding serves Ti a good adhesion material between the Pd layer and SiO₂/Si substrate in Pd/Ti film [34].

Depositing Ti on Si substrate increases surface roughness as seen in Figure 16. The higher roughness of Ti film on Si substrate could be due to the metal-metal interaction of Ti and Si. The Ti-Si bond restricts the diffusion of incoming Ti atoms on Si substrate [34]. This bond resulted in the incoming Ti atoms sticking to the place where it strikes on Si substrate and also due to shadowing effect, large Ti islands are formed [29, 34]. This can be seen in AFM image shown in Figure 18(a) for 1 nm Ti deposited at 3 Pa, where the large white spots indicates a large Ti islands deposited on Si substrate.

Due to the similarity in roughness results of SiO₂/Si and Ti/SiO₂/Si substrates and also due to the lower surface roughness resulted for Ti/SiO₂/Si films than Ti/Si films, SiO₂/Si substrate was chosen for the further analysis of Ti/SiO₂/Si and Pd/Ti/SiO₂/Si films. The surface roughness will increase with increase in thickness of films [10, 29].

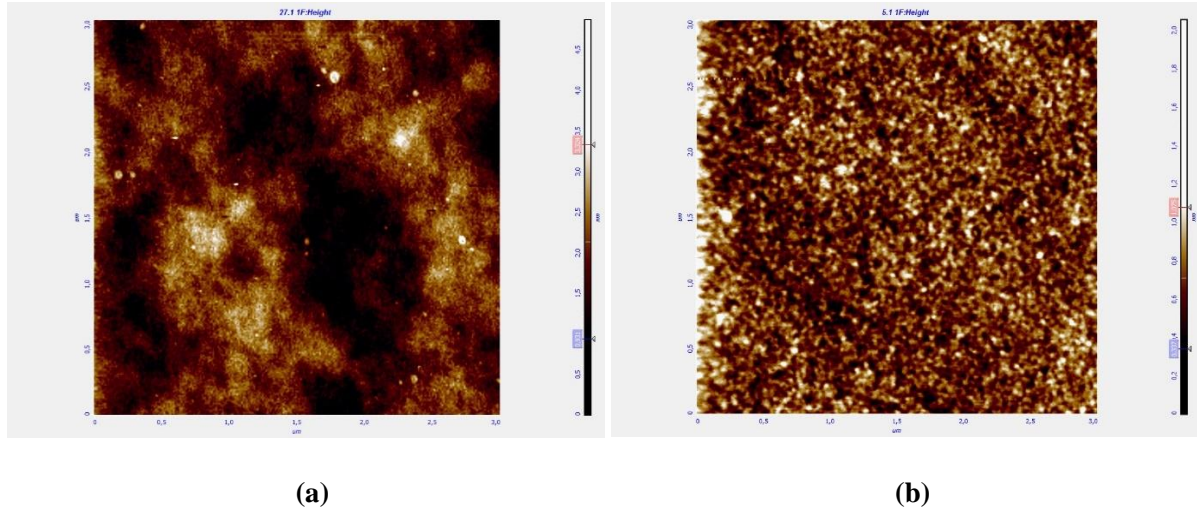


Figure 18. AFM images of 1 nm thick intermediate layer Ti deposited at 3 Pa on (a) Si substrate and (b) SiO₂/Si substrate. The white spots are the deposited Ti film and the dark regions are the respective substrate. The scan size area for both images is 3 μm x 3 μm.

The AFM images obtained for Ti deposited films on SiO₂/Si substrate were analysed with Gwyddion software as explained earlier in Section 2.3 [16]. The skewness, kurtosis and the mean spacing parameters obtained from the line scan profile for the AFM images of 3 μm x 3 μm scan size area for the Ti intermediate layer deposited on oxidized Si substrate (Ti/SiO₂/Si) are listed in Table 4.

| Deposited film | Argon Sputtering Pressure (Pa) | Film Thickness (nm) | RMS Roughness (nm) | Skewness | Kurtosis | Mean Spacing (nm) |
|----------------|--------------------------------|---------------------|--------------------|----------|----------|-------------------|
| | | | 3 μm x 3 μm | | | |
| Ti | 0.4 (3mTorr) | 3.0 | 0.26 | 0.06 | 0.03 | 55 |
| | | 4.3 | 0.26 | 0.15 | 0.11 | 60 |
| | | 6.0 | 0.27 | 0.10 | 0.09 | 90 |
| | 3 (23mTorr) | 1.0 | 0.17 | 0.18 | 0.56 | 130 |
| | | 3.8 | 0.26 | 0.12 | 0.13 | 85 |
| | | 6.4 | 0.21 | 0.44 | 0.90 | 110 |

Table 4. Roughness parameters for Ti intermediate layer deposited on SiO₂/Si substrate.

4. Results and Discussion

Based on the obtained values of different roughness parameters shown in Table 4, an approximate top surface profile of Ti intermediate layer deposited at two different argon pressures on an oxidized Si (SiO_2/Si) substrate is shown in Table 5. The top surface roughness profile obtained for Ti intermediate layer shows the deposition and the growth structure of Ti films on SiO_2/Si substrate.

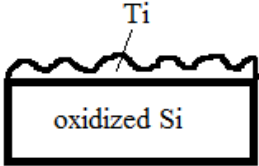
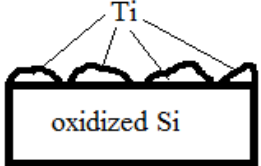
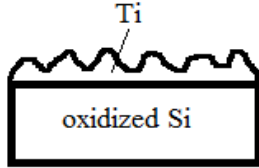
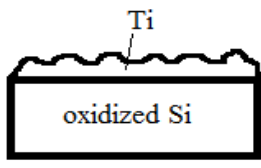
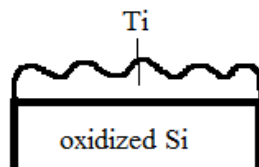
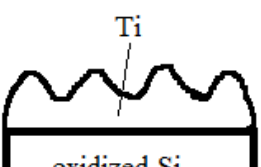
| Ti argon sputtering pressure | | | |
|------------------------------|---|-------------------|---|
| 0.4 Pa | | 3 Pa | |
| Ti Thickness (nm) | Ti surface profile | Ti Thickness (nm) | Ti surface profile |
| 3.0 |  | 1.0 |  |
| 4.3 |  | 3.8 |  |
| 6.0 |  | 6.4 |  |

Table 5. Approximate thin film growth schematic diagrams for Ti intermediate layer deposited on oxidized Si substrate.

Table 5 shows that for 1 nm Ti film deposited at 3 Pa argon pressure, an island formation results [31, 35]. The lower RMS surface roughness and the large mean spacing of 130 nm as shown in Table 4 for 1 nm Ti layer at 3 Pa on SiO_2/Si substrate indicates a large Ti islands were formed as seen from the large white spots shown in Figure 19(b). Deposition of Ti films at higher argon pressures of 3 Pa results in low mobility of the incoming sputtered Ti atoms on the substrate surface and also a little diffusion of Ti was resulted due to the presence of an oxide layer in SiO_2/Si substrate. The collisions between the

sputtered Ti atoms and the argon atoms at elevated pressures of 3 Pa makes the Ti atoms to arrive at the substrate in a randomized directions which promote shadowing leading to the open structures according to Thornton's SZM [36]. Due to this shadowing effect and the low mobility of Ti atoms, the initially deposited Ti film does not spread uniformly but sticks to the place where it strikes on SiO₂/Si substrate forming large islands [35]. The shadowing effect also results in spiky islands which reflected in the higher kurtosis value obtained for Ti films deposited at 3 Pa compared to the values obtained for 0.4 Pa argon pressure as shown in Table 4. The skewness with near zero values indicates a random top surface with both peaks and valleys are equally dominant for all Ti/SiO₂/Si films deposited at 3 Pa [18, 37].

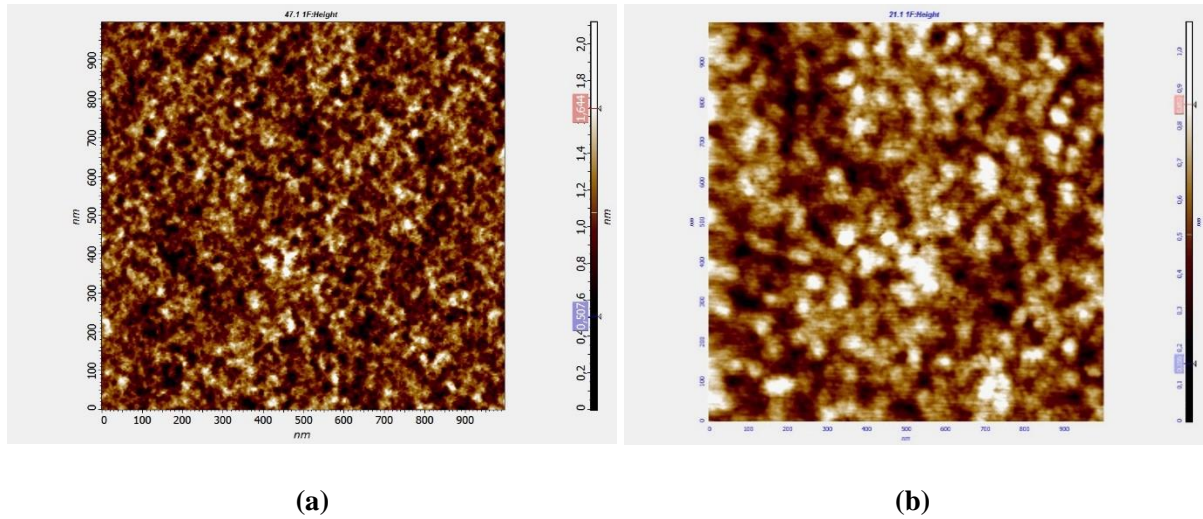


Figure 19. AFM images of Ti intermediate layer deposited on SiO₂/Si substrate at argon pressures of (a) 0.4 Pa (3 nm Ti thickness) and (b) 3 Pa (1 nm Ti thickness). The white spots represents the Ti film and the dark regions corresponds to the substrate. The scan size area of both images is 1 μm x 1 μm.

The Ti intermediate layer deposited on SiO₂/Si substrate at 0.4 Pa results in the formation of smaller Ti islands for an initial Ti film deposition as shown in Figure 19(a). The smaller Ti islands was due to the higher mobility of incoming sputter Ti atoms at lower argon pressures and the diffusion of Ti atoms on the substrate due to the presence of an oxide layer on SiO₂/Si substrate. The higher mobility and diffusion makes the Ti atoms to spread uniformly and easily reach the lower surface energy areas on the SiO₂/Si substrate [35]. The smaller Ti islands formed can also be proved by the lower mean spacing values obtained for Ti films sputtered at 0.4 Pa argon pressure as shown in Table 4, when compared to Ti films deposited at 3 Pa. The uniform spread and diffusion of Ti results in the development of uneven Ti surface atoms as the kurtosis value obtained was lower. The near zero values for skewness shown in Table 4 for Ti films deposited at 0.4 Pa indicates an equally dominant peaks and valleys in the Ti top surface profile.

4. Results and Discussion

An increase in Ti thickness deposition at both argon pressures results in the growth of a uniform Ti layer on SiO₂/Si substrate as seen from the thin film growth schematic diagrams shown in Table 5. The growth of pure polycrystalline films will follow the process of nucleation and island growth to the impingement and coalescence of islands. The formation of polycrystalline islands and channels leading to the development of a uniform layer of film growth [31]. The deposition of Ti intermediate layer at 3 Pa on SiO₂/Si substrate results in the accumulation of large Ti islands for initial 1 nm Ti deposition as shown by the large white spots in Figure 20(a), which matched well with the obtained large mean spacing roughness parameter shown in Tables 4 and 5. An increase in Ti thickness deposition results in the initially deposited large Ti islands to spread uniformly due to the coalescence of islands as seen from the white spots in Figure 20(b) for 6.4 nm Ti thickness AFM image. The dark regions of the AFM image in Figure 20(b) represents the uniform Ti layer due to higher Ti thickness of 6.4 nm but in Figure 20(a), the dark regions corresponds to SiO₂/Si substrate due to the very small Ti thickness of 1 nm.

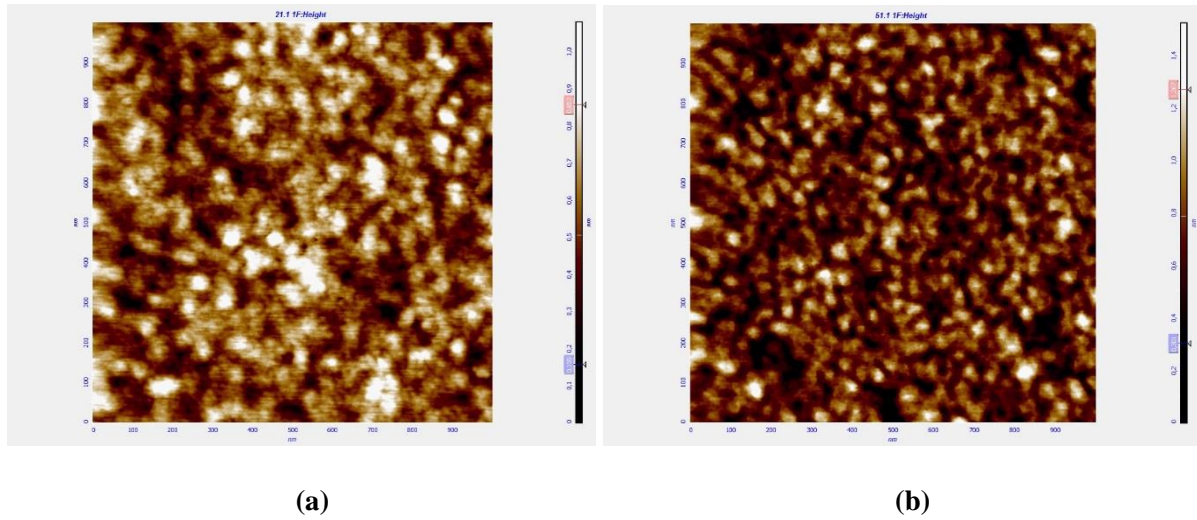


Figure 20. AFM images of Ti intermediate layer deposited on SiO₂/Si substrate at 3 Pa for (a) 1.0 nm Ti thickness and (b) 6.4 nm Ti thickness. The white spots represents the Ti film and the dark regions corresponds to the (a) substrate and (b) Ti film. The scan size area of both images is 1 μm x 1 μm .

The average RMS surface roughness values were similar for Ti films of same thickness deposited on SiO₂/Si substrate for different argon sputtering pressures as seen in Figure 17. Also Figure 17 shows that the average RMS roughness increases with an increase in Ti thickness deposition on SiO₂/Si substrate.

4.1.1.3. Pd film with Ti intermediate layer (Pd/Ti/SiO₂/Si)

The 100 nm thick Pd film deposited at 3 Pa on Ti intermediate layer of different thickness was measured for surface roughness and the results are shown in Table 4. The two extreme thickness of Ti were chosen

from Table 4 to show the influence of thickness and its corresponding film growth on Pd layer of Pd/Ti/SiO₂/Si (Pd/Ti) films at different argon pressures. The Ti layer thickness of 3.0 and 6.0 nm were chosen for 0.4 Pa argon sputtering pressure and for 3 Pa argon pressure, 1.0 and 6.4 nm Ti thickness were chosen as explained earlier in Section 3.2. The RMS roughness were measured at three different scan size areas of 1 μm x 1 μm , 3 μm x 3 μm and 10 μm x 10 μm for a particular Pd/Ti film.

The average RMS roughness values were calculated from the obtained roughness values for different scan size areas and are shown in Table 6. The average RMS roughness value obtained for Pd/Ti films are shown in Figure 21 for different Ti thickness and argon pressures. An increase in roughness was resulted for an increase in Ti thickness deposition of Pd/Ti films. The roughness of Pd/Ti films are similar at particular Ti thickness irrespective of the Ti argon sputtering pressure. Thus the influence of Ti argon pressures on Pd/Ti film surface roughness was negligible.

| Deposited films | Ti Argon Sputtering Pressure (Pa) | Ti Film Thickness (nm) | RMS Roughness (nm) | | | Average RMS surface roughness value (nm) |
|--------------------|---|---------------------------------|----------------------------|----------------------------|------------------------------|--|
| | | | Scan Size | | | |
| | | | 1 x 1 (μm) ² | 3 x 3 (μm) ² | 10 x 10 (μm) ² | |
| Pd/Ti | 0.4 (3 mTorr) | 3.0 | 3.61 | 3.51 | 3.92 | 3.68 ± 0.17 |
| | | 6.0 | 4.68 | 4.78 | 4.79 | 4.75 ± 0.04 |
| | 3 (23 mTorr) | 1.0 | 3.12 | 3.03 | 2.94 | 3.03 ± 0.09 |
| | | 6.4 | 4.73 | 4.49 | 5.3 | 4.84 ± 0.35 |

Table 6. RMS surface Roughness of Pd/Ti/SiO₂/Si samples.

The average RMS roughness values obtained for Pd/Ti films as shown in Figure 21 was higher than Ti/SiO₂/Si films (Figure 17). An increase in roughness of approximately 3 to 4 nm were observed for Pd/Ti films when compared to Ti/SiO₂/Si films. The higher roughness for Pd/Ti films was due to its higher film thickness of both Pd and Ti intermediate layer than the smaller thickness of only Ti layer in Ti/SiO₂/Si films [10, 29]. Similar to Ti/SiO₂/Si films, an increase in Ti thickness of Pd/Ti films also resulted in an increase of RMS surface roughness as seen in Figure 21 where a steady linear increase in roughness was observed at both argon sputtering pressures.

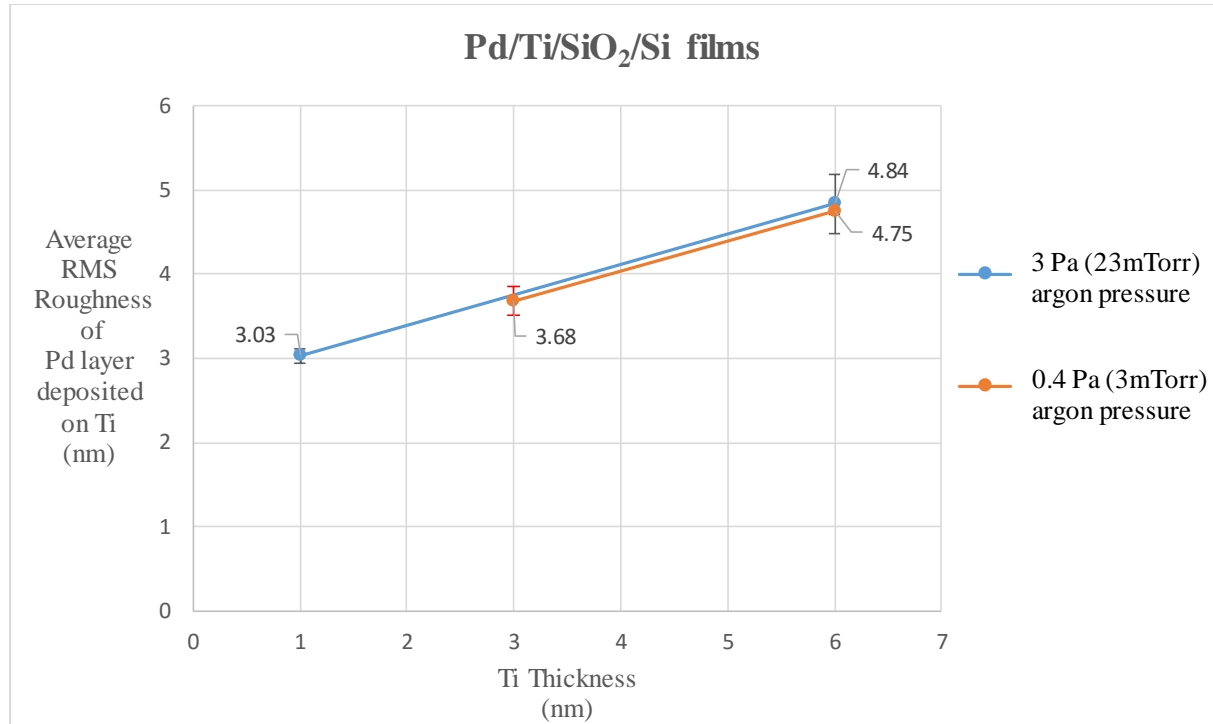


Figure 21. Average RMS Roughness of Pd deposited on Ti of various thickness and argon pressures.

The AFM images shown in Table A.4 (Appendix A) also shows a similar Pd top surface structure for all Pd/Ti films with the mean spacing of about 60 nm. This also proves that the influence of Ti argon pressure was negligible for top Pd surface structure in Pd/Ti films.

4.1.1.4. Pd film without Ti intermediate layer (Pd/SiO₂/Si)

The 100 nm Pd film deposited on SiO₂/Si substrate at 3 Pa argon pressure was measured for RMS surface roughness with AFM. The RMS roughness values obtained for different scan size areas and its average roughness are shown in Table 7.

| Deposited film | Argon Sputtering Pressure (Pa) | Substrate | RMS Roughness (nm) | | | Average RMS surface roughness value (nm) |
|----------------|---------------------------------------|----------------------|-------------------------|-------------------------|---------------------------|--|
| | | | Scan Size | | | |
| | | | 1 x 1 (μm) ² | 3 x 3 (μm) ² | 10 x 10 (μm) ² | |
| Pd | 3 (23 mTorr) | SiO ₂ /Si | 5.39 | 6.21 | 6.61 | 6.07 ± 0.50 |

Table 7. RMS surface roughness of Pd film without Ti intermediate layer.

The RMS roughness of Pd/SiO₂/Si was approximately 6 nm and introducing Ti as an intermediate layer reduces the roughness by 2 nm for Pd/Ti films as seen in Tables 6 and 7.

4.1.2. Texture results

The texture of Pd/SiO₂/Si and Pd/Ti/SiO₂/Si films were measured for the {111} reflection, the type of texture is the result of the XRD as explained earlier in Section 2.4. The {111} fibre texture results obtained are shown in Table 8. A weak texture pole figure obtained for Pd/SiO₂/Si film is shown in Figure 22. And an example of both weak and strong textures obtained for Pd/Ti/SiO₂/Si films are shown in Figures 23 and 24 respectively.

The weak {111} texture of Pd/SiO₂/Si and Pd/Ti/SiO₂/Si films was due to the deposition of Pd and Ti intermediate layer at higher argon pressure of 3 Pa developing porous structure according to Thornton's SZM [29]. The less mobility of the sputtered Ti and Pd atoms on the substrate surface while deposition and also due to the shadowing effect at higher argon pressures, the sputtered atoms cannot reach the lower surface energy area resulting in a weak texture development. But for Pd/Ti/SiO₂/Si film with 1 nm Ti sputtered at 3 Pa argon pressure shows a strong {111} texture despite an expected weak texture. This anomalous texture behaviour of Pd/Ti film 1 nm Ti deposited at 3 Pa is explained later in Section 4.1.4.

For Pd/Ti/SiO₂/Si films, with Ti layer deposited at 0.4 Pa and Pd layer at 3 Pa argon pressure resulted in a strong {111} texture. The low argon pressure deposition of Ti results in the high mobility of incoming sputtered atoms as the atoms can easily reach the lower surface energy area. This well-developed Ti film resulted in influencing the Pd film developing strong {111} texture of Pd/Ti films. Thus Ti sputtered at low argon pressures influences the Pd layer sputtered at 3 Pa over Ti developing a strong texture despite the development of weak texture Pd for 3 Pa argon sputtering pressure.

| Deposited films | Ti argon Sputtering Pressure (Pa) | Ti thickness (nm) | {111} Texture | Maximum Pole density of {111} texture |
|----------------------------|-----------------------------------|-------------------|---------------|---------------------------------------|
| Pd/SiO ₂ /Si | N.A. | N.A. | Weak | 1.91 |
| Pd/Ti/SiO ₂ /Si | 0.4 (3 mTorr) | 3.0 | Strong | 58.41 |
| | | 6.0 | Strong | 26.62 |
| | 3 (23 mTorr) | 1.0 | Strong | 21.99 |
| | | 6.4 | Weak | 1.56 |

Table 8. Texture results of Pd/SiO₂/Si and Pd/Ti/SiO₂/Si films.

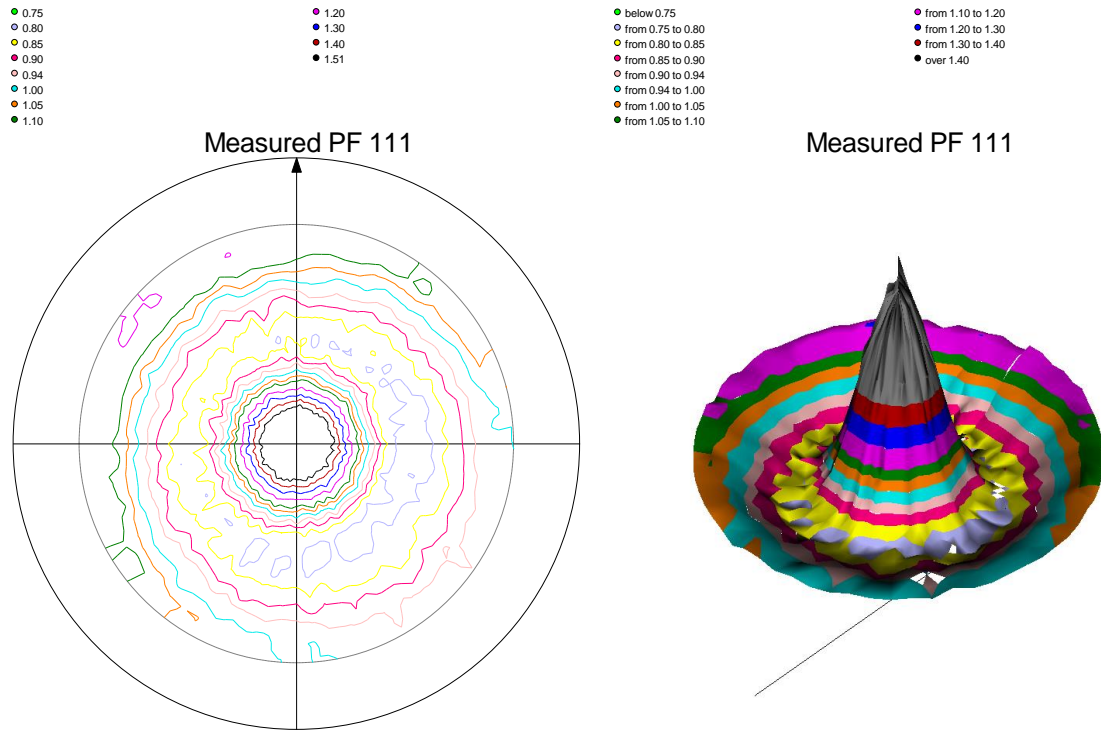


Figure 22. Weak {111} fibre texture pole figure of Pd/SiO₂/Si film.

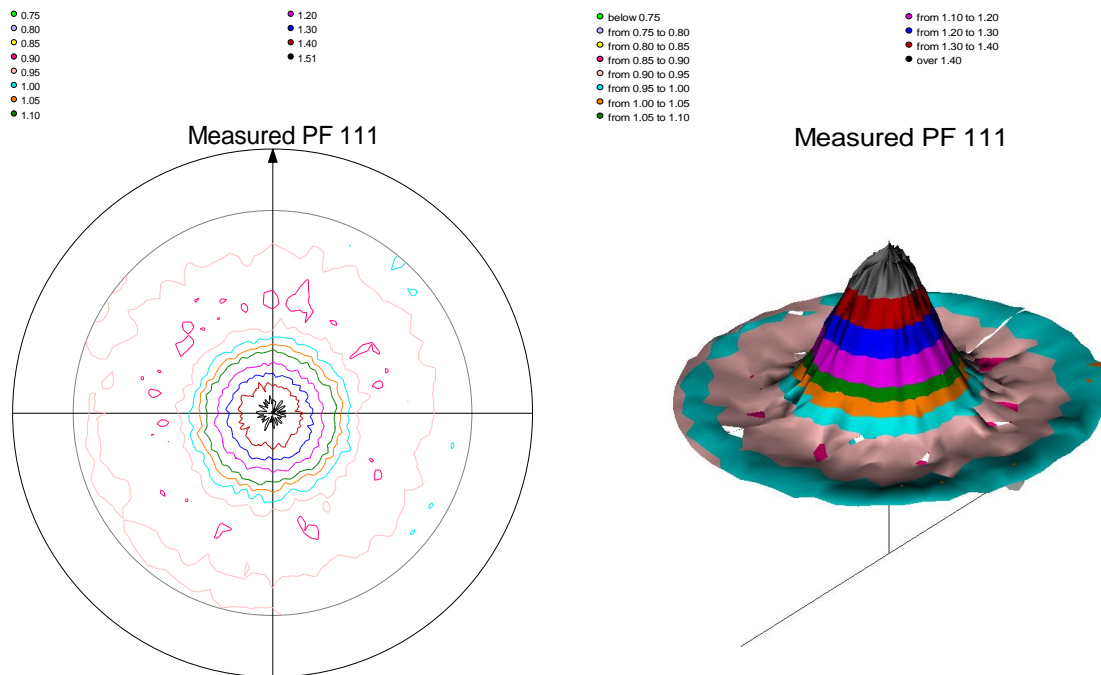


Figure 23. Weak {111} fibre texture pole figure for 6 nm Ti intermediate layer deposited at 3 Pa argon pressure of Pd/Ti/SiO₂/Si film.

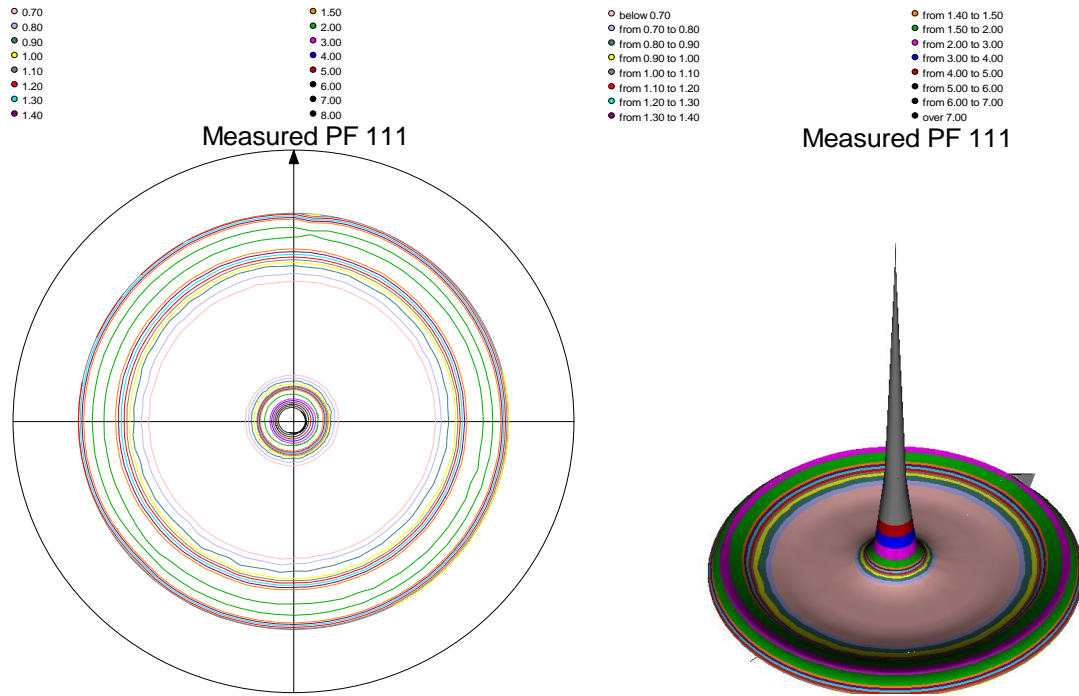


Figure 24. Strong $\{111\}$ fibre texture pole figure for 6 nm Ti intermediate layer deposited at 0.4 Pa argon pressure of Pd/Ti/SiO₂/Si film.

The maximum pole density for the corresponding pole figures obtained for Pd/Ti films are shown in Table 8. The strong textured Pd/Ti films with 3 and 6 nm Ti deposited at 0.4 Pa are stronger as the respective maximum pole density was 58.41 and 26.62 times the random orientation than the anomalous strong textured behaviour of Pd/Ti film with 1 nm thick Ti deposited at 3 Pa where the maximum pole density was 21.99 times the random orientation. The stronger pole density for Pd/Ti films with Ti deposited at 0.4 Pa was due to the higher mobility of the sputtered atoms on the surface. The maximum pole density was less for the weak textured Pd/Ti film and the Pd film without Ti intermediate layer and also similar with respective pole densities of 1.56 and 1.91 times the random orientation respectively. The lower pole density for weak texture could be due to the low mobility of the sputtered atoms at 3 Pa for the respective films. The weak textured Pd/Ti film has lower pole density than the Pd film without Ti layer and this could be due to the larger film thickness of 106 nm in case of Pd/Ti films (Pd (100 nm) and Ti (6 nm)) than 100 nm thick Pd film. Thus the texture developed becomes weaker with an increase in film thickness.

4.1.3. Stress Measurements

Both the Pd/SiO₂/Si and Pd/Ti/SiO₂/Si (Pd/Ti) prepared films were measured for stresses in the films with XRD. The stress values obtained for $[111]$ oriented grains from $\{311\}$ reflection of Pd/SiO₂/Si and

4. Results and Discussion

Pd/Ti/SiO₂/Si films are shown in Table 9. The stresses obtained are tensile for all deposited films. The tensile growth stress of the films are ascribed to the attractive forces between the islands at the coalescence stage of film growth [33]. The stress developed in Pd film without Ti intermediate layer was less when compared to Pd films with Ti intermediate layer. This indicates an influence of Ti on Pd layer in Pd/Ti films. Depositing Ti as an intermediate layer increases the tensile stress of approximately 150 MPa for Pd/Ti films when compared to Pd film without Ti intermediate layer as seen in Table 9.

| Deposited films | Ti argon Sputtering pressure (Pa) | Ti Thickness (nm) | Stress values of (111) oriented grains from {311} reflection (MPa) |
|------------------------------------|-----------------------------------|-------------------|--|
| Pd/SiO ₂ /Si | N.A. | N.A. | 73.2 ± 8.0 |
| Pd/Ti/SiO ₂ /Si (Pd/Ti) | 0.4 (3mTorr) | 3.0 | 257.7 ± 75.9 |
| | | 6.0 | 240.6 ± 47.8 |
| | 3 (23mTorr) | 1.0 | 264.1 ± 37.1 |
| | | 6.4 | 235.7 ± 15.5 |

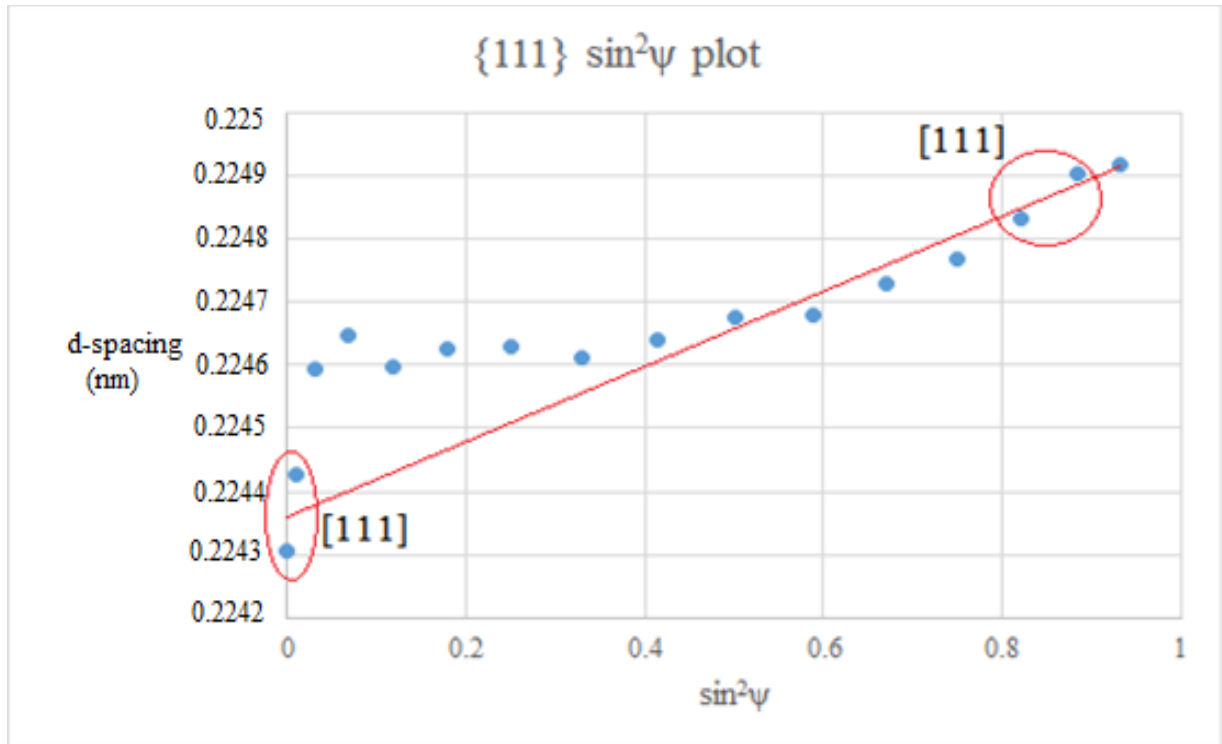
Table 9. Stress values for [111] oriented grains from {311} reflection of Pd/SiO₂/Si and Pd/Ti/SiO₂/Si films.

The stress values are obtained from the slope of d-spacing versus $\sin^2\psi$ plots. The Hill weighted grain interaction model used to fit the values obtained is shown in Figure 25(a) as a red straight line. The [111] oriented grains in {111} reflection $\sin^2\psi$ plot occurs at ψ (tilt) angles of 0° and 70.5°. The corresponding intensity versus ψ plot are also shown for the corresponding Pd/Ti film. Figure 25 shows the $\sin^2\psi$ plots obtained for strong textured Pd/Ti film with 6 nm Ti deposited at 0.4 Pa argon pressure. And Figure 26 shows the $\sin^2\psi$ plots obtained for the weak textured Pd/Ti film with 6 nm Ti deposited at 3 Pa argon pressure.

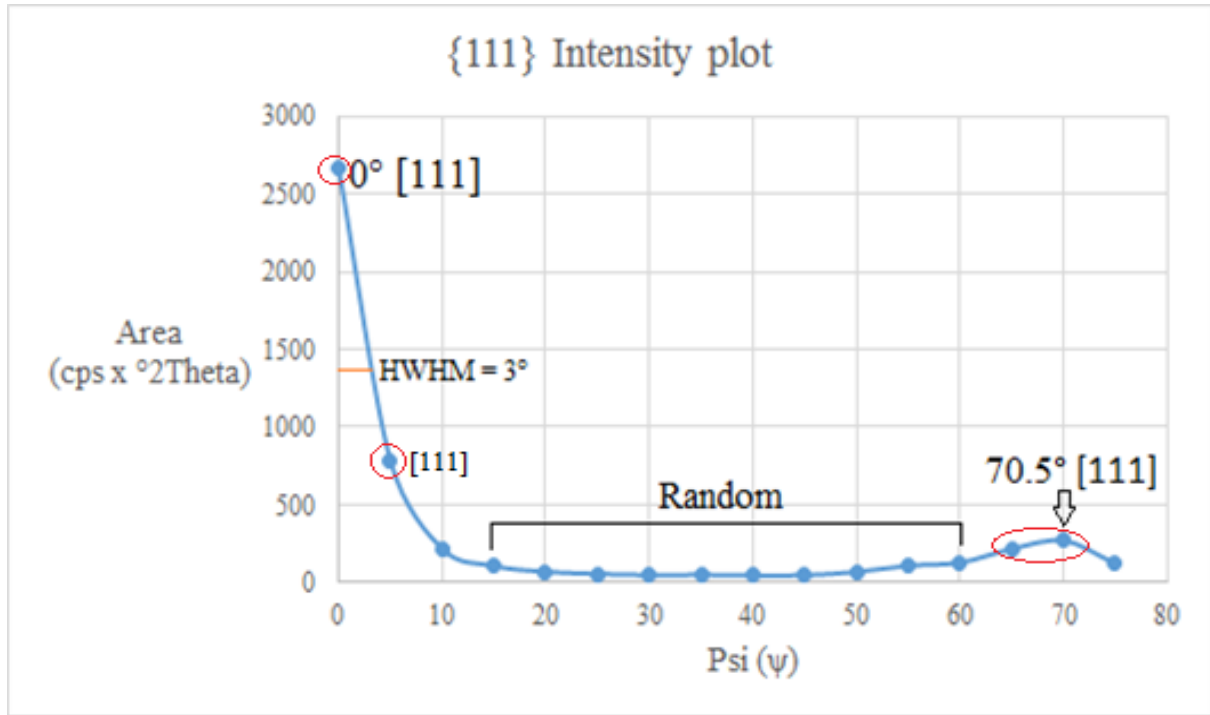
The d-spacing versus $\sin^2\psi$ plots obtained are not linear as seen in Figures 25(a) and 26(a) due to the anisotropy of the Pd and Ti films. But the grain interaction models available in X'Pert Stress Plus are for isotropic systems and as such not suitable for analysis of all grain orientations. So for stress calculation only selected $\sin^2\psi$ values were chosen based on [111] oriented grains from {111} reflection as shown by the intensity versus tilt angle plots in Figures 25(b) and 26(b).

The selection of [111] oriented grains for stress measurements depends upon the intensity curves obtained as shown in Figures 25(b) and 26(b) for Pd/Ti films. The maximum intensity is observed at 0°

and 70.5° tilt (ψ) angles for $\{111\}$ reflection. The grains which are lying in the peak area at 0° and 70.5° tilt (ψ) angles are considered for stress measurements. The sharpness of the half-peak obtained at $\psi = 0^\circ$ can be represented by Half Width Half Maximum (HWHM). A sharp peak with HWHM of 3° observed at 0° tilt (ψ) angle implies a very strong textured Pd/Ti film as shown in Figure 25(b) for Pd/Ti film with 6 nm Ti deposited at 0.4 Pa. A HWHM of 3° tilt angle indicates that the peak width is small and also the peak is steep resulting in a very strong texture Pd/Ti film. The random orientation exists for the remaining tilt angles. But a large HWHM of 23° tilt angle was observed for weak textured Pd/Ti film with 6 nm Ti deposited at 3 Pa as seen in Figure 26(b) with a wide peak. This broadened peak poses a difficulty in choosing appropriate $[111]$ grains for the stress measurements. The stress values in $\sin^2\psi$ plot varies depending on the selection of $[111]$ grains from the intensity plots.

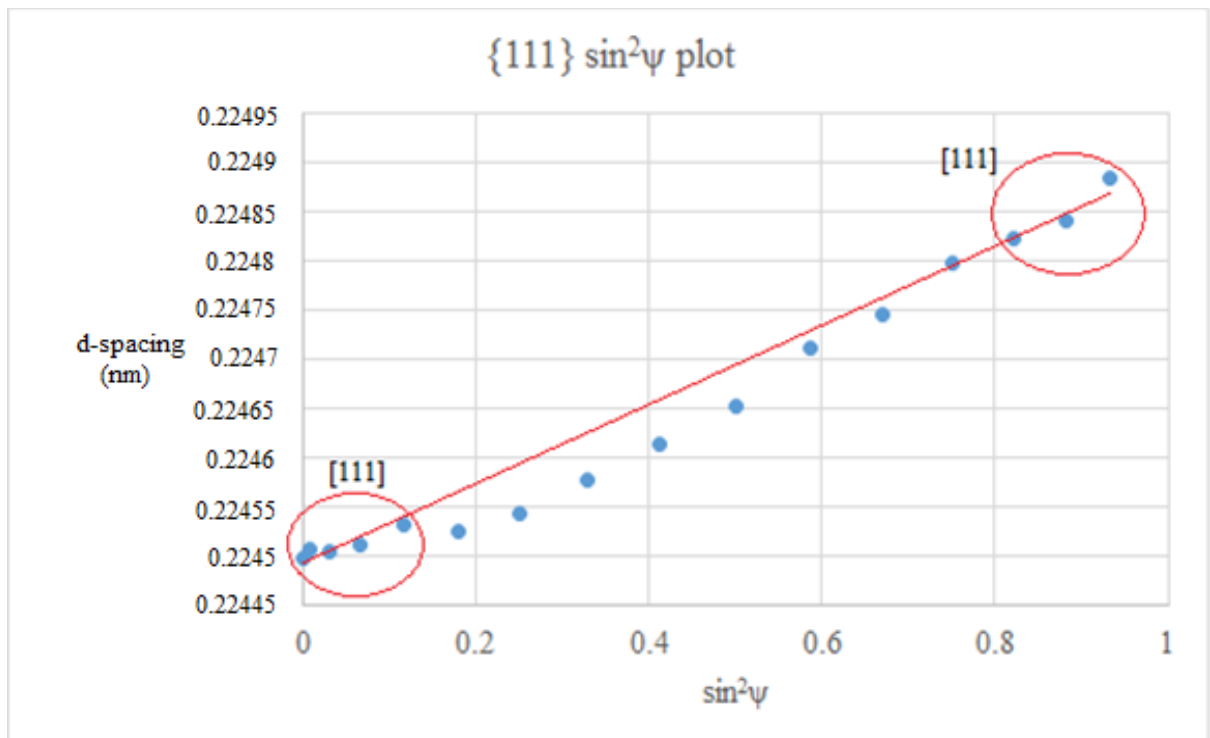


25 (a). d-spacing vs $\sin^2\psi$ plot.

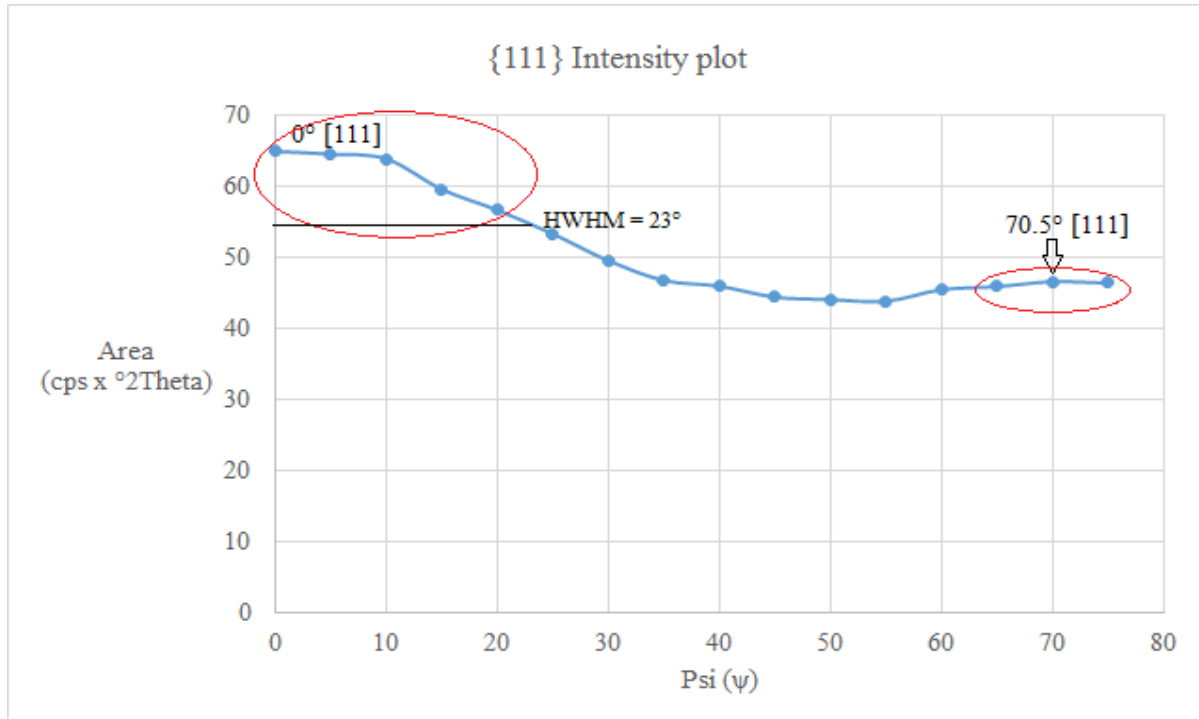


25(b). Intensity vs tilt angle (ψ) plot

Figure 25. Strong textured Pd/Ti film with 6 nm Ti deposited at 0.4 Pa argon pressure for {111} reflection. [111] oriented grains are selected for stress measurements. HWHM= Half Width Half Maximum.



26(a). d-spacing vs $\sin^2\psi$ plot.



26(b). Intensity vs tilt angle (ψ) plot

Figure 26. Weak textured Pd/Ti film with 6 nm Ti deposited at 3 Pa argon pressure for {111} reflection. [111] oriented grains are selected for stress measurements. HWHM= Half Width Half Maximum.

4.1.4. Discussion

The surface roughness obtained was similar for Pd/Ti films, when Ti was sputtered for same thickness at both argon pressures as shown in Figure 21. The same phenomenon was observed and explained earlier in Section 4.1.1.2 for Ti/SiO₂/Si films sputtered for same Ti thickness at both argon pressures as shown in Figure 17. Thus the uniformity in surface roughness was resulted for all Pd/Ti films and also for all Ti/SiO₂/Si films irrespective of the Ti argon sputtering pressures implies that the influence of different Ti argon sputtering pressures on the surface roughness of the deposited Pd/Ti films was negligible.

The RMS surface roughness results obtained for Pd/Ti films are then compared with the Pd film without Ti intermediate layer deposited on SiO₂/Si substrate to deduce the influence of Ti on the surface roughness of top Pd layer. The average RMS surface roughness obtained for Pd film without Ti layer was 6.07 ± 0.50 nm. But the average RMS roughness values for Pd/Ti films was less for small Ti thickness as shown in Figure 21. Thus introduction of Ti intermediate layer of very small thickness reduces the Pd film roughness by 2 to 3 nm. This proves as a reason for the selection of lower thickness range of 1 to 6 nm for Ti intermediate layer in this thesis for better hydrogen absorption and desorption in Pd/Ti films as explained later in Section 4.2.4.

An open columnar structure develops for the deposited Pd layer in Pd/Ti films and also in Pd films without Ti intermediate layer according to Thornton's SZM [31]. The SEM surface topographic images shown in Figure 27 exhibits more open/loose structures as seen by the presence of big gaps on the top surface of Pd film for Pd film without Ti layer than the Pd film with Ti intermediate layer (Pd/Ti). Thus Ti intermediate layer influences the Pd layer resulting in less gap between the open columnar structures for Pd/Ti films.

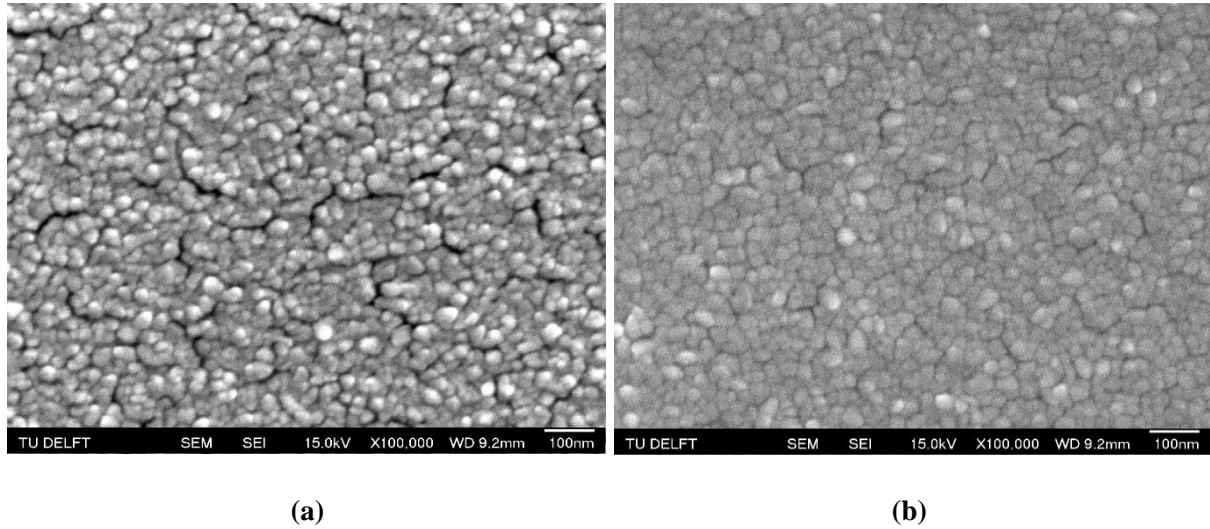


Figure 27. SEM surface topographic images of 100 nm thick Pd layer (3 Pa argon pressure) (a) without Ti intermediate layer and (b) with 6 nm thick Ti intermediate layer (3 Pa argon pressure) deposited on SiO₂/Si substrate.

The introduction of Ti intermediate layer also influences the texture of Pd film in Pd/Ti films as seen from the texture results explained earlier in Section 4.1.2. The Pd/Ti film with 6 nm Ti layer sputtered at 3 Pa shows similar weak {111} texture behaviour as the Pd film without Ti intermediate layer as seen in Table 8. The deposition of Ti and Pd film at same argon pressure of 3 Pa makes Pd/Ti film behaves texturally same as Pd film deposited at same 3 Pa pressure without Ti intermediate layer.

But an anomalous strong {111} texture behaviour was encountered for Pd/Ti/SiO₂/Si film with 1 nm Ti sputtered at 3 Pa as shown in Section 4.1.2 despite the development of a weak texture at higher argon pressure of 3 Pa. To deduce a reason for this strange textural behaviour of the corresponding Pd/Ti film, the Transmission Electron Microscope (TEM) was used. The cross-sectional image obtained from TEM for the Pd/Ti/SiO₂/Si film of 1 nm Ti intermediate layer sputtered at 3 Pa argon pressure is shown in Figure 28.

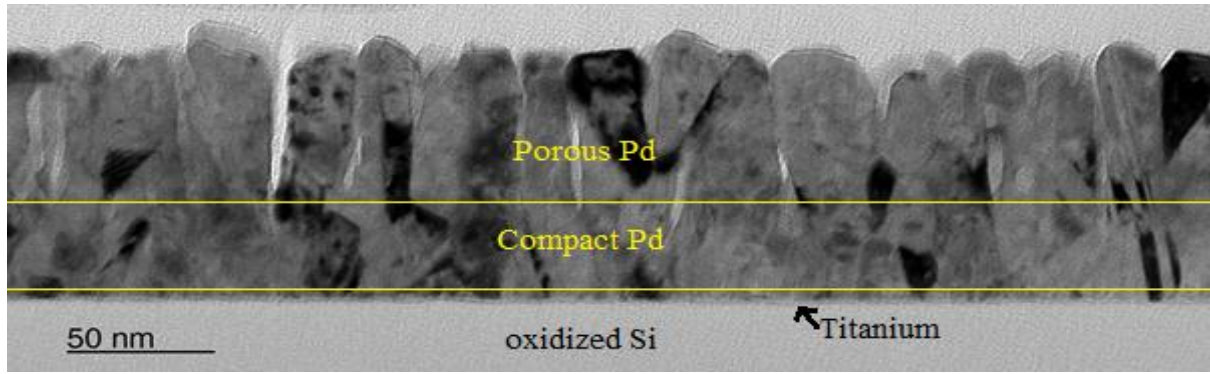


Figure 28. TEM Bright Field (BF) image of Pd/Ti/SiO₂/Si film with 1 nm Ti intermediate layer sputtered at 3 Pa argon pressure.

The TEM image obtained was then analysed with Energy Dispersive X-ray Spectroscopy (EDX) for layer material identification. The EDX maps of the layer obtained for the Pd/Ti/SiO₂/Si film are shown in Figure 29. The EDX maps also confirms the presence of Ti layer (in TiK α 1 map) deposited at 3 Pa argon pressure of the Pd/Ti/SiO₂/Si film.

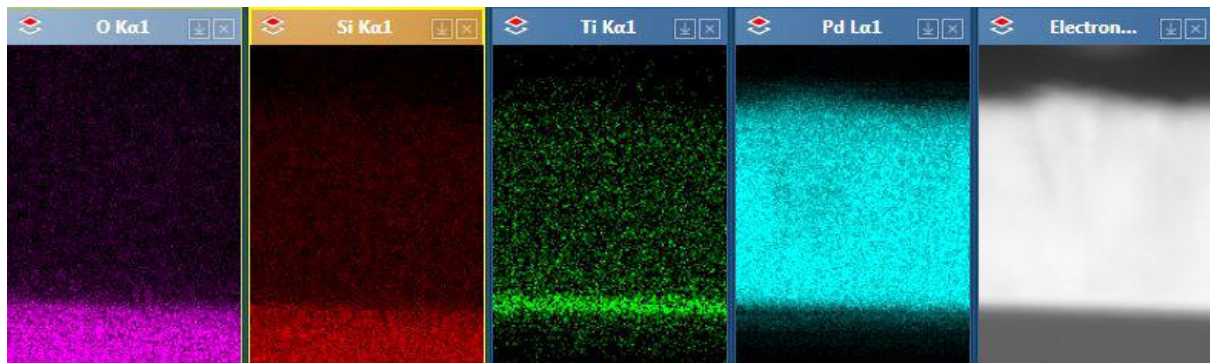


Figure 29. Elemental EDX maps of the layers of Pd/Ti/SiO₂/Si film.

The TEM image in Figure 28 shows the development of compact structure for the 1 nm thick Ti layer and initial Pd layer deposited at 3 Pa on SiO₂/Si substrate despite an expected porous/open structure according to Thornton's SZM [31]. The partial compact and partial open structure influences the texture development of the corresponding Pd/Ti film resulting in the strong {111} texture. The reason is still unknown for the development of the compact structure for an initial thickness of Pd layer in Pd/Ti films.

The stresses in Ti and Pd films developed during deposition for Pd/Ti films were measured with XRD as explained earlier in Sections 2.4 and 4.1.3. The stress results obtained for [111] oriented grains of {311} reflections of Pd/Ti films are shown in Table 9. The stress obtained for Pd film without Ti

intermediate layer was 73.2 ± 8.0 MPa. The deposition of Ti as an intermediate layer increases the stress developed on an average of 150 MPa for all Pd/Ti films as seen in Table 9. The stresses developed in Ti and Pd films was due to the film constraints imposed by the different Ti and Pd crystal structures at Pd/Ti interface in Pd/Ti films (Ti- hexagonal closed packed and Pd- f.c.c) and also the film constraints due to the limited expansion of the Ti film on the confined substrate [5].

The deposition of Ti as an intermediate layer in Pd/Ti/SiO₂/Si (Pd/Ti) films influences the Pd film structure and its growth. Reduction in surface roughness was observed for Pd/Ti films than the Pd film without Ti layer due to the better bonding and adhesion of Ti on SiO₂/Si substrate and the diffusion of Ti in the oxide layer of SiO₂/Si substrate. Columnar structures were developed for Pd, which was deposited at 3 Pa argon pressure over Ti layer, according to Thornton's SZM as proved by the SEM surface topographic images of Pd/Ti films showing the top surface of columnar structures. A change in textural behaviour was resulted for Pd layer in Pd/Ti films depending upon argon sputtering pressures of Ti. A stress increase was observed for Pd/Ti films than Pd/SiO₂/Si films due to the film constraints at Pd/Ti interface.

4.2. AFTER HYDROGENATION AND DE-HYDROGENATION

The Pd film with and without Ti intermediate layer deposited on SiO₂/Si substrate are subjected to the hydrogen loading (hydrogenation) and hydrogen de-loading (de-hydrogenation) processes in XRD as explained earlier in Section 2.4. The results of hydrogen loading and de-loading through Pd/Ti film are described in Section 4.2.1. The textural behaviour and the stress in the films measured with XRD after hydrogen loading and de-loading of Pd/Ti/SiO₂/Si (Pd/Ti) and Pd/SiO₂/Si films are described in section 4.2.2 and 4.2.3 respectively. The influence of Ti layer on Pd film of Pd/Ti films due to hydrogen loading and de-loading are discussed by comparing with the Pd film without Ti intermediate layer later in Section 4.2.4.

4.2.1. Hydrogen loading and De-loading (H-L&DL) processes

The Pd/SiO₂/Si and Pd/Ti films were subjected to H-L&DL processes. The samples are loaded into MRI high temperature XRD chamber as shown in Figure 13(a). The hydrogenation process were carried out at room temperature. The H₂-N₂ gas mixture (5 % H₂ and 95 % N₂) with flow rate of 0.5 L/min was introduced in the chamber. The hydrogen dissociation and diffusion takes place through the Pd layer. The XRD patterns were recorded during H-L&DL processes on Pd films with and without Ti layer for every 2 minutes after allowing H₂/N₂ gas mixture and N₂ gas in the chamber during loading and de-loading process respectively. The Pd/SiO₂/Si and Pd/Ti films, which will be in α -phase of the Pd material before hydrogenation, resulted in a phase transformation from α -Pd phase to a stable β -phase of Palladium Hydride (PdH) after hydrogenation as can be seen in Figures 30, 31 and 32 showing the {111} reflections [2, 3].

The phase transformation is due to the absorption of hydrogen by the Pd layer which results in the hydrogen occupying octahedral interstices of the Pd lattice leading to the formation of PdH [3]. The phase transformation resulted in the shift of {111} diffraction peak from original α -phase Pd peak at 2θ angle of 40.12° to a stable β -phase of PdH at 2θ angle of 38.5° for Pd/Ti film with 6 nm Ti deposited at 3 Pa argon pressure as shown in Figure 30. The reason for peak shift in Pd/Ti films during hydrogen loading was due to the H^+ atoms occupy the octahedral and tetrahedral interstices in Pd and Ti lattices respectively resulting in an increase in the volume of unit cell leading to dislocations [2, 5]. The time taken for the phase transformation from original α -Pd phase to a stable β -PdH phase during hydrogen loading shown in Table 10 will give an insight about the effect of hydrogen dissociation and diffusion through the Pd/Ti films and the Pd film without Ti layer.

The hydrogen absorption is reversible in Pd films [2]. The de-hydrogenation process of Pd/Ti films and the Pd film without Ti layer was carried out after hydrogenation process. The N_2 gas (100% N_2) with the flow rate of 0.5 L/min was introduced in the chamber. The phase transformation obtained during hydrogenation process is reversed during hydrogen de-loading process. A stable β -phase of PdH obtained is transformed to the α -Pd phase during reverse phase transformation. The time taken for the reverse phase transformation from the β -phase of PdH to a stable α -Pd phase by completely suppressing the β -phase during hydrogen de-loading process as shown in Table 10 indicates the time to retrieve the stored hydrogen from Pd layer in Pd/Ti films and the Pd film without Ti layer.

The {111} diffraction patterns during hydrogen loading and de-loading processes are shown in Figure 30 and 31 for the weak textured and the strong textured Pd/Ti film. Figure 32 shows the corresponding diffraction patterns of hydrogen loading and de-loading for the Pd film without Ti intermediate layer.

| Deposited films | Ti Argon Sputtering pressure (Pa) | Ti thickness (nm) | Hydrogen Loading time (min) | Hydrogen De-loading time (min) |
|----------------------------|-----------------------------------|-------------------|-----------------------------|--------------------------------|
| Pd/ SiO ₂ /Si | N.A | N.A | 4 | 14 |
| Pd/Ti/SiO ₂ /Si | 0.4 (3 mTorr) | 3.0 | 66 | 38 |
| | | 6.0 | 42 | 18 |
| | 3 (23 mTorr) | 1.0 | 60 | 26 |
| | | 6.4 | 12 | 18 |

Table 10. Hydrogen loading and de-loading times of Pd film with and without Ti intermediate layer.

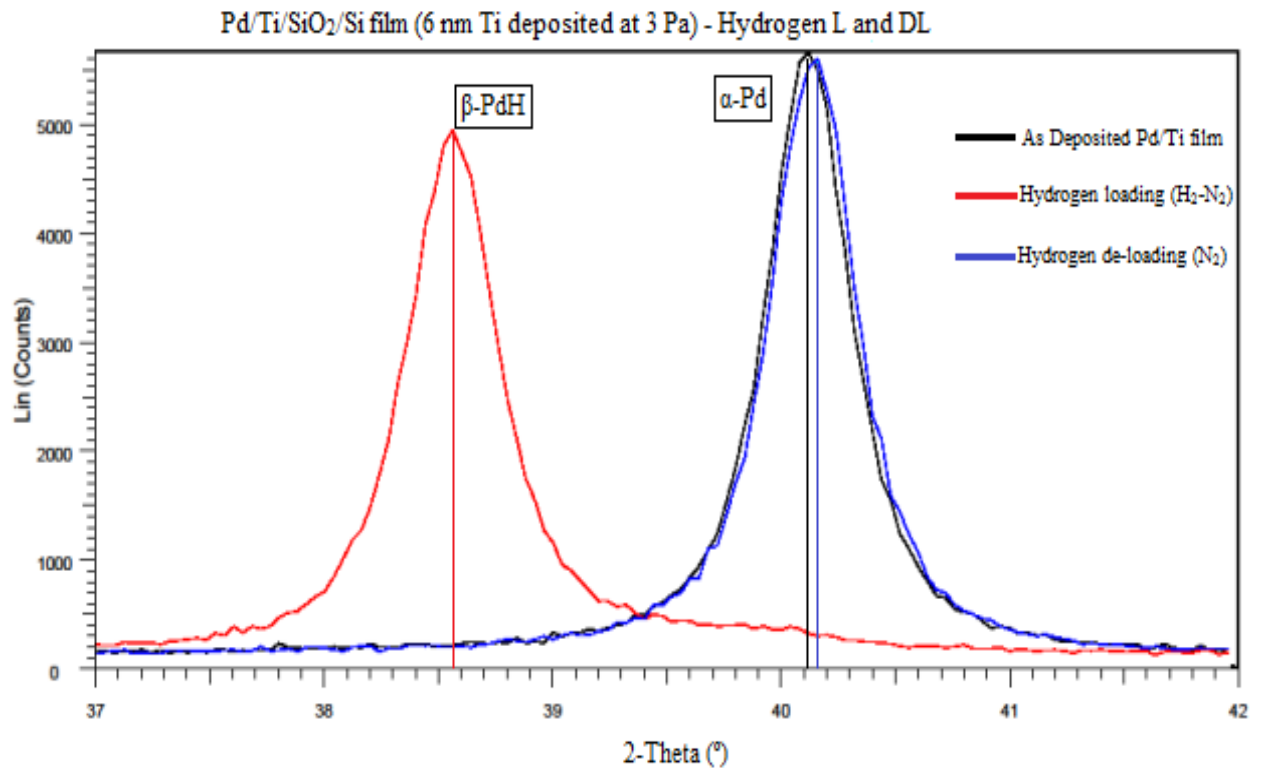


Figure 30. Hydrogen Loading and De-loading intensity scans for a weak textured Pd/Ti film with 6 nm Ti intermediate layer deposited at 3 Pa.

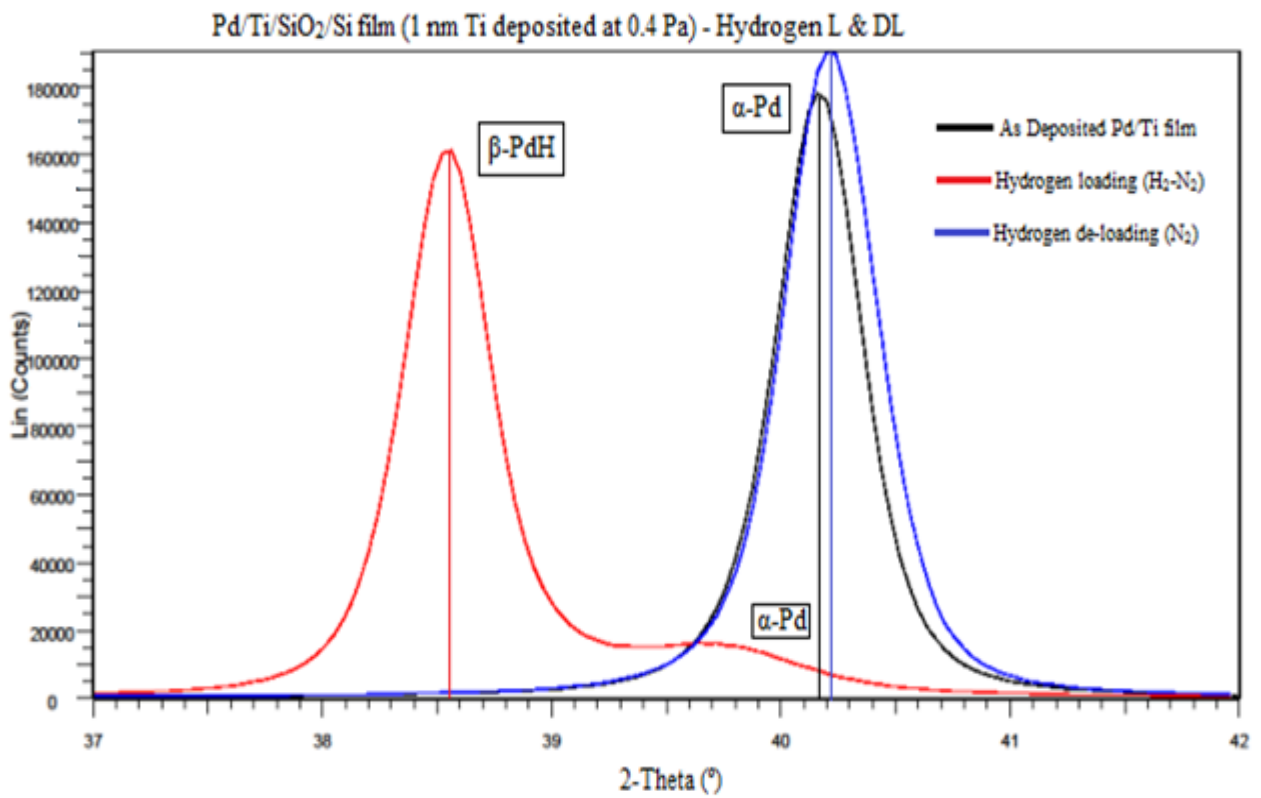


Figure 31. Hydrogen Loading and De-loading intensity scans for a strong textured Pd/Ti film with 3 nm Ti layer deposited at 0.4 Pa.

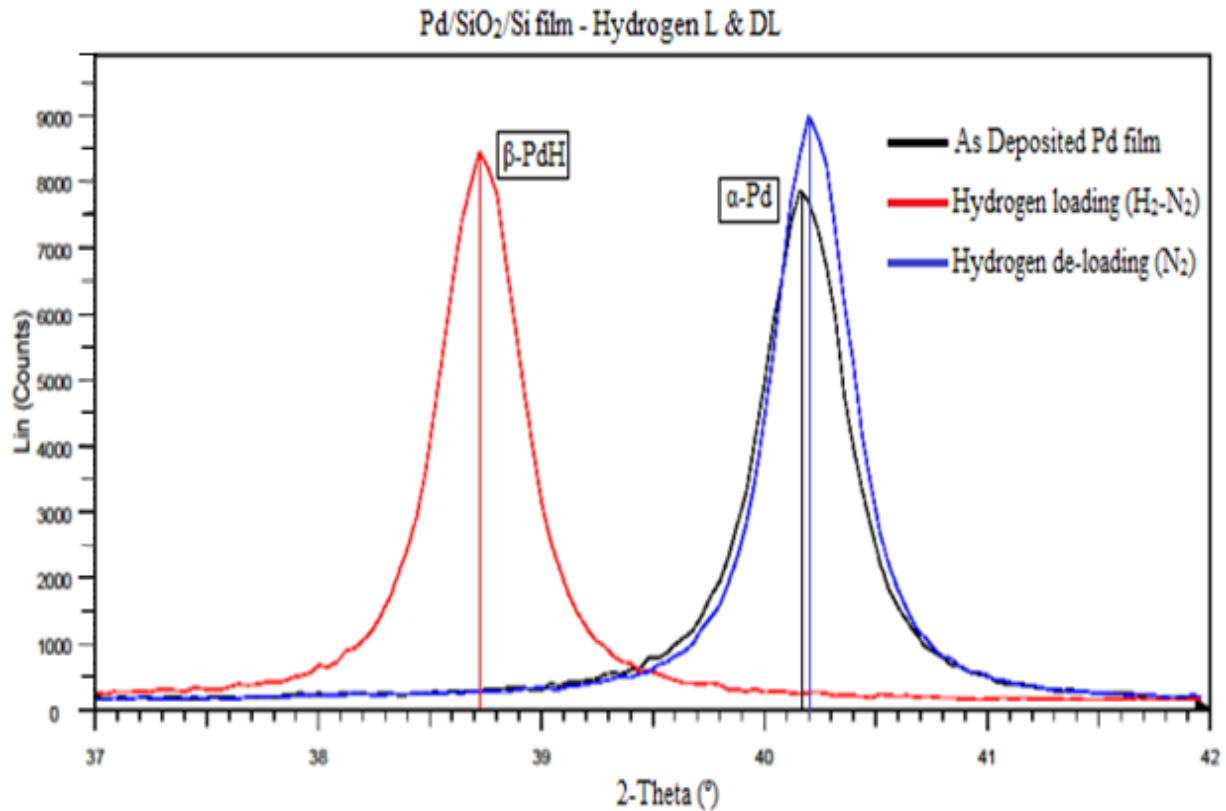


Figure 32. Hydrogen Loading and De-loading intensity scans Pd film without Ti intermediate layer.

A complete suppression of α -phase of Pd was obtained for the Pd film without Ti intermediate layer as shown in Figure 32 during hydrogen loading process. The hydrogen loading {111} diffraction patterns in Figure 31 and Appendix D for the as-deposited strong textured Pd/Ti films shows a small presence of α -phase Pd. The α -phase was not suppressed completely during hydrogen loading due to the different structures of Ti (Compact structure deposited at 0.4 Pa) and Pd (porous structure deposited at 3 Pa). The Pd tries to expand initially during hydrogen loading but due to the constraints imposed by Ti and Pd film near Pd/Ti interface, as the Pd film was confined to the Ti film and the substrate, only limited Pd lattice expansion occurs resulting in a small presence of α -phase of Pd along with stable β -phase during hydrogenation of all strong textured Pd/Ti films. The small presence of α -phase Pd during hydrogen loading is also seen in Figure 35 for strong textured Pd/Ti films. The net area of Pd phase does not reach zero with time indicating its presence along with β -phase of PdH during hydrogen loading.

The α -Pd phase peak width was broadened and the peak intensity was higher after H-L&DL processes shown as a blue line in Figures 30, 31 and 32 when compared to the original as deposited α -Pd peak of the film shown as a black line. The peak broadening was due to the defects like dislocations and the stresses in the films resulted from the Pd lattice expansion during hydrogen loading and de-loading

4. Results and Discussion

process [5]. The peak refers to the {111} planes of the Pd film. The increase in peak intensity was due to the re-orientation of the grains resulted from the dislocations during the H-L&DL processes. Alignment of more {111} texture grains parallel to the surface during grain re-orientation resulted in an increase of peak intensity.

Figure 33 describes the time taken for the formation of stable β -phase of PdH for strong textured Pd/Ti films during hydrogen loading and the suppression of β -phase to form a stable α -phase of Pd during hydrogen de-loading. And Figure 34 describes the same for weak textured Pd/Ti film and the Pd film without Ti intermediate layer. Figure 35 describes the time taken for the suppression of stable α -phase of Pd for strong textured Pd/Ti films during hydrogen loading and the formation of stable α -phase of Pd during hydrogen de-loading. And Figure 36 describes the same for weak textured Pd/Ti film and the Pd film without Ti intermediate layer. The vertical axis in Figures 33, 34, 35 and 36 represents the area under the peaks of β - phase PdH obtained from the {111} diffraction pattern shown above during H-L&DL processes. The corresponding area under the peak for each consecutive 2 minute H-L&DL scans were plotted as a function of time for the films as seen in Figures 33, 34, 35 and 36. The arrows indicates the path followed during hydrogen loading and de-loading by corresponding films.

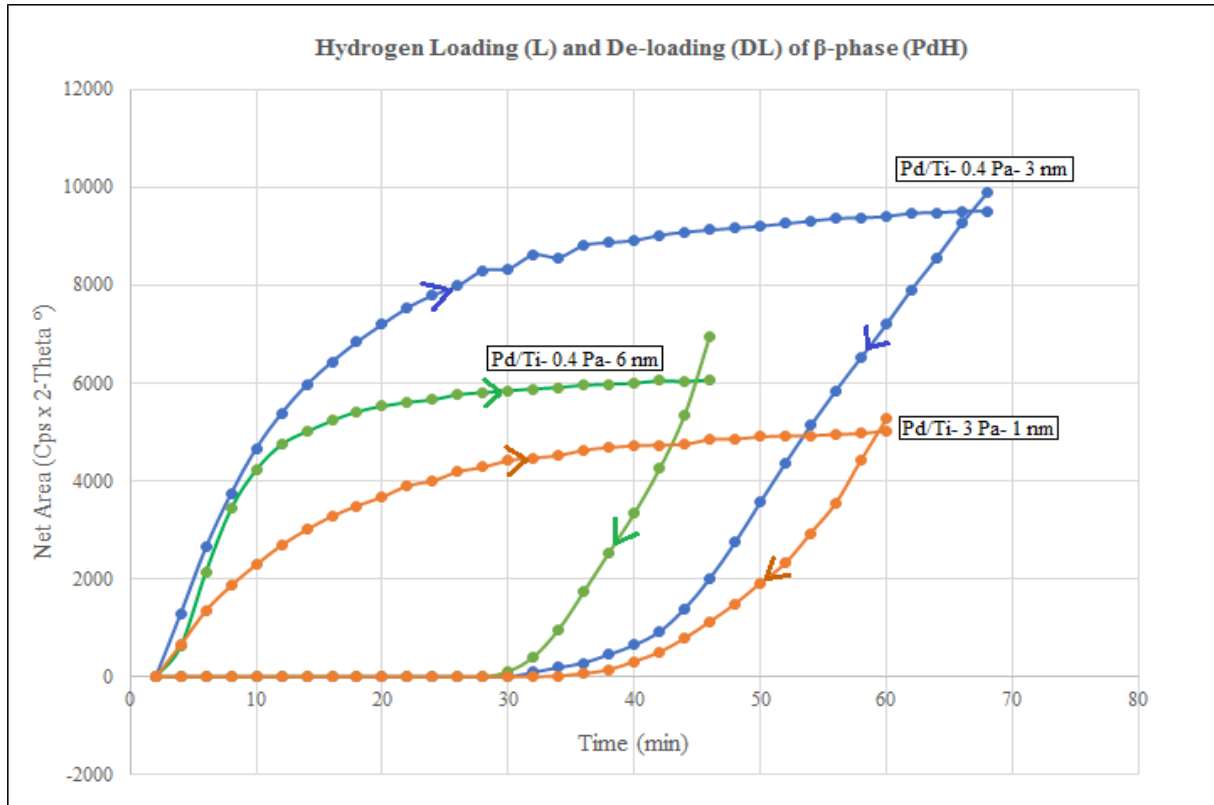


Figure 33. Formation and decrease of β - Phase (PdH) during respective hydrogen loading and de-loading processes in strong textured Pd/Ti films.

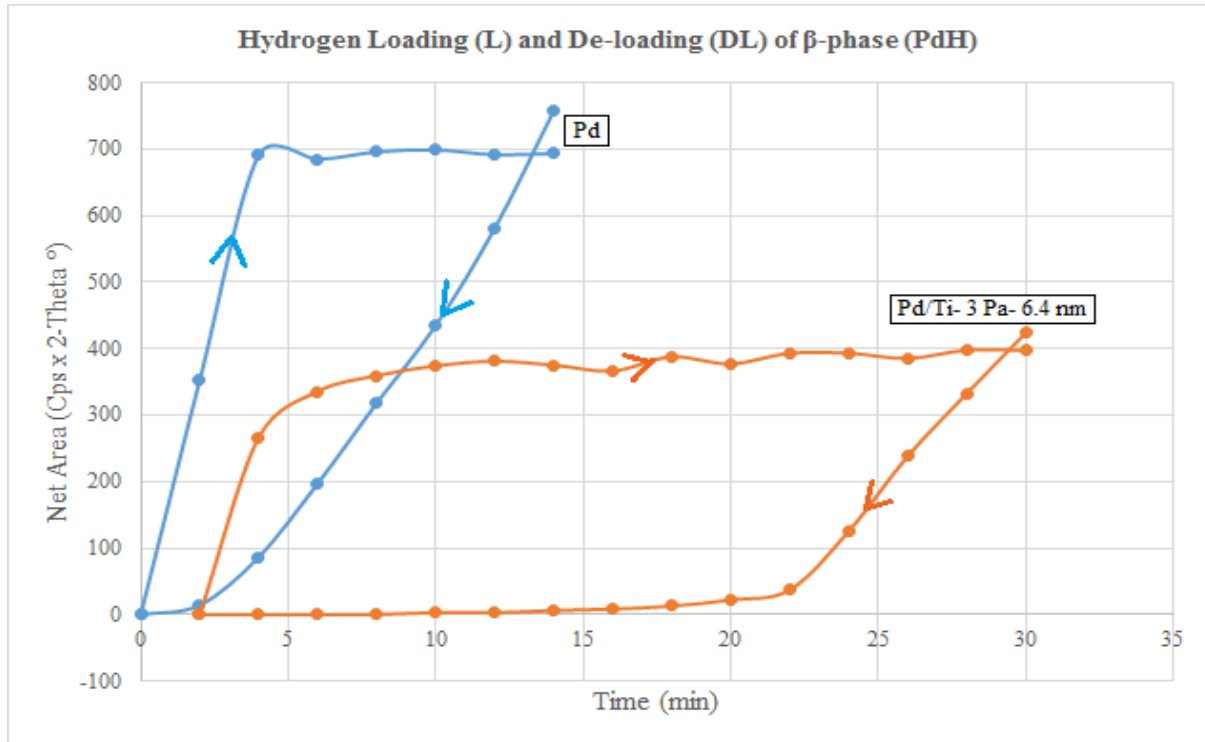


Figure 34. Formation and decrease of β - Phase (PdH) during respective hydrogen loading and de-loading processes in weak textured Pd/Ti film and Pd film without Ti intermediate layer (Pd/SiO₂/Si).

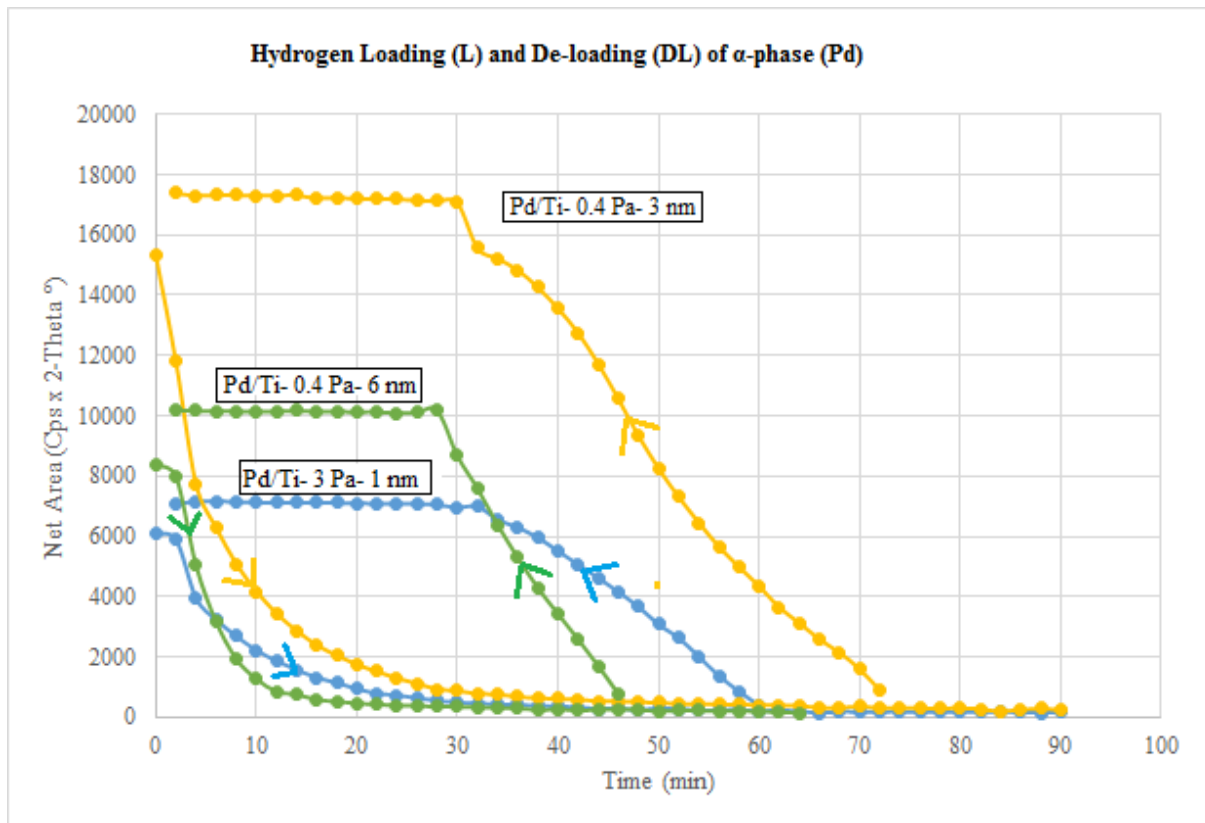


Figure 35. Suppression and formation of α -Phase (Pd) during respective hydrogen loading and de-loading processes in strong textured Pd/Ti films.

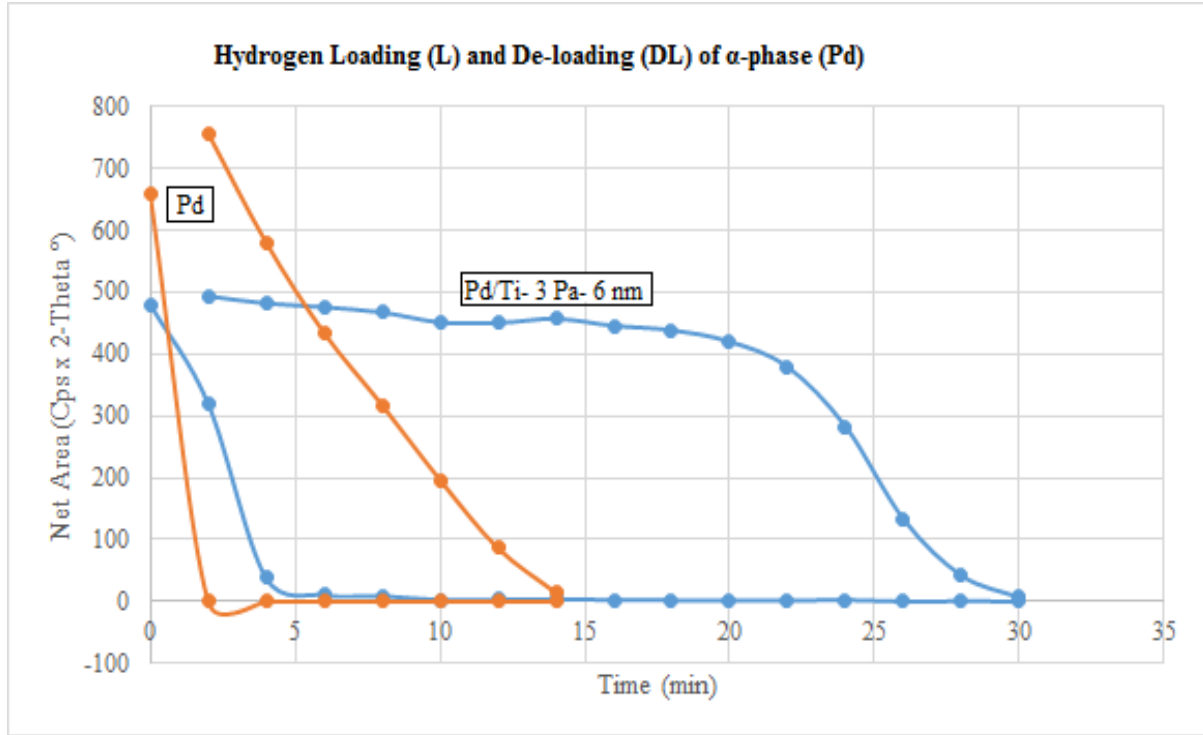


Figure 36. Suppression and formation of α -Phase (Pd) during respective hydrogen loading and de-loading processes in weak textured Pd/Ti film and Pd film without Ti intermediate layer (Pd/SiO₂/Si).

The β -PdH peak area obtained during hydrogen loading was normalized to the before hydrogenated α -Pd peak area of the XRD {111} diffraction patterns shown in Figures 30, 31 and 32 and Appendix D. This normalization of β -PdH peak area to α -Pd peak area plotted with respect to hydrogen loading time as shown in Figure 37. For the Pd film without Ti intermediate layer, normalized β -PdH is more than 1 which implies β -PdH peak area is more than α -Pd peak area as seen from Figure 32. This is due to the easy diffusion of hydrogen through the porous structures of Pd layer which result in the expansion of the Pd lattice. The {111} grain re-orientation occurs parallel to the surface during hydrogen loading which also resulted in more bigger β -PdH peak area in {111} diffraction pattern than α -Pd peak area.

For Pd film with Ti intermediate layer (Pd/Ti), normalized β -PdH is less than 1 which implies β -PdH peak area is less than before hydrogenated α -Pd peak area as seen from Figure 31 and Appendix D. Due to the Pd and Ti film constraints near Pd/Ti interface, the expansion of the Pd lattice was less during hydrogen loading near Pd/Ti interface which results in the presence of little α -Pd peak in strong textured Pd/Ti films. The presence of compact structure of Ti also influenced Pd by developing strong textures of Pd/Ti as seen from Table 8 and 11. And due to this, the expansion of Pd lattice and grain re-orientation will also be less resulting in lower β -PdH peak area than α -Pd peak area.

The normalized β -PdH is also less than 1 for weak textured Pd/Ti film. This is also due to Pd and Ti film constraints near Pd/Ti interface. But due to the porous structures of both Pd and Ti, the barrier for

expansion of Pd lattice was less resulting in the complete suppression of α -Pd peak as seen from Figure 30. This resulted in higher value of normalized β -PdH observed than strong textured Pd/Ti films as seen for the time range until 30 minutes in Figure 37. With an increase in hydrogen loading cycles, an increase of β -PdH peak area could be observed relative to before hydrogenated α -Pd peak area.

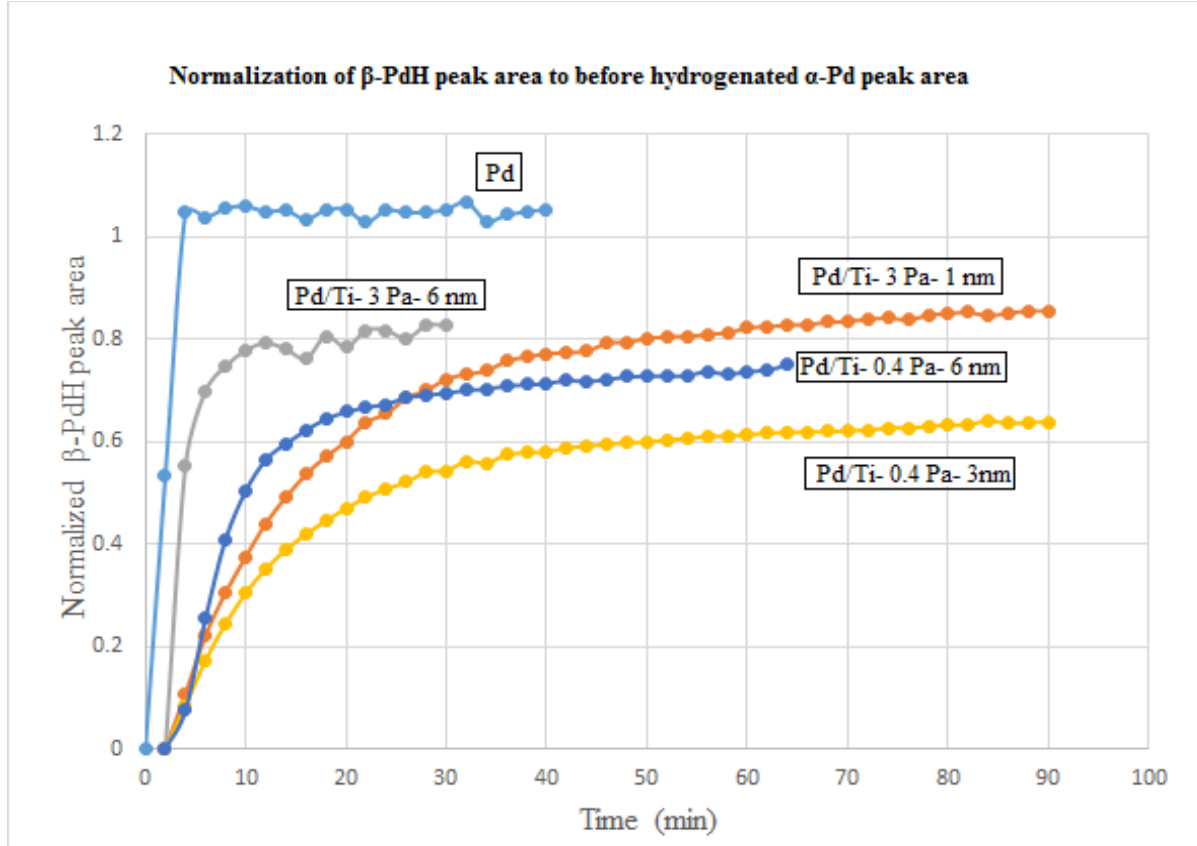


Figure 37. Normalization of β -PdH peak area to before hydrogenated α -Pd peak area with respect to hydrogen loading time.

4.2.2. Texture results

The $\{111\}$ texture scans were carried out for the Pd film with and without Ti intermediate layer after subjected to H-L&DL processes. The texture results obtained are shown in Table 11. The results proves that $\{111\}$ texture results were similar for Pd/Ti films but an increase in maximum pole density was observed for $\{111\}$ texture orientation for Pd film with and without Ti intermediate layer after H-L&DL processes. This pole density increase was due to the increase in the amount of grains oriented with $\{111\}$ parallel to the surface as seen in Table 11. The pole figure for weak textured Pd film without Ti layer is shown in Figure 38. And Figures 39 and 40 shows the pole figure for the weak and strong textured Pd/Ti films respectively.

4. Results and Discussion

| Deposited films | Ti Argon Sputtering pressure (Pa) | Ti thickness (nm) | {111} Texture | | Maximum Pole density of {111} texture | |
|----------------------------|-----------------------------------|-------------------|-----------------|----------------|---------------------------------------|----------------|
| | | | Before H - L&DL | After H - L&DL | Before H - L&DL | After H - L&DL |
| Pd/ SiO ₂ /Si | N.A | N.A | Weak | Weak | 1.91 | 2.13 |
| Pd/Ti/SiO ₂ /Si | 0.4 (3 mTorr) | 3.0 | Strong | Strong | 58.41 | 71.83 |
| | | 6.0 | Strong | Strong | 26.62 | 34.33 |
| | 3 (23 mTorr) | 1.0 | Strong | Strong | 21.99 | 26.50 |
| | | 6.4 | Weak | Weak | 1.56 | 1.59 |

H – L&DL = Hydrogen Loading and De-loading.

Table 11. {111} Texture results of Pd film without and with Ti intermediate layer before and after hydrogen loading and de-loading processes.

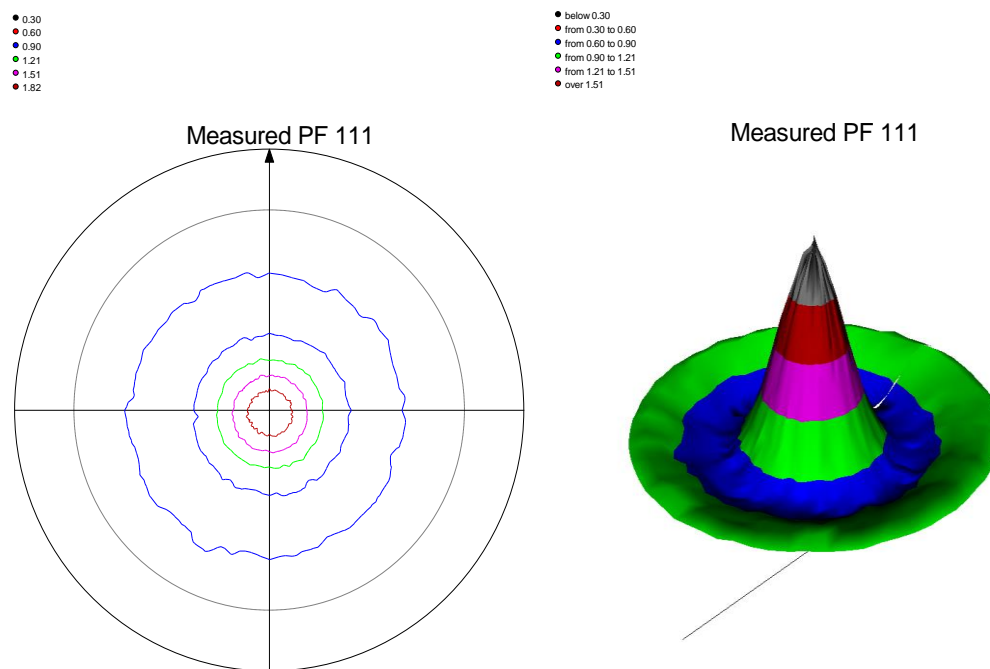


Figure 38. Weak {111} texture pole figure of Pd/SiO₂/Si film after H-L&DL processes.

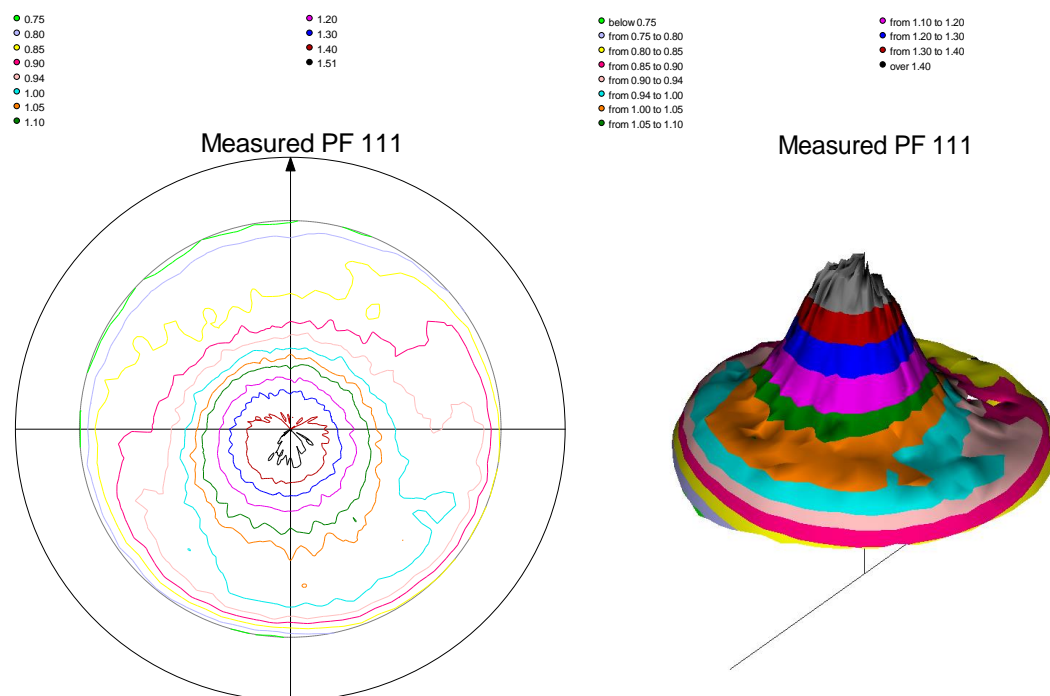


Figure 39. Weak $\{111\}$ texture pole figure for 6.4 nm thick Ti intermediate layer deposited at 3 Pa argon pressure of Pd/Ti/SiO₂/Si film after H-L&DL processes.

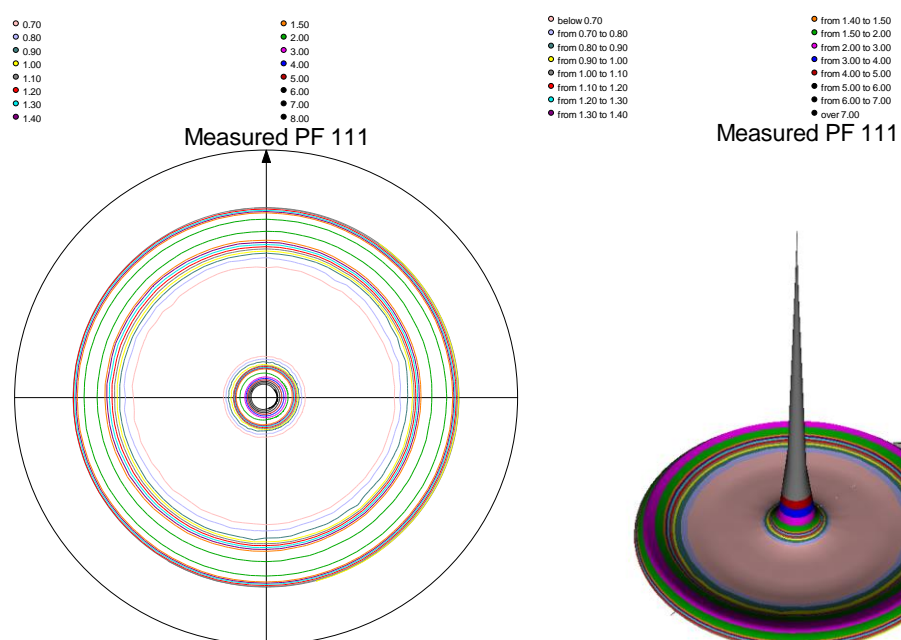


Figure 40. Strong $\{111\}$ texture pole figure for 6 nm thick Ti intermediate layer deposited at 0.4 Pa argon pressure of Pd/Ti/SiO₂/Si film after H-L&DL processes.

4.2.3. Stress measurements

The stresses in the Pd film with and without Ti intermediate layer after HL&DL processes are calculated from XRD. The stress values are deduced from the slopes of d-spacing versus $\sin^2\psi$ plot in X'Pert Stress Plus software as explained earlier in Sections 2.4 and 4.1.3. The stresses of Pd film with and without Ti layer obtained for [111] oriented grains of {311} reflection before and after H-L&DL processes are shown in Table 12.

The stresses obtained were tensile for all films before and after HL&DL processes. The tensile growth stress of the films were ascribed to the attractive forces between the islands at the coalescence stage of film growth [33]. A compressive stress was resulted during hydrogen loading at the Pd and Ti film interface in Pd/Ti films, as the films were confined to the substrate dimensions [25, 30]. The compressive stresses relax during hydrogen de-loading resulting in the deformation of the lattice structure of Pd/Ti film. This deformation causes an increase of tensile stress of the Pd/Ti films after H-L&DL processes. An increase of 150 MPa were resulted for Pd/Ti films before and after H-L&DL processes.

An increase in stress of 70 MPa were resulted for the porous Pd film without Ti intermediate layer (Pd/SiO₂/Si) after HL&DL processes as seen in Table 12. This stress increase was due to the expansion of the Pd lattice resulting from the hydrogen occupying the octahedral interstices of Pd lattice during hydrogen loading [5]. A stress increase of approximately 200 MPa was resulted for Pd/Ti films than the Pd film without Ti layer after H-L&DL processes as seen in Table 12. This higher stress increase in Pd/Ti films when compared to the Pd film without Ti layer was due to the influence of the compact (0.4 Pa) and porous (3 Pa) structures of Ti deposited on the porous structure of Pd (3 Pa) resulting in the constraints of the Pd and Ti film at Pd/Ti interface and also the expansion of Pd lattice was limited due to its confinement to Ti film and hence the substrate during HL&DL processes.

| Deposited films | Ti argon Sputtering pressure (Pa) | Ti Thickness (nm) | Stress values of (111) oriented grains from {311} reflection (MPa) | |
|----------------------------|-----------------------------------|-------------------|--|----------------|
| | | | Before H - L&DL | After H - L&DL |
| Pd/SiO ₂ /Si | N.A | N.A | 73.2 ± 8.0 | 139.3 ± 7.1 |
| Pd/Ti/SiO ₂ /Si | 0.4 (3mTorr) | 3.0 | 257.7 ± 75.9 | 383.3 ± 80.6 |
| | | 6.0 | 240.6 ± 47.8 | 307.8 ± 62.8 |
| | 3 (23mTorr) | 1.0 | 264.1 ± 37.1 | 434.0 ± 51.1 |
| | | 6.4 | 235.7 ± 15.5 | 302.9 ± 5.1 |

Table 12. Stress values for [111] oriented grains from {311} reflection of Pd/SiO₂/Si and Pd/Ti/SiO₂/Si films before and after hydrogen loading and de-loading processes.

4.2.4. Discussion

The H-L&DL times were 4 and 14 minutes for Pd film without Ti intermediate layer, as seen in both Table 10 and Figure 34, because of the effective hydrogen dissociation and diffusion into the porous Pd film [5]. The Pd film with Ti as an intermediate layer increases the H-L&DL times due to the influence of Ti on Pd layer and the constraints imposed by the Pd and Ti films at Pd/Ti interface as seen from Figure 33 and Table 10. The Ti influence was also shown by normalization of β -PdH peak area to α -Pd peak area as shown in Figure 37.

The H-L&DL times for Pd/Ti films varies depending upon the argon sputtering pressures used for the Ti and Pd layers. The strong textured Pd/Ti film with Ti layer deposited at lower argon pressures of 0.4 Pa (3 mTorr) resulted in more time as seen from Figure 33 for the H-L&DL processes. The larger time taken as shown in Figure 33 for the formation of β -phase of PdH during hydrogen loading and for the formation of α -Pd phase during hydrogen de-loading was due to the different Ti and Pd film structures (compact for Ti and porous for Pd) imposing the film constraints near Pd/Ti interface. The limited expansion of Pd lattice due to the confinement of Pd film on Ti film and the substrate also resulted in a larger time for H-L&DL processes in Pd/Ti films.

The weak textured Pd/Ti film with 6 nm Ti layer deposited at higher argon pressures of 3 Pa (23 mTorr) resulted in less time of 12 and 18 minutes for H-L&DL processes as seen from Figure 34. This was due to the porous structures of both Pd and Ti films. The porous structures of Pd and Ti film helps in faster hydrogen diffusion due to the presence of voids [3]. But a larger H-L&DL time were resulted for an anomalous behaviour strong textured Pd/Ti film with 1 nm Ti deposited at 3 Pa higher pressure. This larger time for H-L&DL processes was due to the presence of compact structure at Pd/Ti interface as seen in TEM image shown in Figure 28.

The SEM surface topographic images were obtained for the top surface of Pd layer of Pd/Ti films after H-L&DL processes. No delamination or the crack occurs on the Pd top surface layer of Pd/Ti films as seen in Figure 41 and 42 for Pd/Ti films with Ti deposited at 0.4 Pa and 3 Pa argon pressures respectively. This eliminates the crack and de-lamination formed for the Pd film deposited on SiO₂/Si substrate without Ti intermediate layer according to the work done by Verma and Böttger [27]. But the cases discussed in this thesis, the Pd film without Ti layer after H-L&DL shows no cracks or delamination which was not the actual scenario.

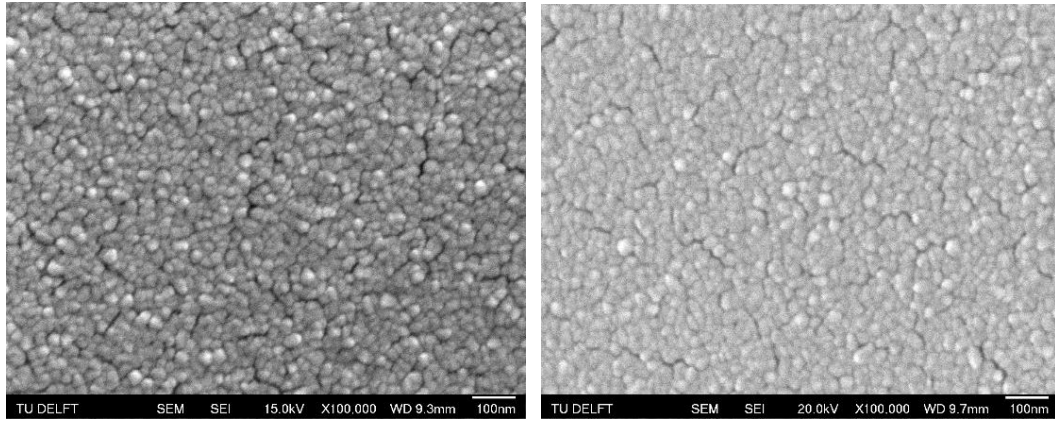


Figure 41. SEM surface topographic images at 100000x magnification for a strong textured Pd/Ti film with 3 nm Ti deposited at 0.4 Pa before H-L&DL (left) and after H-L&DL (right).

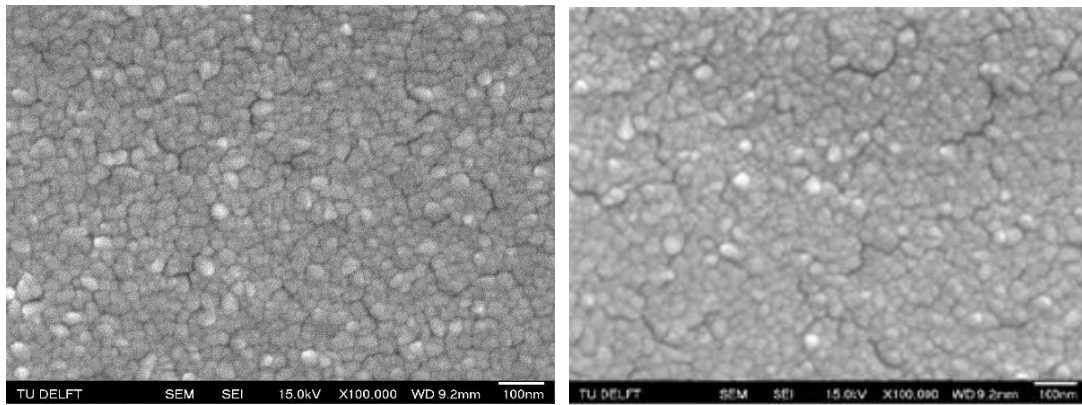


Figure 42. SEM surface topographic images at 100000x magnification for a weak textured Pd/Ti film with 6 nm Ti deposited at 3 Pa before H-L&DL (left) and after H-L&DL (right).

A very less H-L&DL time and the fully suppressed α -phase of Pd during hydrogen loading for weak textured Pd/Ti film with 6 nm Ti deposited at 3 Pa resulted in a very close behaviour to the Pd film without Ti intermediate layer unlike other Pd/Ti films. Also the porous structures of Ti and Pd resulted in a small increase of stress in the films after H-L&DL unlike a larger increase in other Pd/Ti films as seen from Table 12. Thus Pd/Ti film with 6 nm Ti and 100 nm Pd deposited at 3 Pa can be selected for hydrogen separation purposes without the formation of crack and delamination in the films at room temperature after H-L&DL processes.

CONCLUSION

To improve the mechanical stability and reduce the hydrogen embrittlement and de-lamination of the Pd film used in the hydrogen separation purposes at room temperature, the Titanium was introduced as an intermediate layer between the Pd and an oxidized Si wafer substrate. The Pd/Ti/SiO₂/Si films were prepared by magnetron sputtering at room temperature and growth of the films were analysed with different techniques like AFM, SEM and XRD before and after hydrogenation and de-hydrogenation processes.

With Ti as an intermediate layer, a better adhesion was achieved between the Pd and an oxidized Si wafer substrate because of Ti having a higher affinity for oxygen. The average RMS roughness was reduced for Pd films with Ti intermediate layer when compared to the Pd film without Ti intermediate layer as shown by the AFM results. Better bonding and adhesion resulted in eliminating the crack formation and delamination of the Pd material from the substrate as shown by SEM images before and after hydrogenation and de-hydrogenation processes for Pd/Ti films.

The texture change resulted for Pd/Ti films measured from XRD shows the influence of Ti on Pd layer. An approximate stress measurements from XRD observed resulted in tensile behaviour and an increase in stress was resulted for the Pd/Ti films after H-L&DL processes due to the expansion of the Pd lattice during H-L&DL and also due to the Pd and Ti film constraints near Pd/Ti interface in Pd/Ti films.

Among the prepared Pd/Ti/SiO₂/Si films, the Ti and Pd films sputtered at same higher argon pressure of 3 Pa (23 mTorr) for 6 nm and 100 nm respective thickness with porous structures shows a better hydrogen diffusion behaviour with less H-L&DL times by eliminating the crack formation and also the de-lamination of the Pd film when compared to Pd film without Ti intermediate layer (Pd/SiO₂/Si). Thus Pd/Ti film with 6 nm Ti deposited at 3 Pa can be selected for hydrogen separation purposes by reducing the damage of the films during hydrogenation and de-hydrogenation processes.

RECOMMENDATIONS FOR FUTURE WORK

- The Pd/Ti sample with 1 nm thick Ti and 100 nm thick Pd sputtered at same higher argon pressure of 3 Pa (23 mTorr) shows a strange behaviour by forming a strong texture Pd/Ti instead of a weak texture for porous structures. A compact structure at Pd/Ti interface was resulted as seen in TEM images rather than an expected porous structure according to Thornton's SZM. So experiments should be carried out again to investigate this respective Pd/Ti film.
- The TEM analysis should also be carried out on all Pd/Ti films which will give more insight about the Ti film growth and its influence on columnar structure of Pd.
- The surface roughness should also be measured for Pd/Ti films after hydrogenation and de-hydrogenation process by AFM. This will give an insight about the mean spacing between the columnar structures from line scan profile from which the expansion of Pd lattice after hydrogen loading and de-loading (H-L&DL) can be calculated by comparing it with Pd lattice before H-L&DL processes. The lattice expansion will also indicate the stresses acting in thin films.
- The available X'Pert Stress Plus software used for the stress calculations are only for isotropic materials. But the anisotropic Pd/Ti films were incompatible with the available software. To overcome this, some other methods should be used for calculating the stresses in thin films. The use of ISODEC software with ODF of different orientations of Pd/Ti films could be a better alternative for stress calculations of anisotropic materials.
- The sputtering and the hydrogenation and de-hydrogenation process were carried out at room temperature. But the films will be subjected to different temperatures depending upon applications like fuel cells. The annealing process should also be carried out on the prepared Pd/Ti films to examine their mechanical stability and de-lamination behaviour before and after hydrogenation and de-hydrogenation at different temperatures

APPENDIX I- AFM

I. AFM for as –deposited samples:

The AFM was done for 3 types of films sputtered at different argon pressures on different substrates before hydrogenation process and the respective images are shown in Tables 13, 14, 15 and 16. The RMS roughness for these images is listed in Tables 2, 3 and 4.

1. Pd film without Ti intermediate layer on oxidized Si wafer substrate (Pd/SiO₂/Si).
2. Ti intermediate layer on Si substrate (Ti/Si) and Oxidized Si wafer substrate (Ti/SiO₂/Si).
3. Pd film with intermediate layer on oxidized Si wafer substrate (Pd/Ti/SiO₂/Si).

1. Pd film without Ti intermediate layer (Pd/SiO₂/Si):

Pd deposited at 3 Pa (23 mTorr) argon pressure for 100 nm thickness.

Scan size = 3 μ m x 3 μ m.

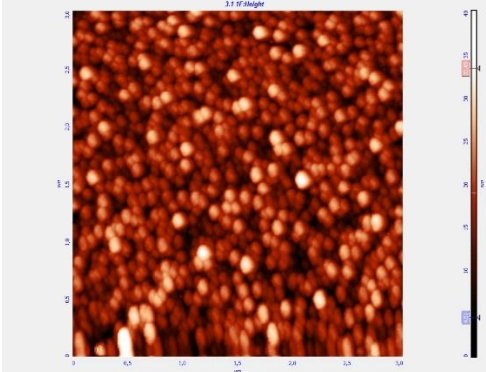
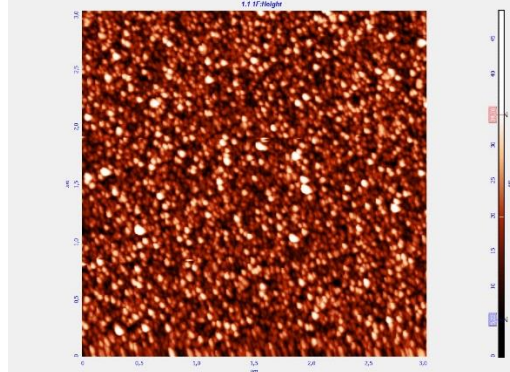
| Pd thickness (nm) | Substrate | |
|----------------------|---|--|
| | Si | Oxidized Si |
| 100 |  |  |

Table A.1. AFM images of reference Pd sample on Si and oxidized Si substrates.

2. Ti intermediate layer on Si (Ti/Si) and Oxidized Si substrate (Ti/SiO₂/Si):

a) Ti deposited at 0.4 Pa (3 mTorr) argon pressure:

Scan Size = 3 μm x 3 μm .

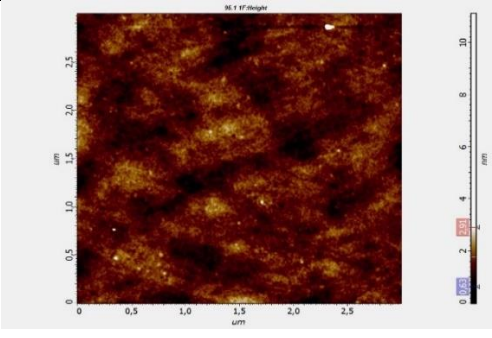
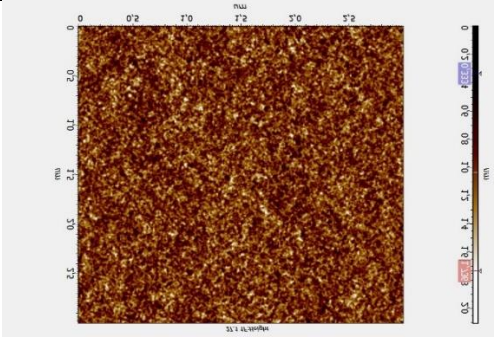
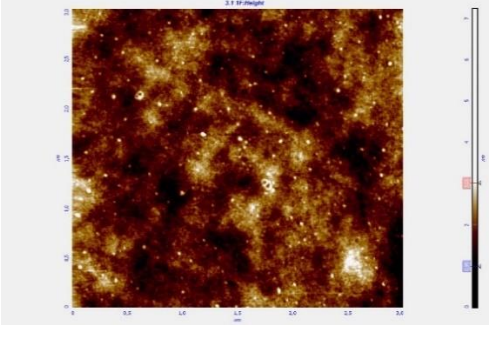
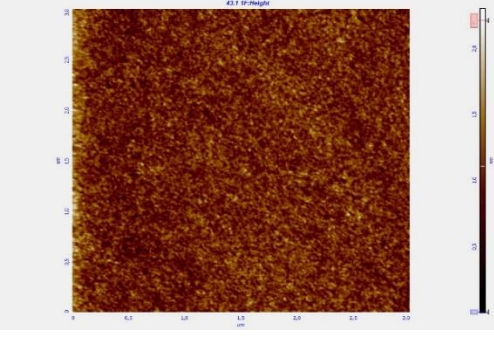
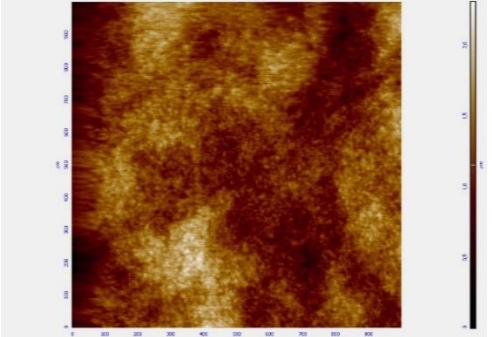
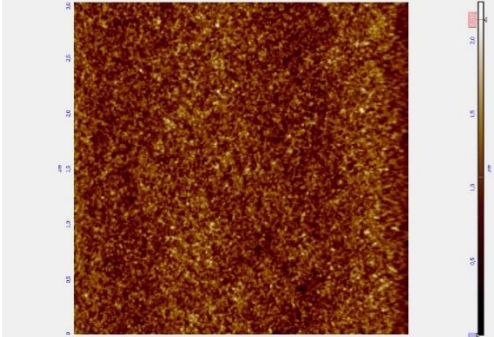
| Ti thickness (nm) | Substrate | Ti thickness (nm) | substrate |
|-------------------|---|-------------------|---|
| | Si | | Oxidized Si |
| 3.0 |  | 3.0 |  |
| 4.4 |  | 4.3 |  |
| 5.8 |  | 6.0 |  |

Table A.2. AFM images of Titanium samples deposited at 0.4 Pa (3 mTorr) argon pressure.

b) Ti deposited at 3 Pa (23 mTorr) argon pressure:

Scan Size = 3 μm x 3 μm .

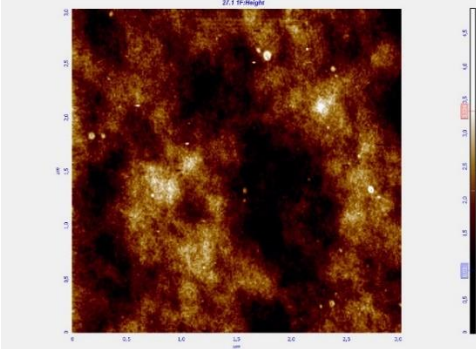
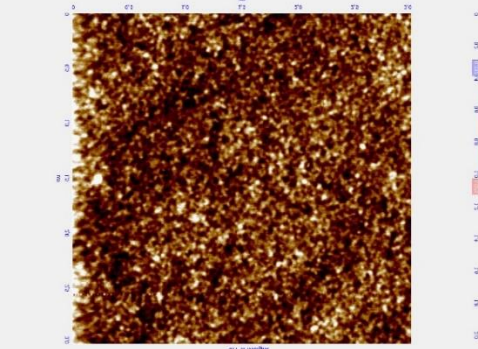
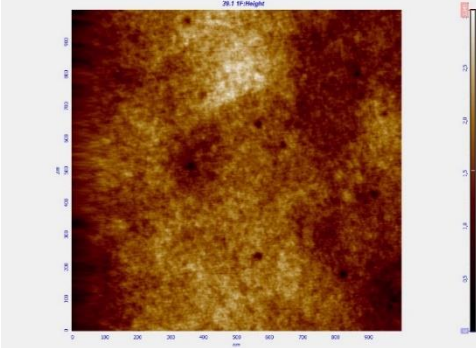
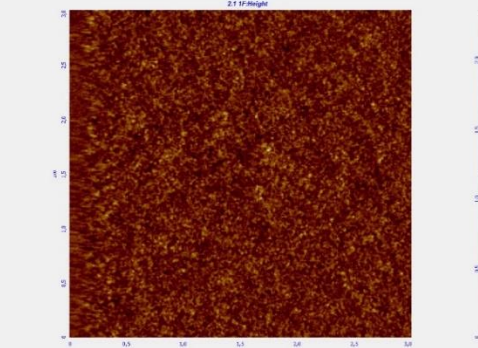
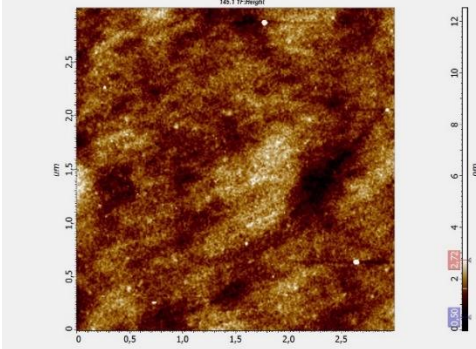
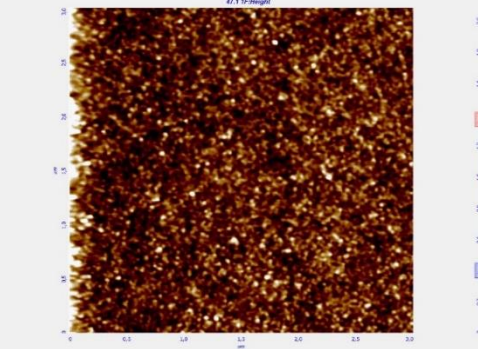
| Ti thickness (nm) | Si Substrate | Ti thickness (nm) | Oxidized Si substrate |
|-------------------|---|-------------------|---|
| 0.2 |  | 1.0 |  |
| 4.0 |  | 3.8 |  |
| 6.5 |  | 6.4 |  |

Table A.3. AFM images of Titanium samples deposited at 3 Pa (23 mTorr) argon pressure.

3. Pd film with Ti intermediate layer (Pd/Ti/SiO₂/Si):

Ti and Pd samples were sputtered on oxidized Si wafer substrate.

Pd was deposited at 3 Pa (23 mTorr) argon pressure. But Ti was deposited at two different argon pressures of 0.4 Pa (3 mTorr) and 3 Pa (23 mTorr).

Scan size = 1 μm x 1 μm .

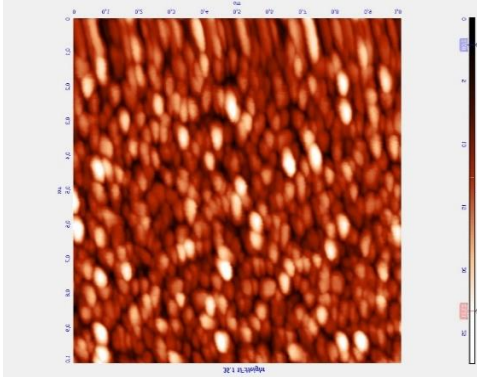
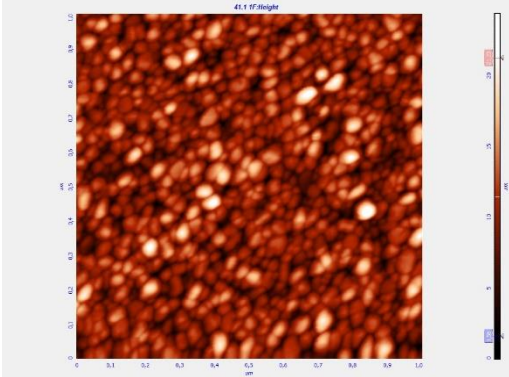
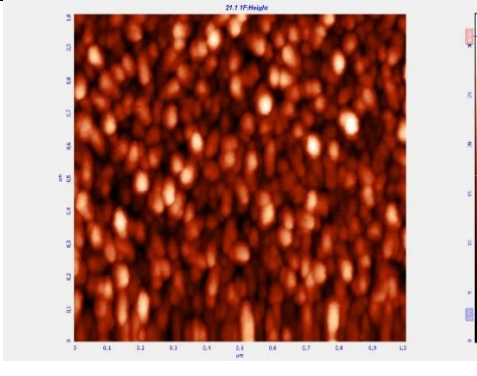
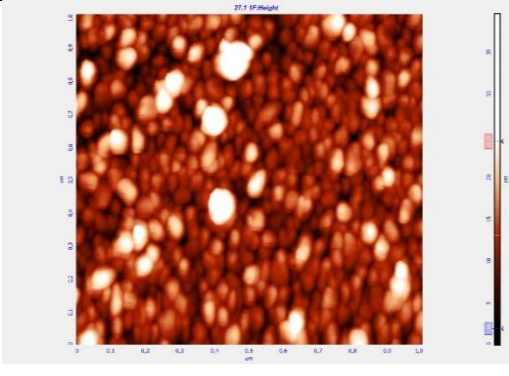
| Ti thickness in Pd/Ti samples (nm) | Argon sputtering pressure 0.4 Pa (3 mTorr) | Ti thickness in Pd/Ti samples (nm) | Argon sputtering pressure 3 Pa (23 m Torr) |
|------------------------------------|---|------------------------------------|---|
| 3.0 |  | 1.0 |  |
| 6.0 |  | 6.4 |  |

Table A.4. AFM images of Pd/Ti samples (Pd/Ti/SiO₂/Si) with Ti sputtered at different pressures and thickness.

APPENDIX II- SEM

The SEM surface topographic images obtained for the Pd film without and with Ti intermediate layer before and after hydrogen loading and de-loading processes. In all cases Pd was deposited at 3 Pa (23 mTorr) argon pressure for 100 nm thickness.

1. Pd film without Ti intermediate layer:

Scan magnification- 40000x

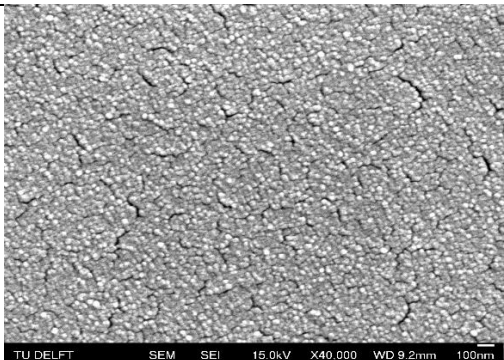
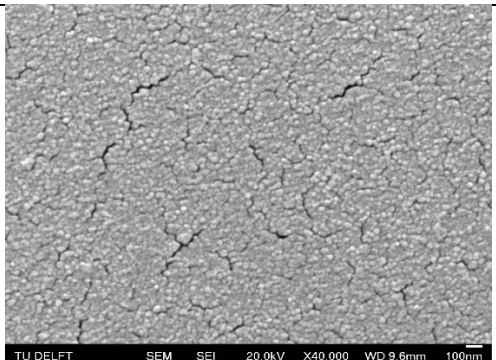
| Deposited film | Before H-L&DL | After H-L&DL |
|-------------------------|--|---|
| Pd/SiO ₂ /Si |  |  |

Table B.1. SEM surface topographic images of Pd film without Ti layer before and after hydrogen loading and de-loading (H-L&DL) processes.

2. Pd/Ti film with Ti deposited at 0.4 Pa (3 mTorr) argon pressure on oxidized Si wafer:

Scan magnification- 40000x

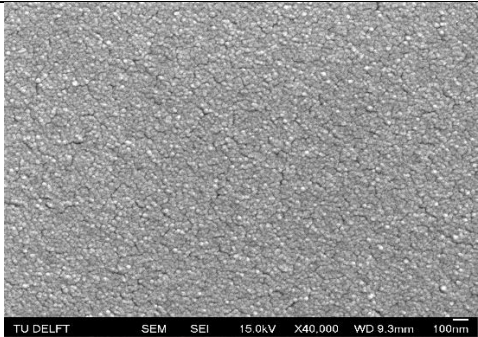
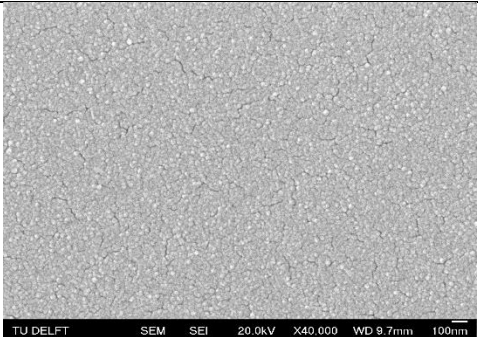
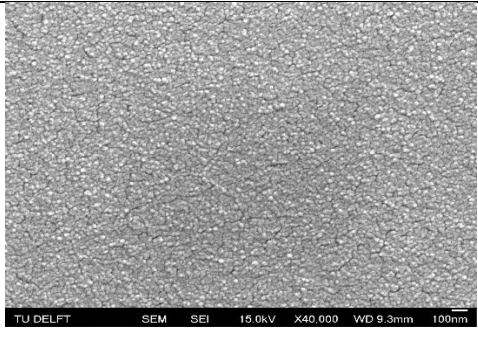
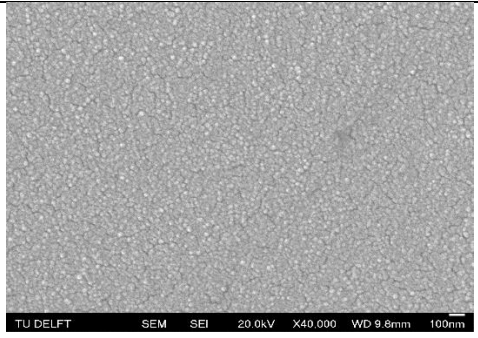
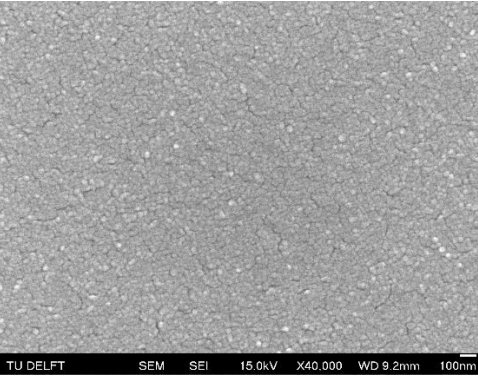
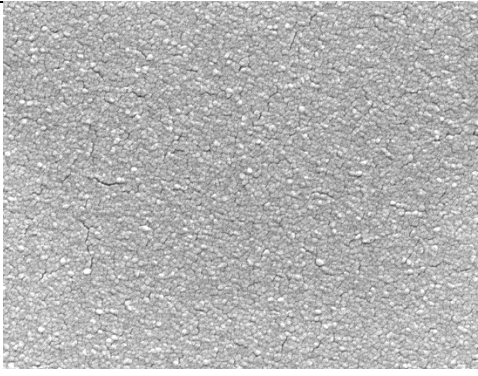
| Ti thickness (nm) | Before H-L&DL | After H-L&DL |
|----------------------|--|---|
| 3.0 |  |  |
| 6.0 |  |  |

Table B.2. SEM surface topographic images of Pd/Ti films with Ti deposited at 0.4 Pa argon pressure before and after H-L&DL processes.

3. Pd/Ti film with Ti deposited at 3 Pa (23 mTorr) argon pressure on oxidized Si wafer:

Scan magnification- 40000x

| Ti thickness (nm) | Before H-L&DL | After H-L&DL |
|----------------------|---|--|
| 1.0 |  |  |

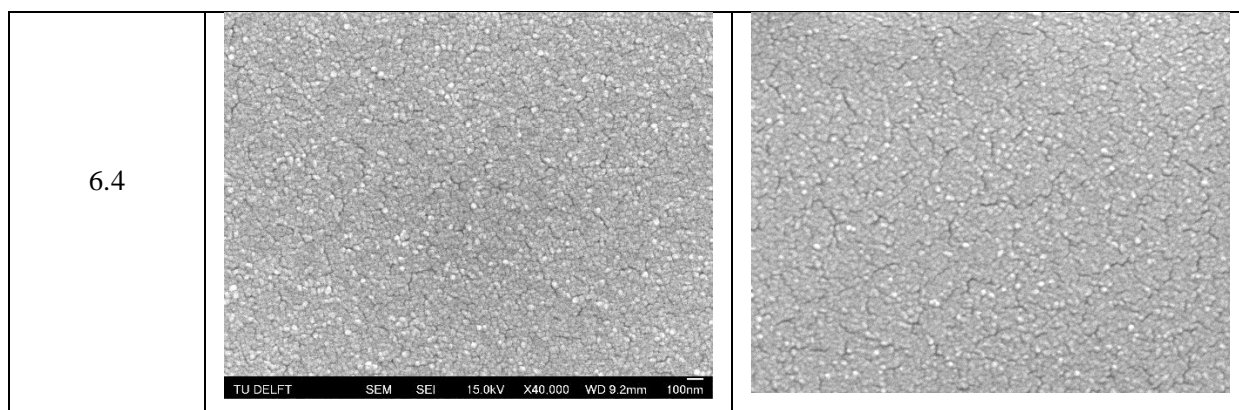


Table B.3. SEM surface topographic images of Pd/Ti film with Ti deposited at 3 Pa argon pressure before and after H-L&DL processes.

APPENDIX III- TEXTURE RESULTS

1. As-Deposited Pd/Ti films:

The pole figures shown in Figures 31 and 32 are for Pd/Ti film with 3.0 nm and 1.0 nm thick Ti deposited at respective 0.4 Pa and 3 Pa argon pressures.

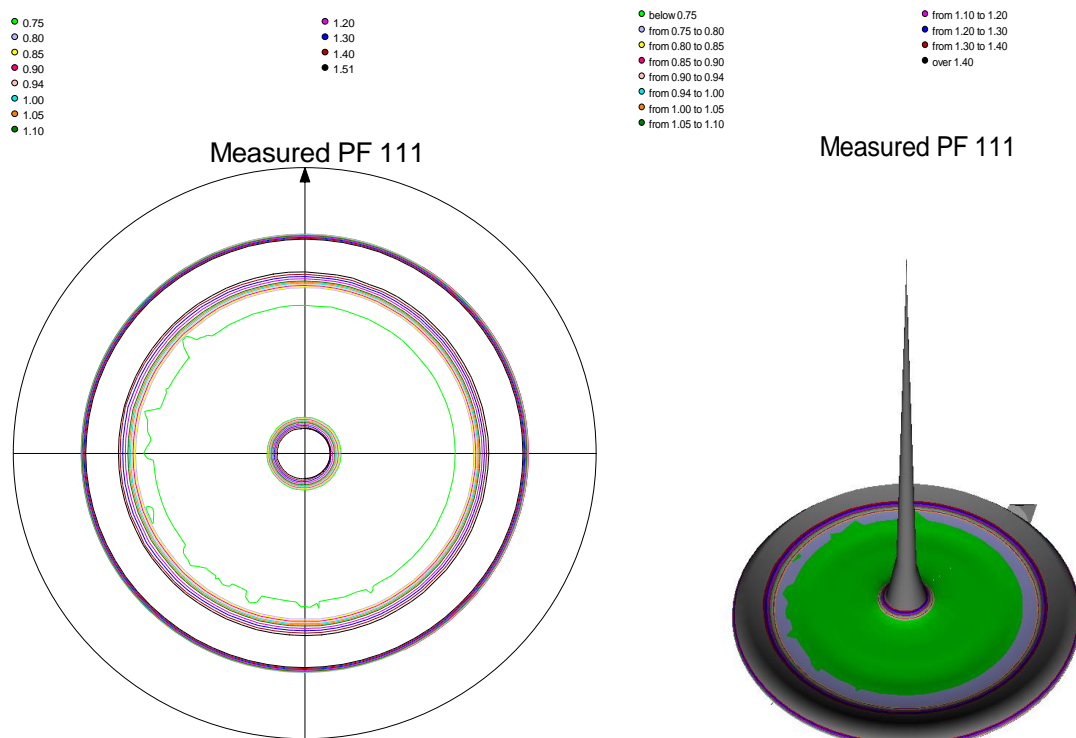


Figure C.1. Strong {111} texture pole figure for 3 nm thick Ti intermediate layer deposited at 0.4 Pa argon pressure of Pd/Ti/SiO₂/Si film.

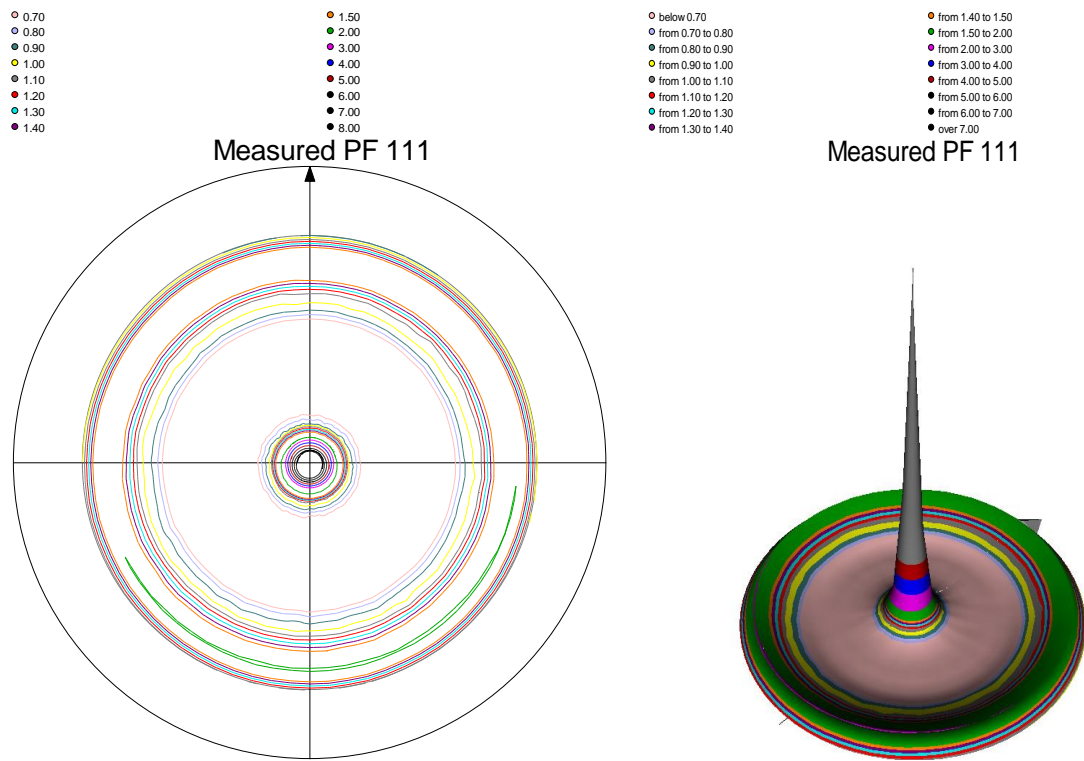


Figure C.2. Strong {111} texture pole figure for 1 nm thick Ti intermediate layer deposited at 3 Pa argon pressure of Pd/Ti/SiO₂/Si film.

2. Pd/Ti films after hydrogen loading and de-loading process (H-L&DL):

The pole figures shown in Figures 33 and 34 are for Pd/Ti film with 3.0 nm and 1.0 nm thick Ti deposited at respective 0.4 Pa and 3 Pa argon pressures after H-L&DL processes.

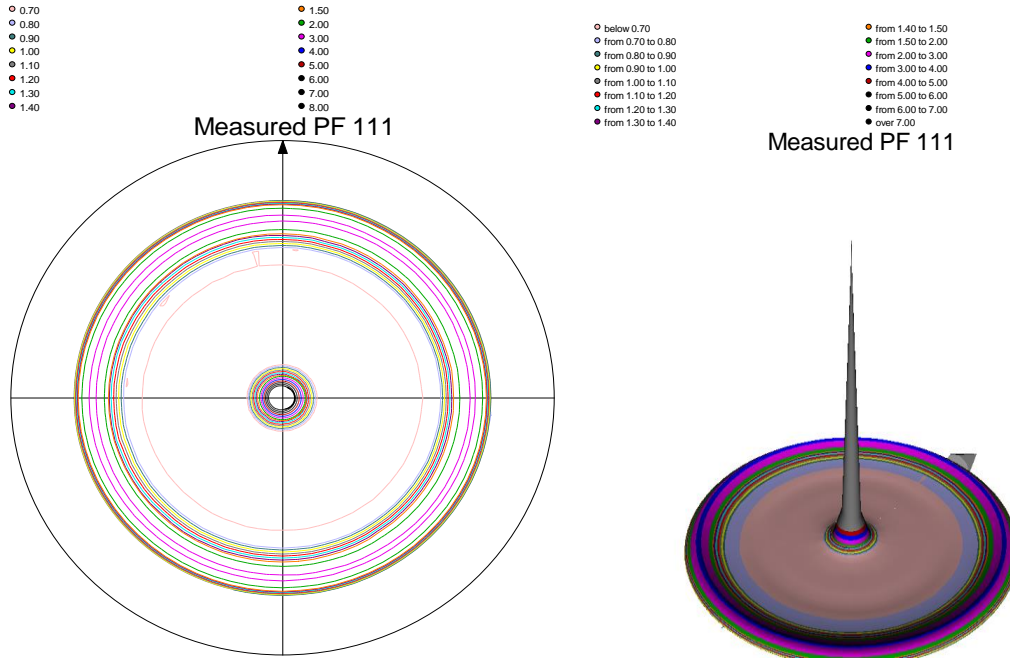


Figure C.3. Strong {111} texture pole figure for 3 nm thick Ti intermediate layer deposited at 0.4 Pa argon pressure of Pd/Ti/SiO₂/Si film after hydrogen loading and de-loading processes.

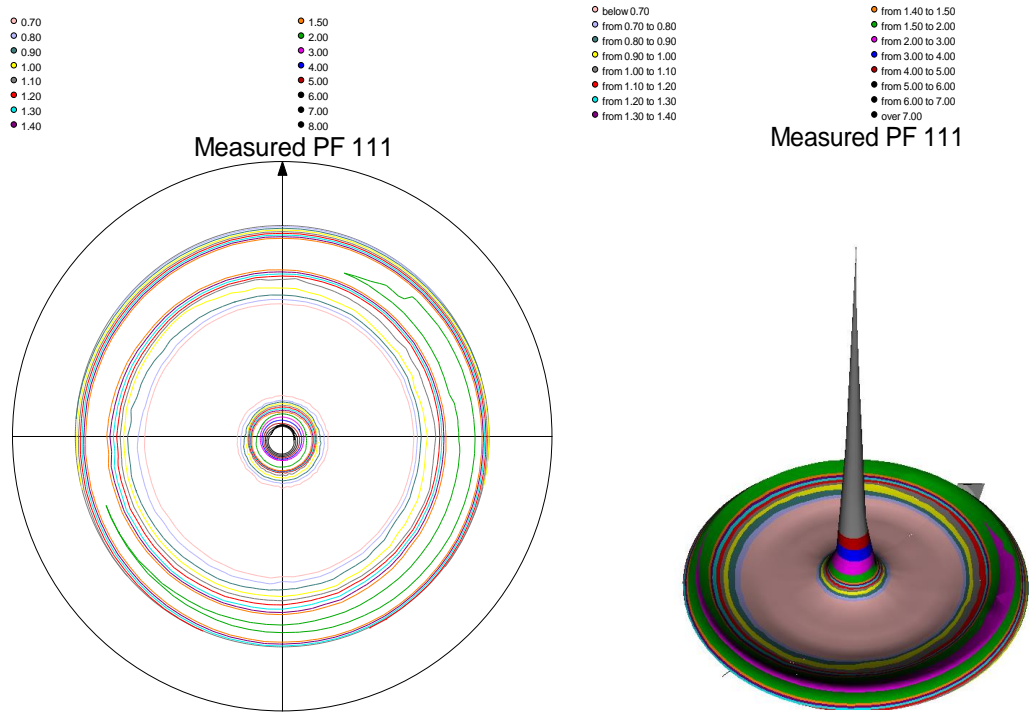


Figure C.4. Strong {111} texture pole figure for 1 nm thick Ti intermediate layer deposited at 3 Pa argon pressure of Pd/Ti/SiO₂/Si film after hydrogen loading and de-loading processes.

APPENDIX IV- HYDROGEN LOADING AND DE-LOADING

1. Pd/Ti films after H-L&DL processes:

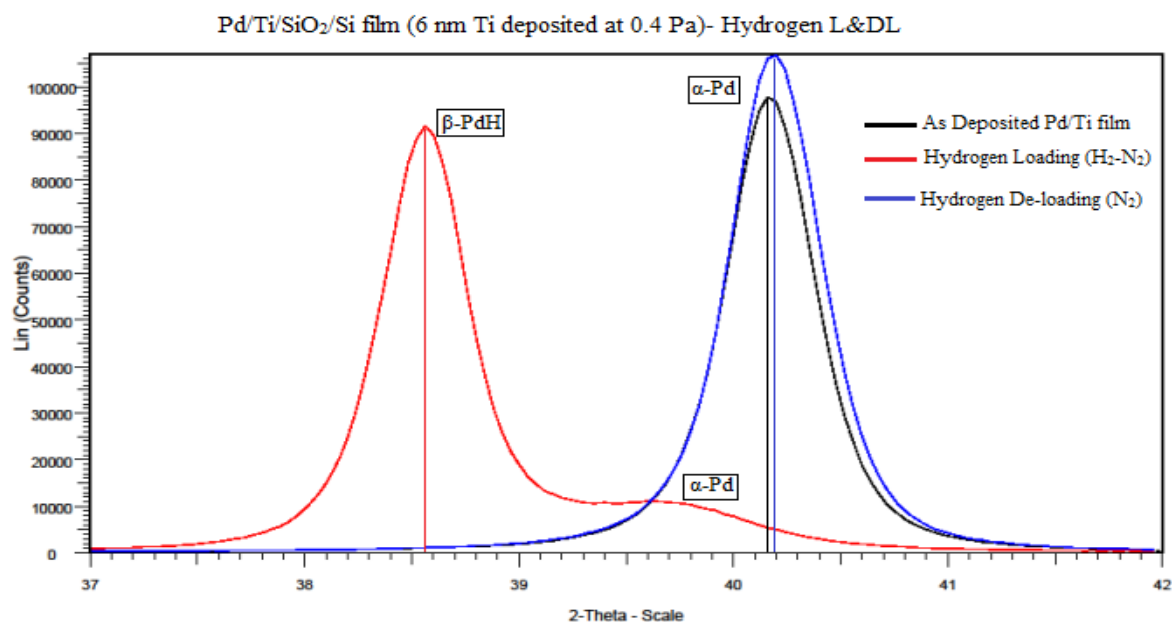


Figure D.1. Hydrogen Loading and De-loading intensity scans for a strong textured Pd/Ti film with 6 nm Ti layer deposited at 0.4 Pa.

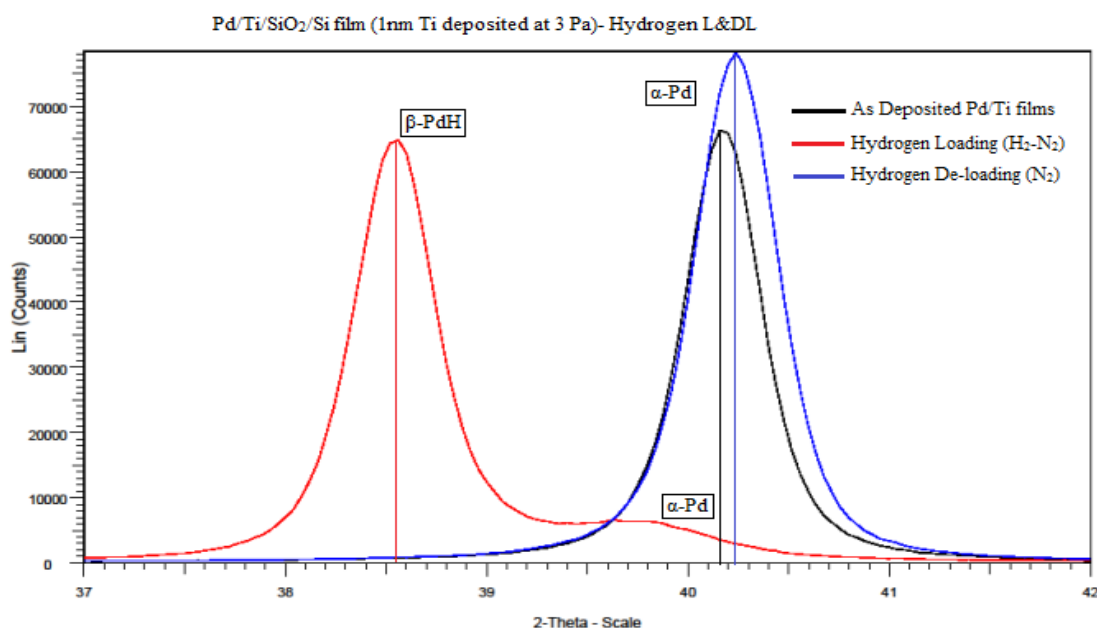


Figure D.2. Hydrogen Loading and De-loading intensity scans for a strong textured Pd/Ti film with 1 nm Ti layer deposited at 3 Pa.

BIBLIOGRAPHY

1. Nenoff, Tina M., Richard J. Spontak, and Christopher M. Aberg. "Membranes for hydrogen purification: an important step toward a hydrogen-based economy." *MRS bulletin* 31.10 (2006): 735-744.
2. Sholl, David S., and Y. H. Ma. "Dense metal membranes for the production of high-purity hydrogen." *MRS bulletin* 31.10 (2006): 770-773.
3. Basile, A., et al. "Pd-based selective membrane state-of-the-art." *Membrane reactors for hydrogen production processes*. Springer London, 2011. 21-55.
4. Saini, Alpna. *An investigation of the cause of leak formation in palladium composite membranes*. 2006.
5. Drogowska, K., et al. "Hydrogen Charging Effects in Pd/Ti/TiO₂/Ti Thin Films Deposited on Si (111) Studied by Ion Beam Analysis Methods." *Advances in Materials Science and Engineering* 2012 (2011).
6. Alfonso, Edgar, Gloria Cubillos, and Jairo Olaya. *Thin film growth through sputtering technique and its applications*. INTECH Open Access Publisher, 2012.
7. Direct vacuum, "Magnetron sputtering technology" (directvacuum.com).
8. Okolo, B., et al. "The effect of deposition parameters and substrate surface condition on texture, morphology and stress in magnetron-sputter-deposited Cu thin films." *Thin solid films* 474.1 (2005): 50-63.
9. Farooq, M., and Z. H. Lee. "Optimization of the sputtering process for depositing composite thin films." *Journal of the Korean Physical Society* 40.3 (2002): 511-515.
10. Bordo, Kirill, and Horst-Günter RUBAHN. "Effect of deposition rate on structure and surface morphology of thin evaporated Al films on dielectrics and semiconductors." *Materials Science* 18.4 (2012): 313-317.
11. Pollack, Gordon. "AJA Magnetron Sputter System Operation Manual." (2006).
12. Pascual, R., et al. "Thin film thickness measurement using the energy-dispersive spectroscopy technique in a scanning electron microscope." *Thin solid films* 185.2 (1990): 279-286.
13. Burnham, N. A., et al. "An introduction to atomic force microscopy." *Computer* 10 (2004): 800V.

14. De Oliveira, R. R. L., et al. *Measurement of the nanoscale roughness by atomic force microscopy: basic principles and applications*. INTECH Open Access Publisher, 2012.
15. School of Crystallography, Birkbeck University of London, "Instrument X-ray optics reflection geometry." *Course Material Master Index*.
16. Klapetek, Petr, David Necas, and Christopher Anderson. "Gwyddion user guide." *Online* <http://gwyddion.net> (2004).
17. Salcedo, K. L., et al. "Morphological study of Palladium thin films deposited by sputtering." *Journal of Physics: Conference Series*. Vol. 274. No. 1. IOP Publishing, 2011.
18. Gadelmawla, E. S., et al. "Roughness parameters." *Journal of Materials Processing Technology* 123.1 (2002): 133-145.
19. Ohring, Milton. *Materials science of thin films*. Academic press, 2001.
20. Cullity, Bernard Dennis. "Elements of X-ray Diffraction." (2001).
21. Illinois education site, "Development of X-ray Crystallography", December 2014.
22. Bruker user manual, *XRD instrument (brukersupport.com)-product details*.
23. Yasaka, Miho. "X-ray thin-film measurement techniques." *The Rigaku Journal* 26.2 (2010).
24. Was, G. S., H. Ji, and Z. Ma. "Texture Control in Thin Films Using Ion Bombardment." *Textures and Microstructures* 34.2-3 (2000): 105-118.
25. Thornton, John A., and D. W. Hoffman. "Stress-related effects in thin films." *Thin solid films* 171.1 (1989): 5-31.
26. Welzel, U., et al. "Stress analysis of polycrystalline thin films and surface regions by X-ray diffraction." *Journal of Applied Crystallography* 38.1 (2005): 1-29.
27. Verma, Neha, and Amarante J. Böttger. "Stress development and adhesion in hydrogenated nano-columnar Pd and Pd/Ti ultra-thin films." *Advanced Materials Research* 996 (2014).
28. Gnäupel-Herold, Thomas. "ISODEC: software for calculating diffraction elastic constants." *Journal of Applied Crystallography* 45.3 (2012): 573-574.
29. Klaus Pagh Almqvist, "Structural characterization of Nano-crystalline thin films grown by Magnetron Sputtering", *Interdisciplinary Nanoscience center (iNANO) and Department of Physics and Astronomy*, University of Aarhus, April 2006.
30. Thornton, John A. "High rate thick film growth." *Annual review of materials science* 7.1 (1977): 239-260.

31. Petrov, I., et al. "Microstructural evolution during film growth." *Journal of Vacuum Science & Technology A* 21.5 (2003): S117-S128.
32. Jie, Wang, et al. "Deposition and characterization of TiZrV-Pd thin films by dc magnetron sputteringSupported by National Natural Science Funds of China (11205155) and Fundamental Research Funds for the Central Universities (WK2310000041)." *Chinese physics C* 39.12 (2015): 127007.
33. Nix, W. D., and B. M. Clemens. "Crystallite coalescence: A mechanism for intrinsic tensile stresses in thin films." *Journal of Materials Research* 14.08 (1999): 3467-3473.
34. Yu, Jian, et al. "Low-Temperature Titanium-Based Wafer Bonding Ti/ Si, Ti/ SiO₂, and Ti/ Ti." *Journal of the Electrochemical Society* 154.1 (2007): H20-H25.
35. Bai, P., et al. "Effect of substrate surface roughness on the columnar growth of Cu films." *Journal of Vacuum Science & Technology A* 9.4 (1991): 2113-2117.
36. Thomas, Senoy, et al. "Influence of substrate topography on the growth and magnetic properties of obliquely deposited amorphous nanocolumns of Fe–Ni." *Journal of Physics D: Applied Physics* 42.21 (2009): 215005.
37. Kumar, B. Rajesh, and T. Subba Rao. "AFM Studies on surface morphology, topography and texture of nanostructured zinc aluminum oxide thin films." *Digest Journal of Nanomaterials and Biostructures* 7.4 (2012): 1881-1889.